AD-A154 718 NAVY TACTICAL APPLICATIONS GUIDE VOLUME 5 PART 1 INDIAN OCEAN (RED SEA/PE..(U) BOHAN (WALTER A) CO PARK RIDGE IL R W FETT ET AL. FEB 85 NEPRF-TR-83-03-REV 1/2

UNCLASSIFIED N00228-82-C-6222 F/G 4/2 NL

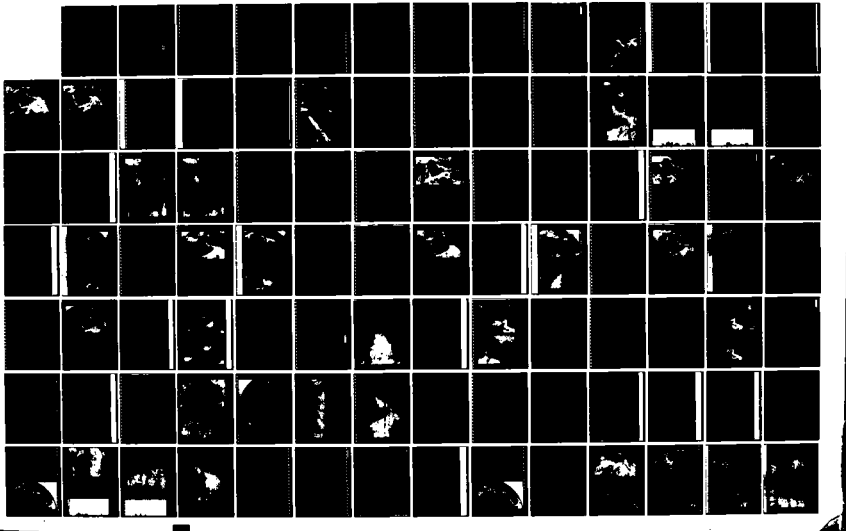

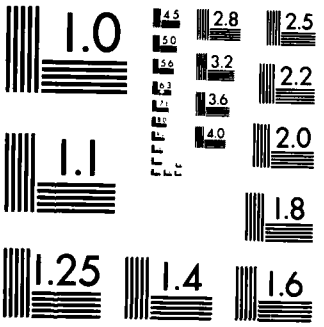

REVISED
January 1985

UNCLASSIFIED
SECURITY CLASSIFICATION OF THIS PAGE (When Data Entered)

REPORT DOCUMENTATION PAGE		READ INSTRUCTIONS BEFORE COMPLETING FORM
1. REPORT NUMBER: NAVENVPREDRSCHFAC Technical Report 83-03	2. GOVT ACCESSION NO.	3. RECIPIENT'S CATALOG NUMBER
4. TITLE (and Subtitle): Navy Tactical Applications Guide. Volume 5. Part 1 Indian Ocean (Red Sea/Persian Gulf) Weather Analysis and Forecast Applications		5. TYPE OF REPORT & PERIOD COVERED 6. PERFORMING ORG. REPORT NUMBER
7. AUTHOR(s): Robert W. Fett, Walter A. Bohan, Ronald E. Englebretson		8. CONTRACT OR GRANT NUMBER(s): The Walter A. Bohan Company N00228-82-C-6222
9. PERFORMING ORGANIZATION NAME AND ADDRESS: The Walter A. Bohan Company, 2026 Oakton Street, Park Ridge, IL 60068		10. PROGRAM ELEMENT, PROJECT, TASK AREA & WORK UNIT NUMBERS: 62759N. WF 59-553. NEPRF WU: 6.3-18
11. CONTROLLING OFFICE NAME AND ADDRESS: Naval Air Systems Command, Department of the Navy, Washington, D.C. 20361		12. REPORT DATE: February 1985 13. NUMBER OF PAGES: 185
14. MONITORING AGENCY NAME & ADDRESS(if different from Controlling Office): Naval Environmental Prediction Research Facility, Monterey, California 93943		15. SECURITY CLASS. (of this report): Unclassified 15a. DECLASSIFICATION/DOWNGRADING SCHEDULE

16. DISTRIBUTION STATEMENT (of this Report)

Approved for Public Release
Distribution Unlimited

17. DISTRIBUTION STATEMENT (of the abstract entered in Block 20, if different from Report)

18. SUPPLEMENTARY NOTES

19. KEY WORDS (Continue on reverse side if necessary and identify by block number)

Meteorological Satellite Systems
Analysis and Forecast Applications
Indian Ocean
Northeast Monsoon
Southwest Monsoon
Coastal Zone Phenomena
Ocean-Atmosphere Interaction

20. ABSTRACT (Continue on reverse side if necessary and identify by block number)

Case studies describing regional environmental analysis and forecast applications based on satellite data and conventional meteorological observations for the Indian Ocean area are presented. Topics include Northeast Monsoon Southwest Monsoon, coastal zone phenomena, and ocean-atmosphere interaction. The studies provide insights into identifiable patterns of weather development that occur frequently, so that once the basic pattern is recognized at an early stage this information can be used for improved weather analysis and forecasting

DD FORM 1 JAN 73 1473 EDITION OF 1 NOV 65 IS OBSOLETE
S/N 0102-014-6601

UNCLASSIFIED
SECURITY CLASSIFICATION OF THIS PAGE (When Data Entered)

UPDATE BULLETIN

Navy Tactical Applications Guide
Volume 5 Part 1
Indian Ocean: Red Sea/Persian Gulf
Weather Analysis and Forecast Applications

Revised pages dated January 1985, additional sections, and additional case studies are enclosed. This is the first mailing since the initial distribution of Volume 5 Part 1.

Replacement pages:
- DD Form 1473
- Acknowledgments (page vi)
- Main Contents (page vii)
- Sectional Contents (page 1A-i)

Additional Case Studies:
- Section 1A Introduction (page 1A-1)
- Section 1B Autumn Transition
  - Case 1 Convective Storms During the Autumn Transition (page 1B-1)
- Section 1C Winter
  - Case 5 Jet Aircraft Generated Condensation Trails (page 1C-47)
- Section 1D Spring Transition
  - Case 1 Desert Front (page 1D-1)
  - Case 2 Detection of the Descending Offshore Branch in a Sea Breeze Circulation (page 1D-25)
  - Case 3 Land Breeze Detection in Infrared Imagery (page 1D-29)
- Section 1E Summer
  - Case 4 Duststorms over the Southern Red Sea (page 1E-41)
  - Case 5 Summer Shamal over the Persian Gulf (page 1E-49)

Foreword

Volume 5 of the Navy Tactical Applications Guide (NTAG) series is devoted to regional weather analysis and forecast applications in the northern Indian Ocean. Part 1 of Volume 5 is dedicated to operationally important weather phenomena affecting the region surrounding and including the Red Sea and Persian Gulf. Part 2 extends the area of interest to the Arabian Sea and Bay of Bengal. The case study technique of relating weather satellite imagery to concurrent conventional weather data and analyses from the surface to the upper troposphere, along with available numerical guidance products, is continued, focusing on the unique weather characteristics of the Indian Ocean region.

Whereas the topics of blocking and cyclogenesis were emphasized in previous volumes, it is the powerful monsoon influences of winter and summer that become the dominant interest in the Indian Ocean. Duststorm generation is a subject of major interest because of its effect on operations thoughout the northern portion of the Indian Ocean region. The ability to detect duststorms over land areas at the time of earliest inception in satellite data, and to forecast the areas most likely to be influenced by the dust, is given special attention.

The Indian Ocean volumes are intended as an evolving series which will be supplemented with additional material presently under development. The initial material is being distributed to the fleet to expedite access of completed work for operational use.

As with case studies developed for previous volumes, many of the principles derived for Indian Ocean weather analysis and forecasting are general in nature and equally applicable to similar weather events in other areas of the world.

It is anticipated that these guides will be useful supplements to other material available for the Indian Ocean region in their emphasis on new aspects of weather satellite interpretation for improved weather analysis and forecasts.

Kenneth L. Van Sickle

KENNETH L. VAN SICKLE
Captain, U.S. Navy
Commanding Officer, NEPRF

REVISED
January 1985

Acknowledgments

This volume could not have been published without the devoted effort of the NEPRF Meteorological Laboratory personnel who obtained required documentation, and who spent many hours on the computer terminal entering information for the analyses utilized in the studies. Directed by AGCM D.M. Ales, the following personnel: AG2 J.V. Klimas, AG2 R.J. Bonaly, AG2 D.B. Elliott, AG3 J.L. Benvick, AG3 B.H. Kenthack, and AGAN J.M. Roy, did an outstanding job in supporting the work effort required for this volume.

PH1 A. Matthews and PH2 W.A. Anderson processed many of the original photos utilized. The correlative meteorological data were provided by the Fleet Numerical Oceanography Center, Monterey, CA, and the U.S. Naval Oceanographic Detachment, Asheville, N.C.

Additional satellite imagery was supplied by the National Environmental Satellite Data and Information Service (NESDIS) of the National Oceanic and Atmospheric Administration (NOAA). METEOSAT imagery was supplied by the European Space Agency.

The assistance of the staff of the Walter A. Bohan Company is again acknowledged; in particular, Lido A. Andreoni for design of the format of the publication and layout of the case studies. Gregory E. Terhune assisted in the preparation of case study graphics and preparation in the editing and formating of the text. The high quality of the reproduction of the satellite imagery used in the case studies and the excellent printing of the publication are due to the combined efforts of Peter M. Samorez and Michael E. Brock.

This work was funded by the Naval Environmental Prediction Research Facility, Monterey, California, under Program Element 63207N, Project 2W0527, Remote Ocean Measuring System

REVISED
January 1985

Contents

REVISED
January 1985

Section 1

Red Sea/Persian Gulf

Introduction

Case Studies

1B Autumn Transition

1C Winter

1D Spring Transition

1E Summer

Red Sea/ Persian Gulf Introduction

—Physiography
—General Weather Patterns

Red Sea/ Persian Gulf

Physiography

The Red Sea lies in the northern extension of the eastern branch of the great Rift Valley of eastern Africa (1A-2a). It is surrounded by mountainous terrain which rises sharply to high elevations from a narrow coastal plain (1A-3a). The Red Sea is about 1,200 n mi long with its greatest width (190 n mi) in the southern part where the mountains are also the highest. The great Nubian and Arabian Deserts are located to the west and east of the Red Sea, respectively.

On the African side, a ridge some 20-30 n mi inland roughly parallels the coast. The ridge is about 3,000 ft (914 m) high in the north, with a significant gap in the north-south barrier near Tokar. South of 16° N, the mountains bordering on the Red Sea are about 6,000 ft (1,828 m) high.

On the Arabian side of the Red Sea, there is a higher and broader mountain barrier. The mountains exceed 4,500 ft (1,372 m) from the northern end of the Red Sea to about 27° N; from there southward to Jidda, they are mostly above 3,000 ft (914 m). South of Jidda, the mountains are over 6,000 ft (1,828 m). The high terrain surrounding the Red Sea forms a large channel which is called the Red Sea basin. This high bordering terrain disrupts the flow around cyclonic disturbances crossing the region, resulting in pronounced channel flow in the Red Sea basin. The gaps and lower portions of the surrounding barriers provide favored areas of flow into the Red Sea basin from the deserts on either side.

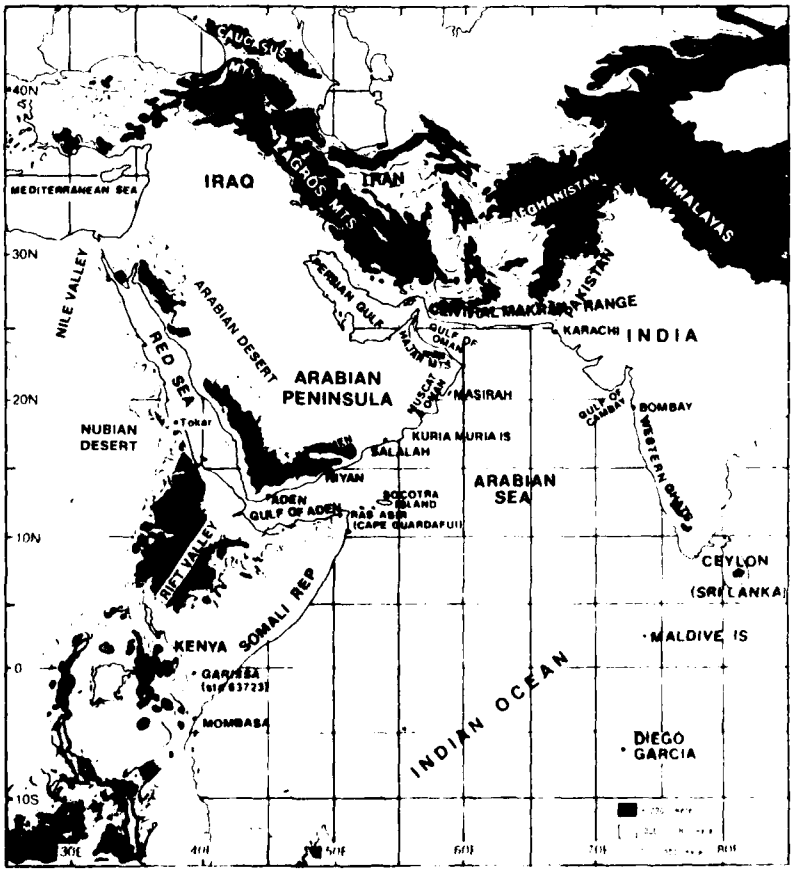

1A-2a. Locator Map of the Red Sea/Persian Gulf Region

The Persian Gulf is located to the east of the Red Sea (1A-2a). The gulf is approximately 450 n mi long, with widths varying from 100 to 180 n mi. The Persian Gulf is bounded on the south and west by the peninsula of Arabia, and on the north and east by the Asian Continent.

Along the Arabian coast of the Persian Gulf is a vast, low-lying desert. Mountainous terrain (Hajar Mountains, 1A-2a and 3a) is located along the southeastern coast of Arabia, bordering on the Gulf of Oman. Mountains rise sharply from the sea to about 6,000 ft (1,828 m) in this coastal region.

To the north and east of the Persian Gulf, the terrain is also mountainous and rises sharply to the tablelands of Iran and Afghanistan. In some places, the tablelands rise to about 3,000 ft (914 m) directly from sea level, and to above 10,000 ft (3,048 m) further inland, with some perennially snow-capped mountains. Wide valleys parallel the mountains, along with strips of low land of varying width between the mountains and the sea.

Reference

NEPRF, 1980: Weather in the Indian Ocean to Latitude 30° S and Longitude 95° E including the Red Sea and Persian Gulf. Vol. 2, Part 1. NAVENVPREDRSCHFAC Technical Bulletin 80-02, Naval Environmental Prediction Research Facility, Monterey, Calif., 83 pp.

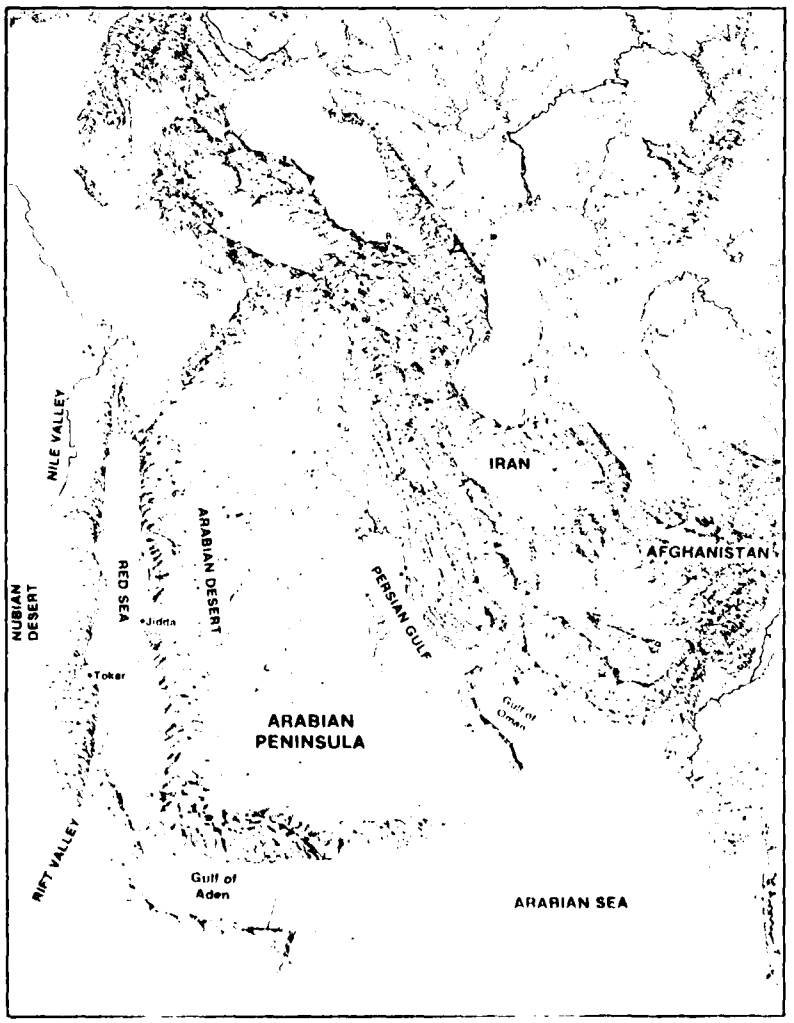

1A-3a Relief Map of the Red Sea-Persian Gulf Region

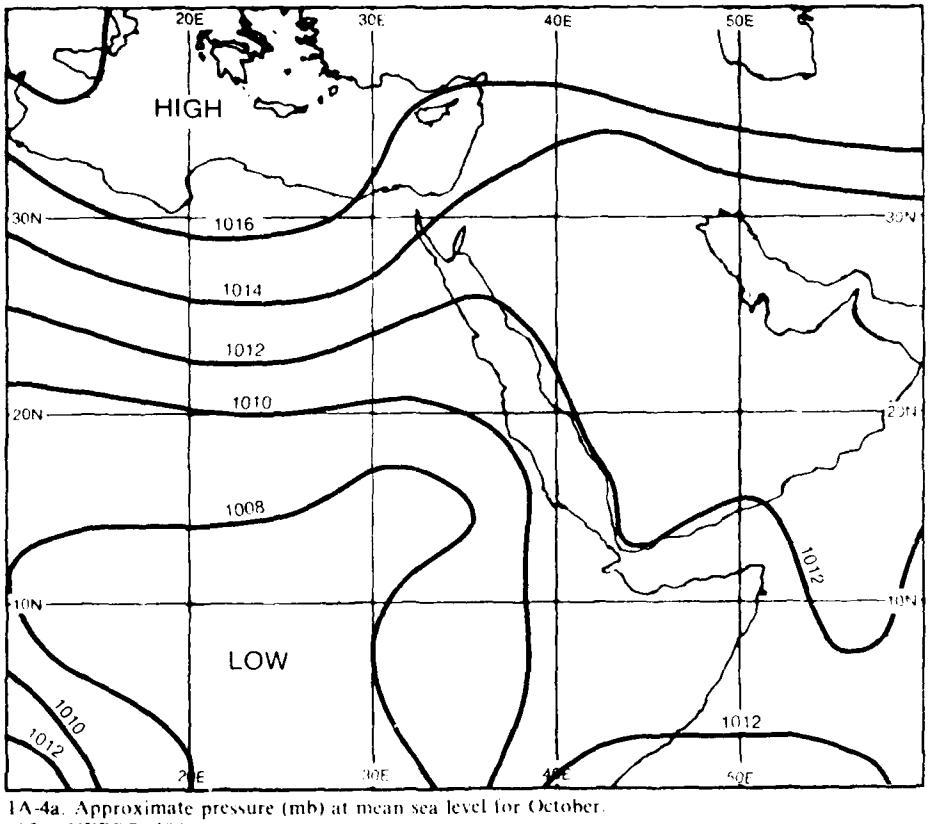

1A-4a. Approximate pressure (mb) at mean sea level for October.
(After NEPRF, 1980.)

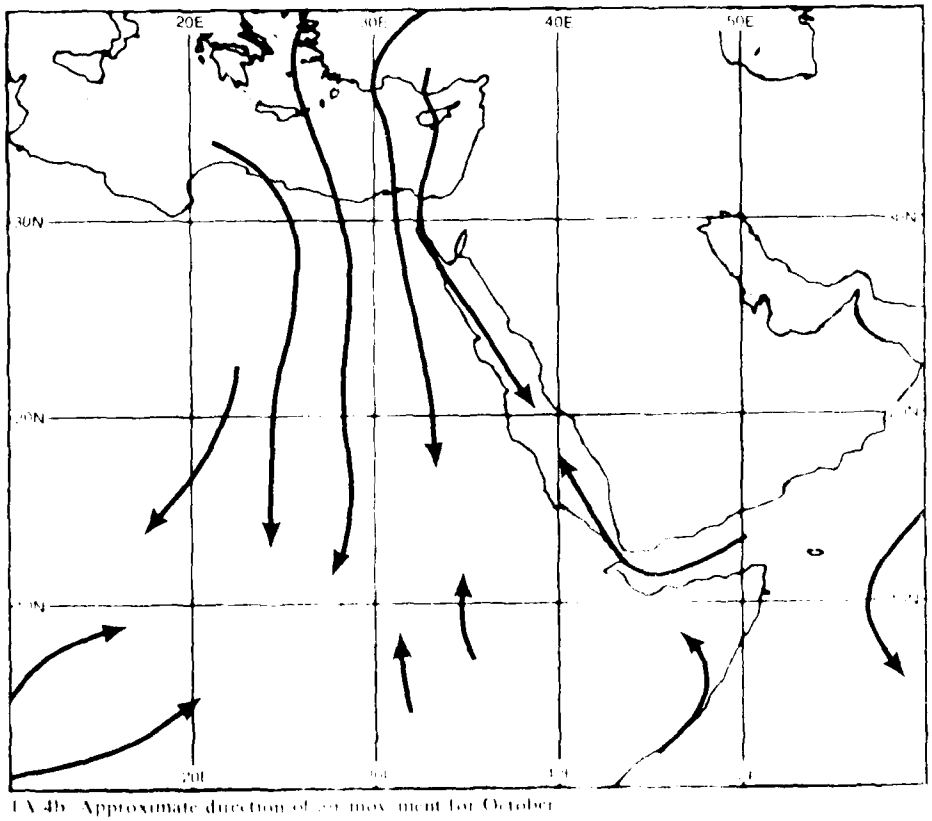

1A-4b. Approximate direction of ice movement for October.
(After NEPRF, 1980.)

Autumn Transition (October–November)

Fall begins the transition to cooler temperatures which prevail over the Red Sea and Persian Gulf region from November through April. The heat lows over the adjacent land areas begin to weaken and finally disappear to be replaced by a cool ridge as the monsoon trough over the Indian Ocean moves southward toward its winter position near the Equator.

Winds are generally northwesterly over the northern Red Sea and Persian Gulf, but may become easterly or southeasterly due to the passage of easterly moving mid-latitude depressions from the Mediterranean.

The southern portion of the Red Sea undergoes a seasonal reversal of wind direction at this time due to monsoonal effects from the Arabian Sea, as winds shift from northwesterly to southeasterly. This reversal produces a convergence of flow, giving rise to the convergence zone cloud band (CZCB), normally located over the Red Sea, near 18° 20° N, from October through February.

The surface pressure pattern and approximate direction of air movement over the Red Sea region during October (IA-4a and 4b) show that the convergence of air over the Red Sea is often linked with similar convergence in a trough or cyclonic wind shear region extending southeastward toward the quasi-permanent low pressure area over Sudan.

The GOES-Indian Ocean visible picture on 20 October 1979 (IA-5a) reveals that the effect of this convergence can produce extensive convective cloudiness in a band covering the northern Red Sea and extending southwestward to Sudan. Disturbances frequently move northeastward along this band, producing first a northward and then a southward displacement of the CZCB over the Red Sea. The concurrent NMC surface streamline analysis (IA-5b) depicts features of flow closely approximating the ocean condition for October (IA-4b).

latitude depression or frontal passage in the northern portion of the Red Sea Persian Gulf region produces occasional squalls which can be especially severe in the Gulf of Aqaba, the northern Red Sea, and in the Persian Gulf, where they are known locally as "Haboob". These squalls occur from early October through late November and, in rare instances, have been reported to have been accompanied by wind speeds exceeding hurricane force (NEPRF, 1980).

Winds in excess of 20 kt, however, are sufficient to create sandstorm conditions detrimental to operations in many areas. Such winds almost always accompany or follow movement of a depression into the northern Persian Gulf region. An example of such an occurrence is shown on the GOES-Indian Ocean visible picture for 26 October 1979 (IA-6a). The corresponding NMC surface streamline analysis (IA-6b) displays southerly winds coming around the west side of the anticyclone over the southern Arabian Peninsula, bringing moist tropical air into juxtaposition with cool, modified polar air from the eastern Mediterranean. This produces active frontogenesis in the northern Persian Gulf region with very strong moisture and temperature discontinuities. Further movement of the depression southward initiates strong northerly shamal conditions which raise sea state very rapidly over the Persian Gulf.

Such disturbed conditions are not the rule, however, during the autumn transition. Generally, weather over the region during this period is benign with very little low cloudiness, good visibility, and only occasional light rain.

Reference

NEPRF, 1980: Weather in the Indian Ocean to Latitude 30° S and Longitude 95° E including the Red Sea and Persian Gulf. Vol. 2, Part 1. NAVENVPREDRSCHFAC Technical Bulletin 80-02. Naval Environmental Prediction Research Facility, Monterey, Calif., 83 pp.

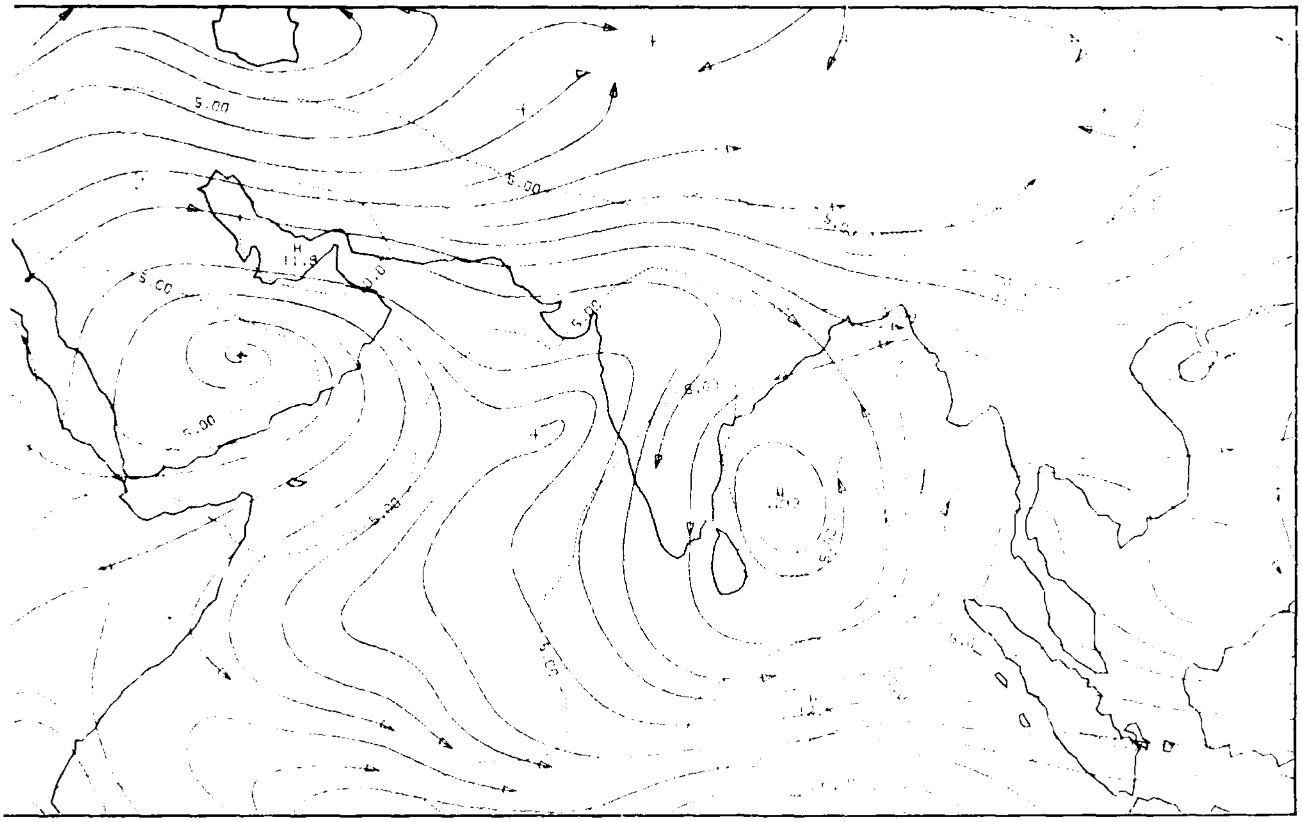

IONEX Mean 700-mb Analysis, 1 15 May 1979.

ıb

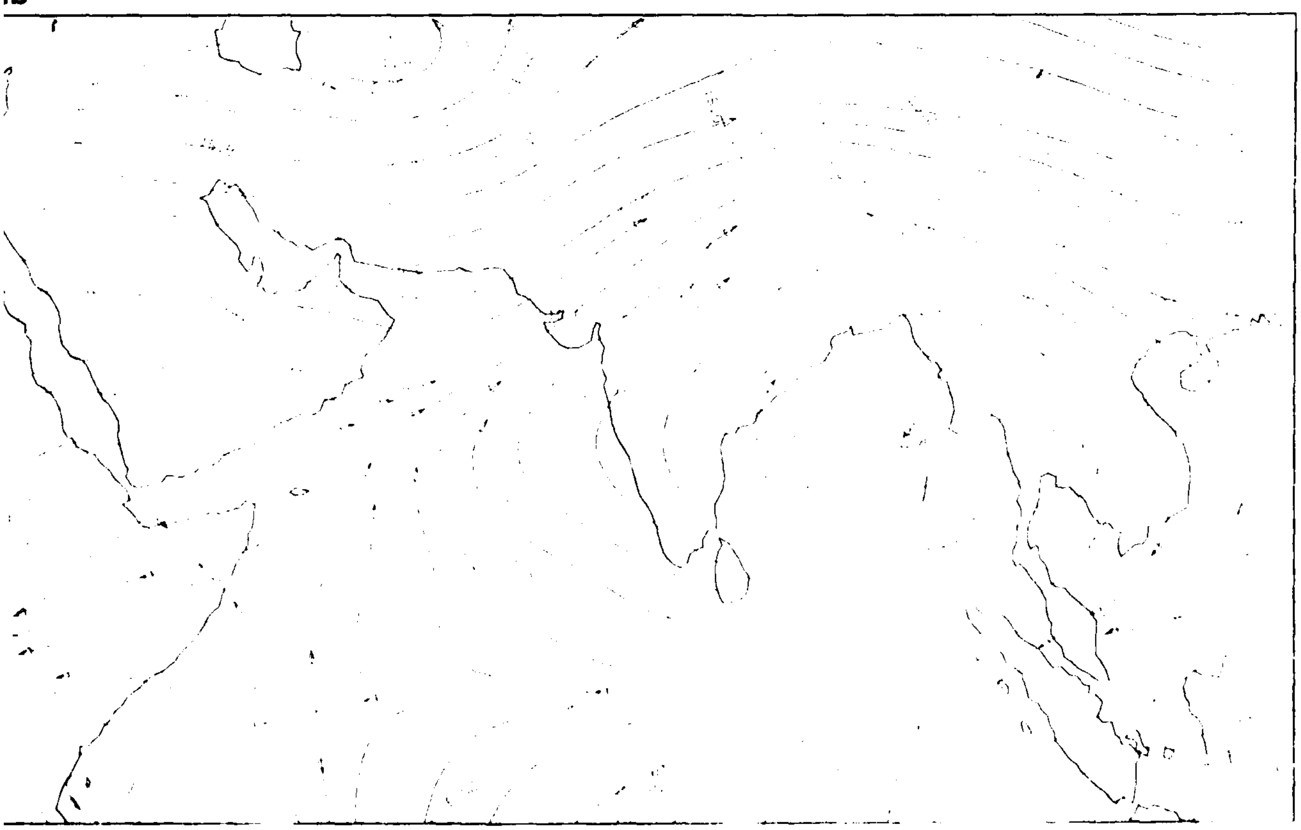

4ONEX Mean 200 mb Analysis 1 15 May 1979

General Weather Patterns

Spring Transition: Early Phase (1–15 May)

The spring transition from the northeast to the southwest monsoon over the northern Indian Ocean region is a result of increased heating of the land areas resulting in relatively lower pressure over land in comparison to that over the water. This constitutes a complete reversal from the winter northeast monsoon regime in that air that had been flowing offshore toward lower pressure now flows onshore toward lower pressure. A very shallow surface heat trough has formed over northern India which extends westward over Pakistan, Iran, Saudi Arabia and across the Red Sea into Africa.

The NMC surface streamline analysis for 8 May 1979 (1A-16a) shows typical conditions of the spring transition, early phase (1–15 May). Cyclonic circulations are depicted ringing the Red Sea, Persian Gulf region from southern India through Pakistan, across Saudi Arabia, the Red Sea, and into the Sudan region of Africa.

The MONEX 850- and 700-mb mean flow fields (1A-16b and 17a) for the 1–15 May 1979 transition period reveal a strong anticyclonic pattern extending over Saudi Arabia with ridging into northern India. The analyses confirm the shallow nature of the surface heat low which occupies only the lowest kilometer of the atmosphere and does not extend upward even to the 850-mb level.

The MONEX 200-mb mean flow field (1A-17b) depicts an extensive anticyclonic cell centered in the [illegible] Bay of Bengal near Burma, which completely [illegible] flow at this level. Zonal westerlies are [illegible] the region from 20–30° N. Short-wave disturbances penetrate at times into the southern portion of this [illegible] severe weather and [illegible]

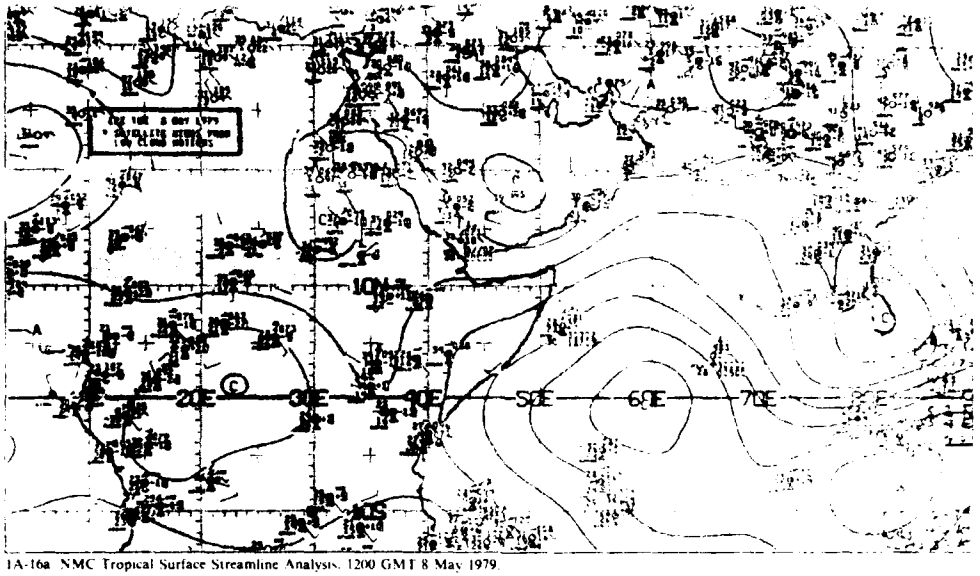

1A-16a NMC Tropical Surface Streamline Analysis, 1200 GMT 8 May 1979.

850 mb

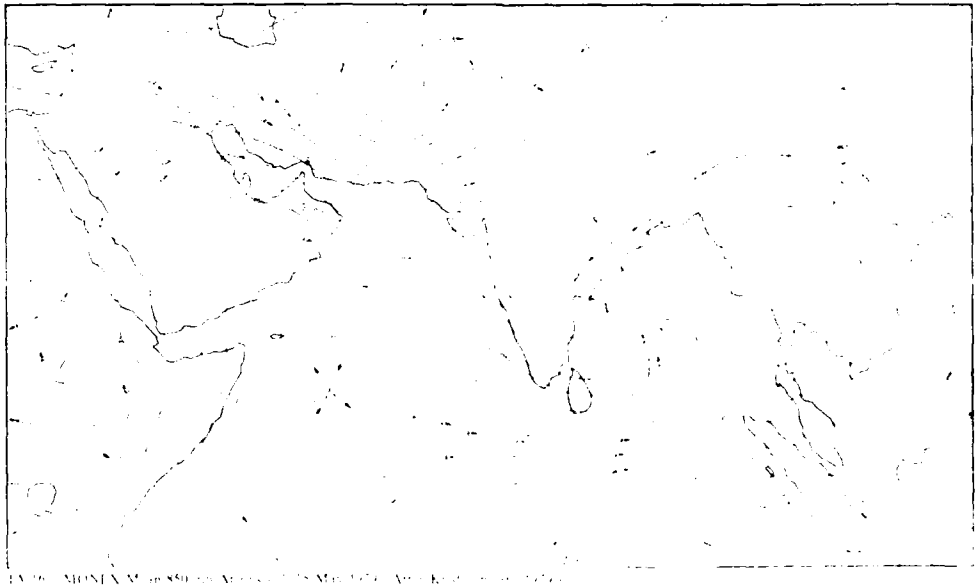

1A-16b MONEX Mean 850-mb Analysis, 1–15 May 1979 (After [illegible])

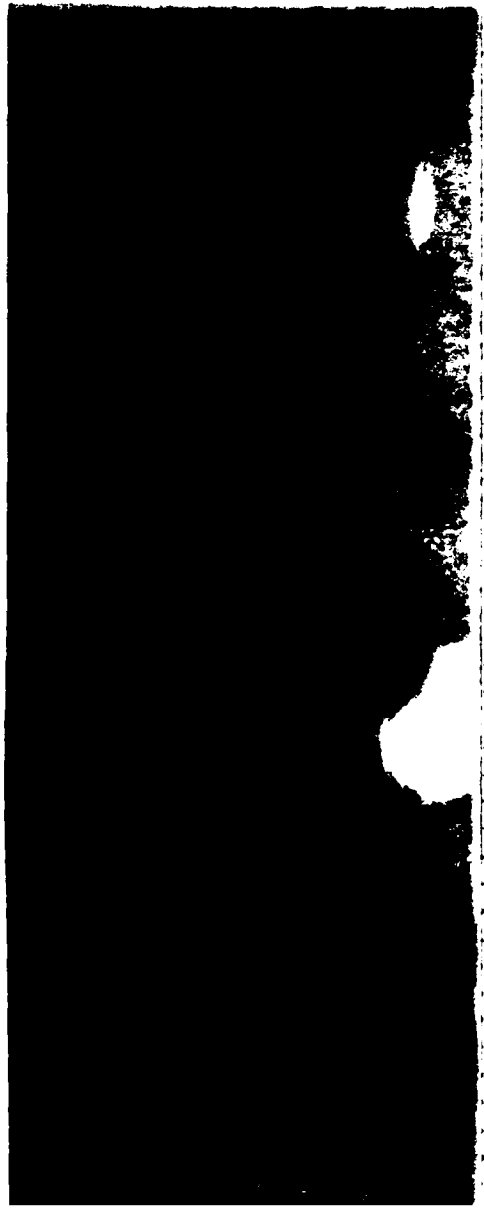

Reference

Red Sea/Persian Gulf

General Weather Patterns

Spring Transition—Early Phase
Spring Transition—Late Phase
Southwest Monsoon

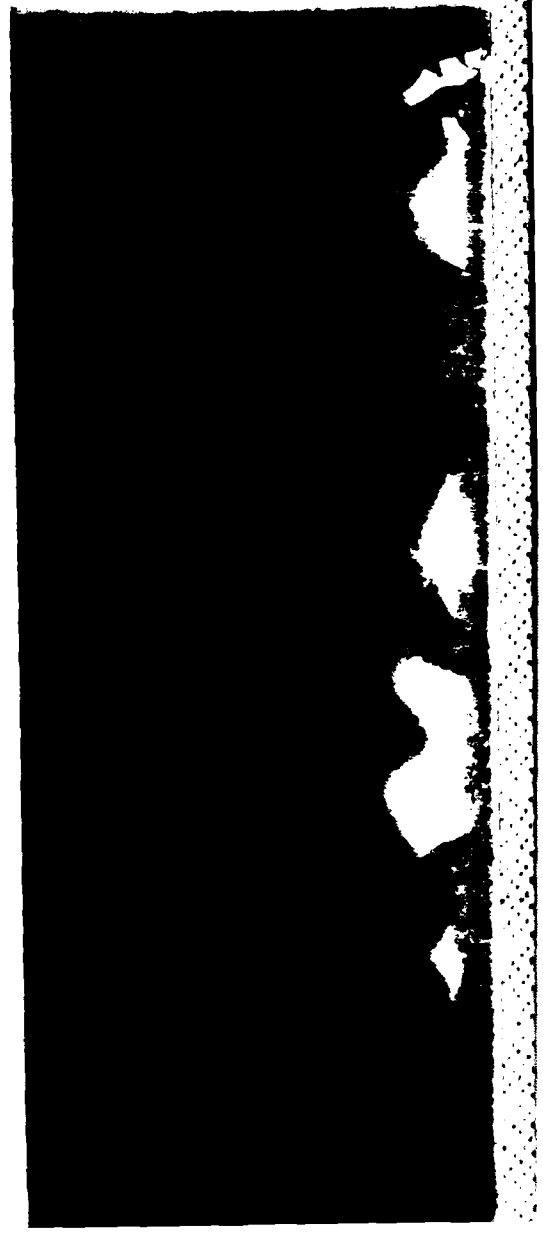

1A-14a. I-4 DMSP FT Normal Enhancement, 0437 GMT 3 January 1980

Northeast Monsoon

50 mb

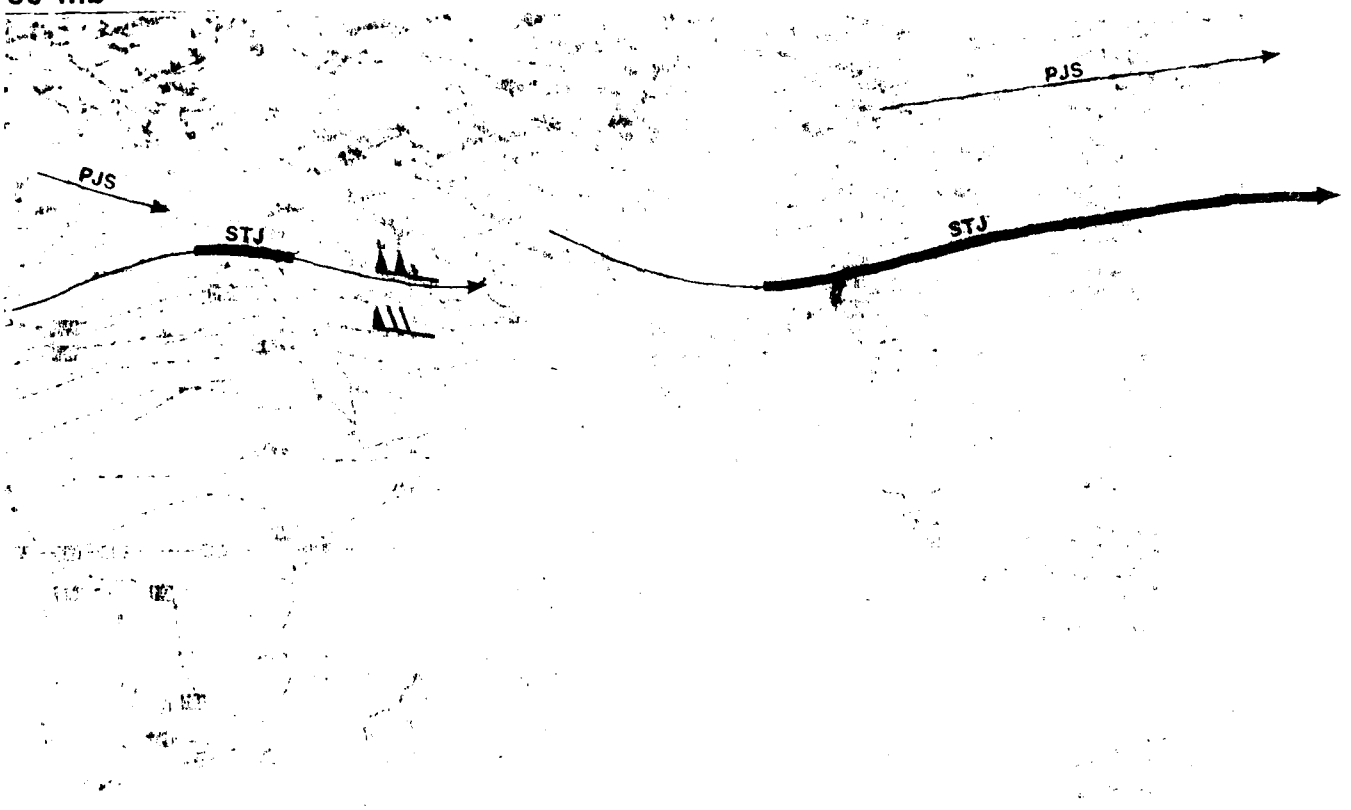

IA-13a. NMC Tropical 250-mb Streamline Analysis, 0000 GMT 3 uary 1980

surface

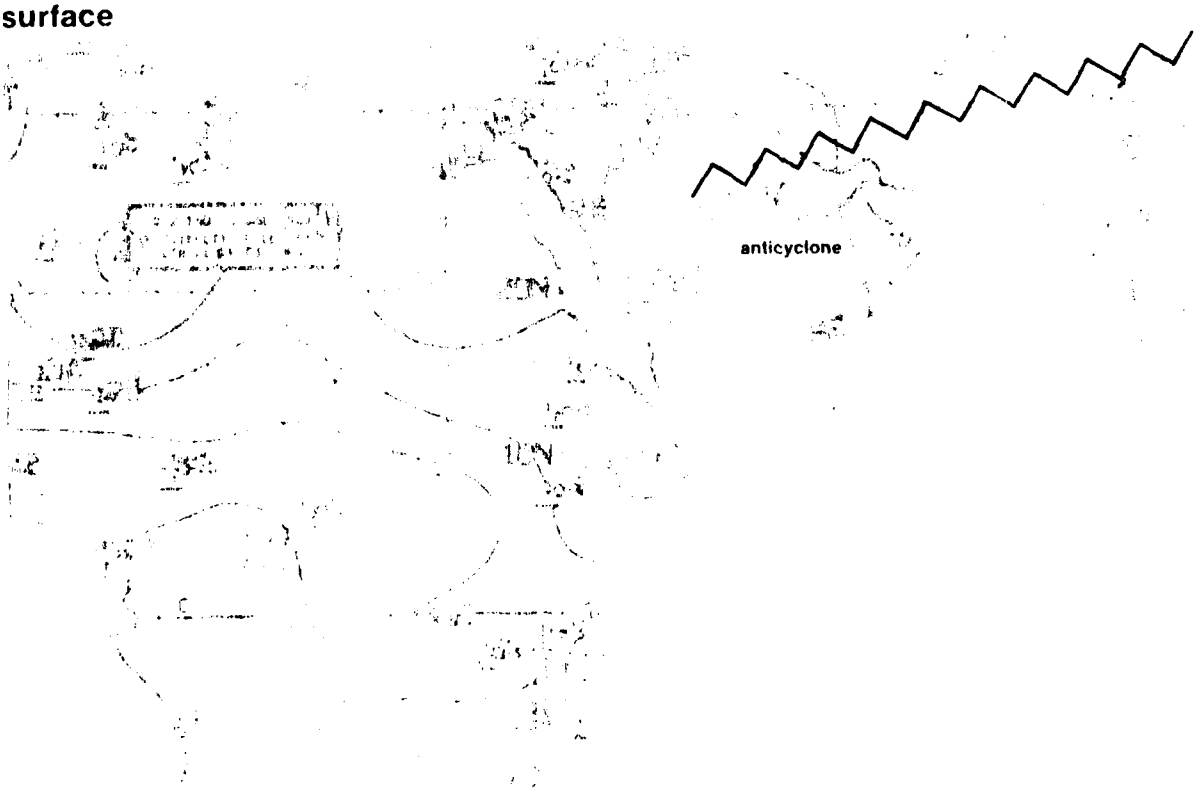

IA-13b. NMC Tropical Surface Streamline Analysis, 0000 GMT 3 January 1980

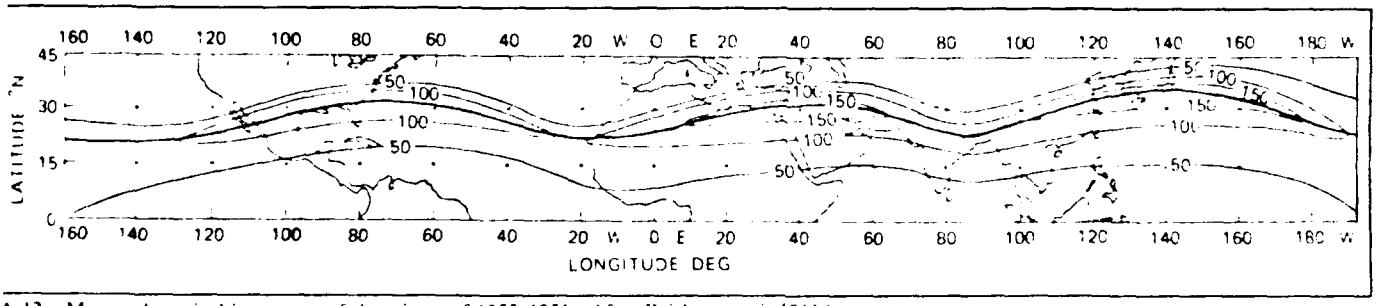

A-12a. Mean subtropical jet stream of the winter of 1955–1956. (After Krishnamurti, 1961.)

00 mb

A-12b. NMC 200-mb Analysis 1200 GMT 12 January 1980.

500 mb

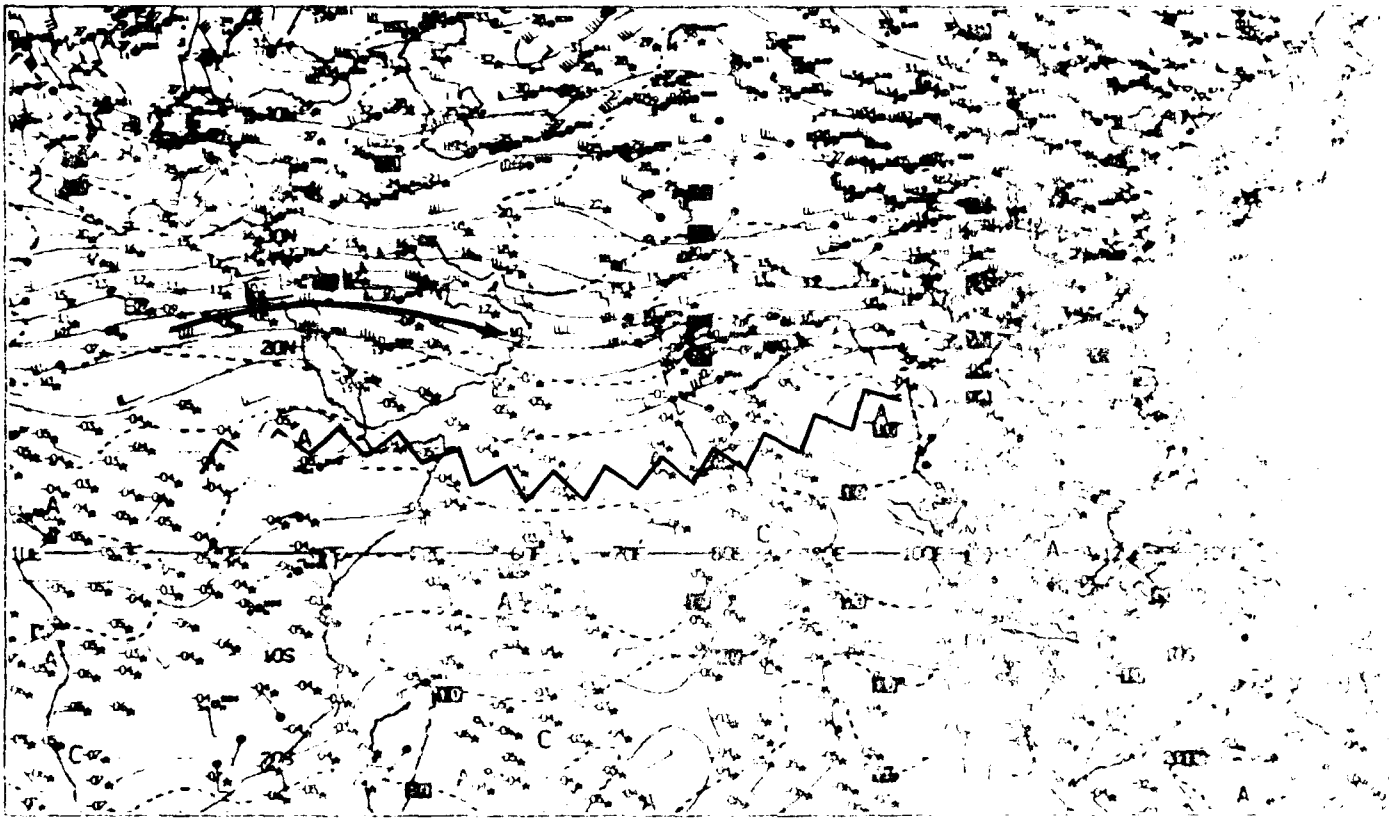

1A-11a. NMC Tropical 500-mb Streamline Analysis 1200 GMT 12 January 1980.

250 mb

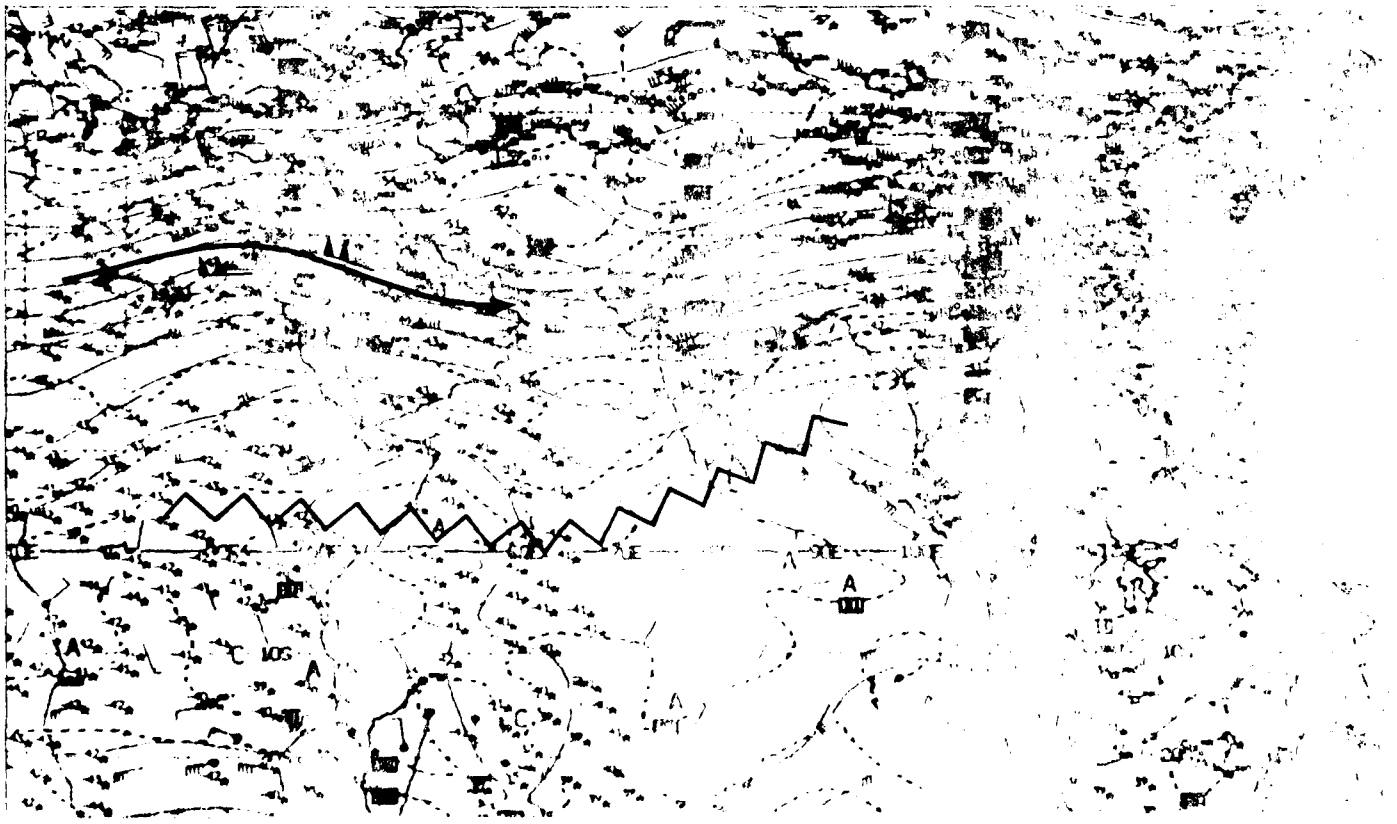

1A-11b. NMC Tropical 250-mb Streamline Analysis 1200 GMT 12 January 1980.

surface

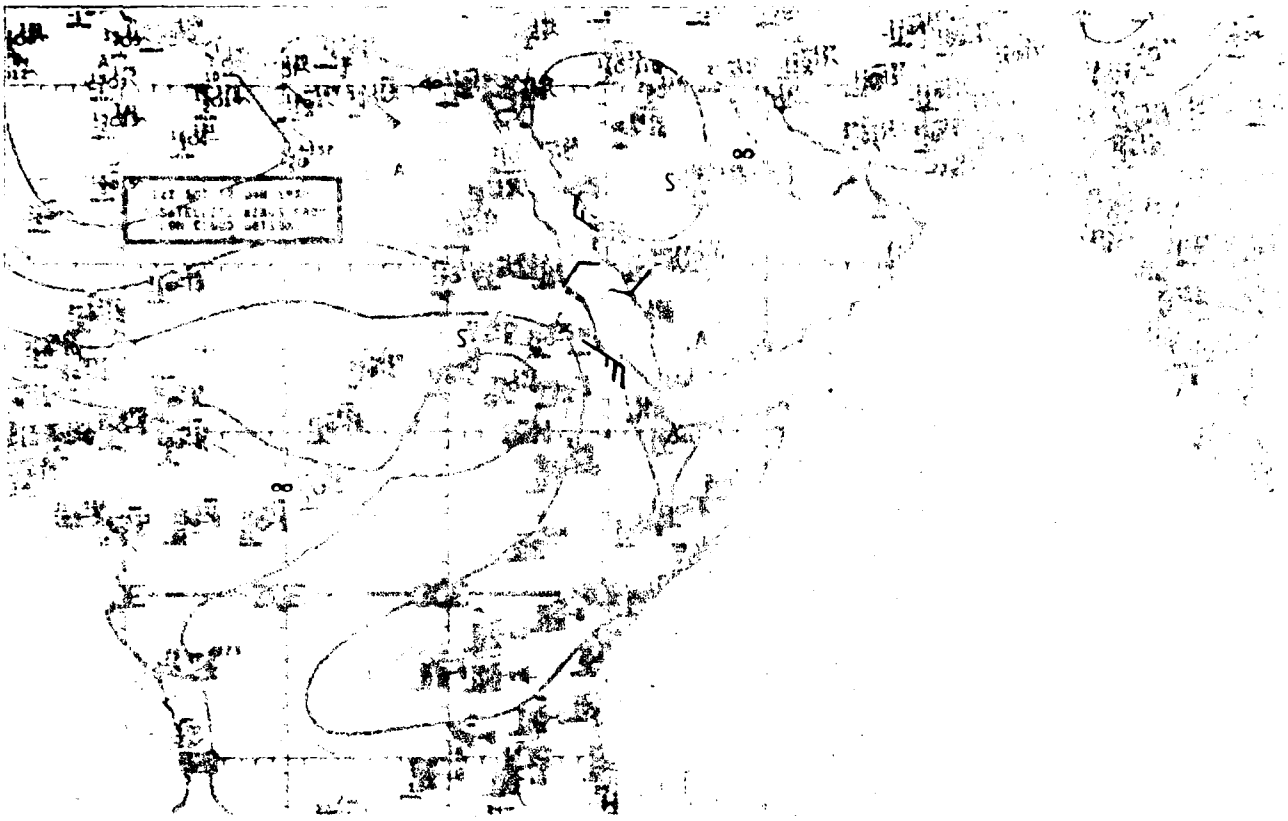

1A-10a NMC Tropical Surface Streamline Analysis. 1200 GMT 12 January 1980.

700 mb

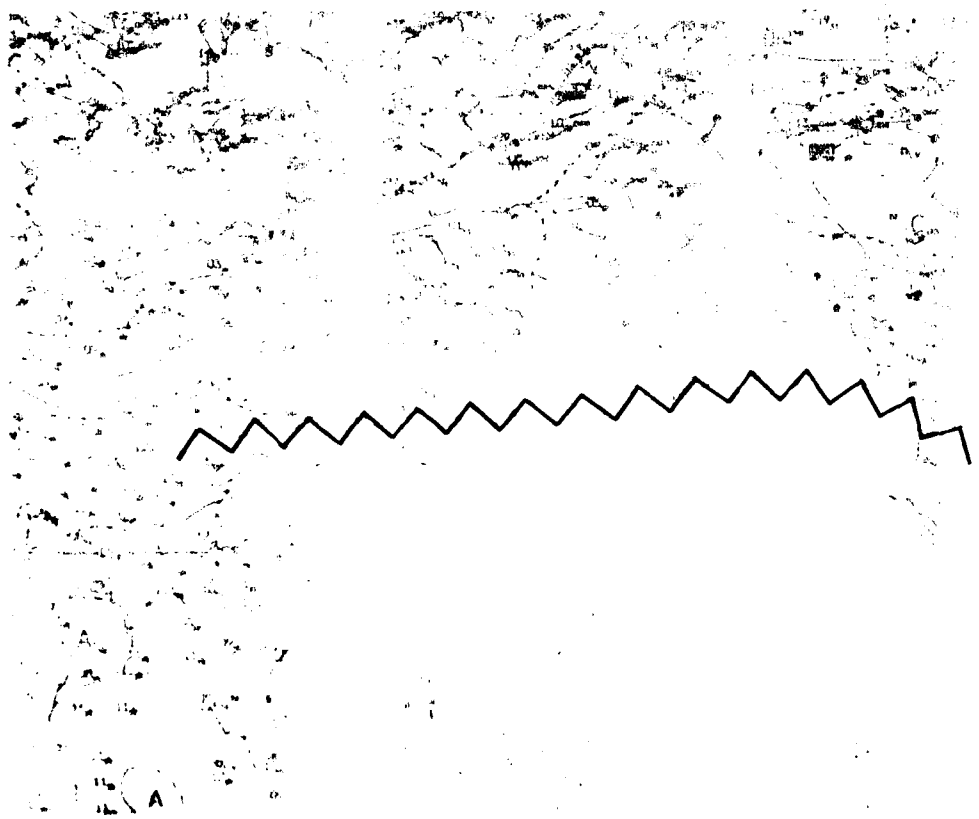

1A-10b NMC Tropical 700-mb Streamline Analysis. 1200 GMT 12 January 1980.

Northeast Monsoon

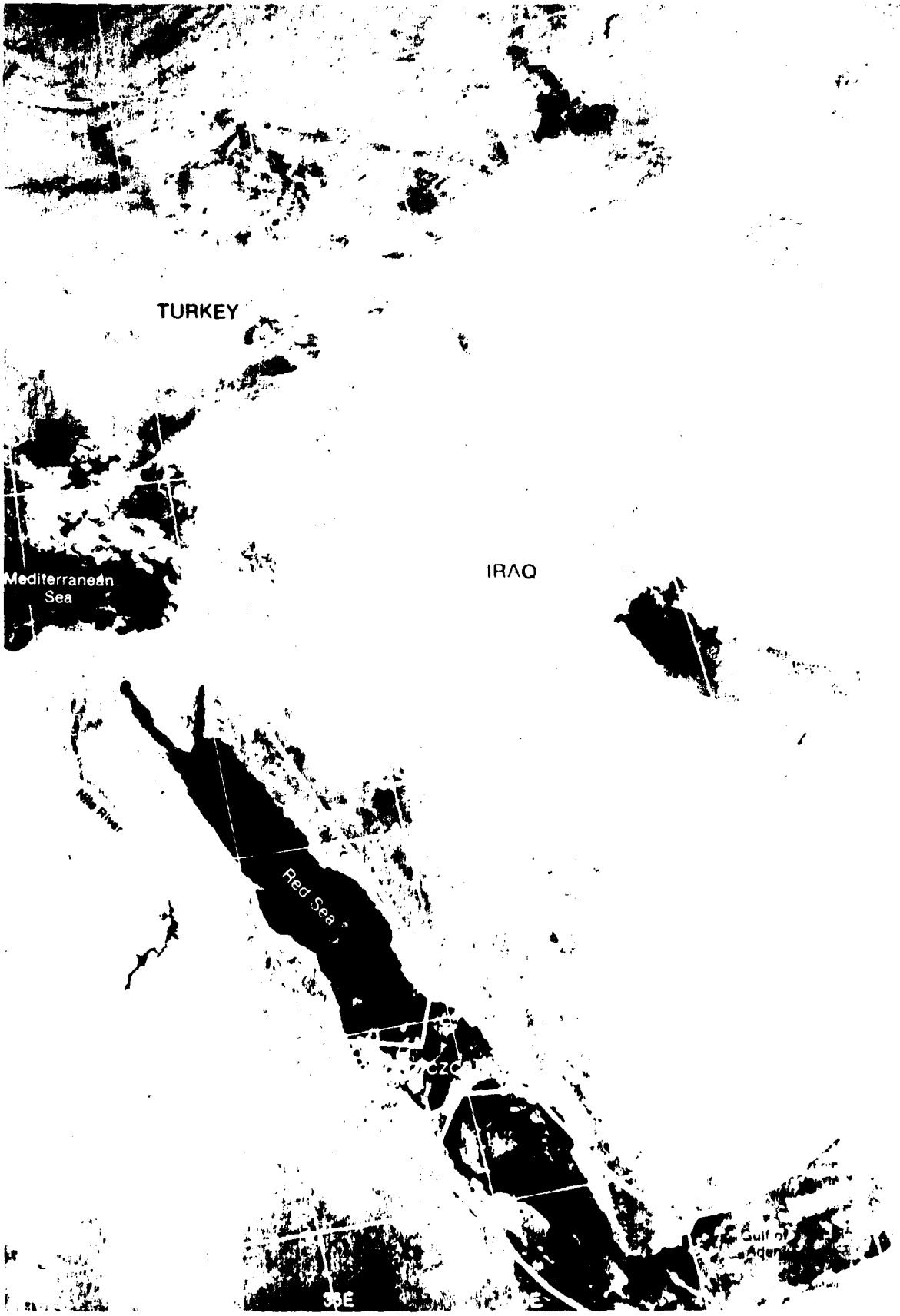

IA-9a. I-4. DMSP FT. Low Enhancement. 0724 GMT 12 January 1980

Northeast Monsoon (December–March)

The northeast monsoon season extends from December through March. This is the cool or cold season for the Red Sea and Persian Gulf. In January, an extension of the winter anticyclone over central Asia protrudes over Iran and into the northern Persian Gulf region (1A-8a). In addition, high pressure is also found over Egypt, while an inverted trough dominates the Red Sea, as shown in the mean surface pressure and wind flow pattern for January over this region (1A-8a and 8b).

Depressions from the Mediterranean frequently move through the Red Sea Persian Gulf region, producing overcast skies, rain, squalls, and thunderstorms. Sand and duststorms almost always accompany these disturbances. Aloft, the depressions show a branch of the polar jet which often interacts with the subtropical jet.

On those occasions when a large-scale blocking pattern is established either over Europe or Asia, a long-wave trough may extend southward over the northern portion of the Indian Ocean. Under these conditions, the mid-latitude jet and related frontal systems will move through the Red Sea and Persian Gulf region and will penetrate well into the central Arabian Sea.

Secondary cyclogenesis frequently forms over the Persian Gulf to the south of the mountain ranges of Iraq and Turkey. With the approach and passage of a disturbance, low-level winds will first be southerly and then northwesterly. The strong northwest wind events over the Persian Gulf are known as the "shamal". Perrone (1979) addresses the winter shamal in detail.

The DMSP visible picture on 12 January 1980 (1A-9a) shows the typical cloudiness over the Red Sea during the northeast monsoon. Northerly low-level flow occurs over the northern and central portions of the Red Sea. This is an extension of the westerly flow from the eastern Mediterranean. The general northeast monsoon flow from the Arabian Sea extends through the Gulf of Aden as easterly flow and then enters the southern Red Sea as southerly flow. The opposing low-level flows of the Red Sea merge near 18° 20° N and produce a climatological cloud feature referred to as the convergence zone cloud band (CZCB, see Sec. 1C, Case 1).

Skies are generally clear north of the CZCB. South of the CZCB, scattered to broken cumulus or stratocumulus prevail. The lack of clarity of the Nile River suggests obscuration by dust or haze. A few stations in the area are reporting suspended dust or haze (1A-10a), which is probably widespread over the region.

The NMC surface streamline analysis for 1200 GMT (1A-10a) shows a 15 kt northerly wind to the north of the CZCB and a 25-kt southerly wind south of it, with light and variable winds in the CZCB. The displacement of the CZCB from its normal winter position (1A-8b) is an indication of a synoptic-scale disturbance over the Red Sea region (see Sec. 1C, Case 2).

The upper-level westerlies penetrate progressively further equatorward with height. The 700-mb analysis (1A-10b) shows the subtropical ridge near 13° N over the southern Red Sea. At 500 mb (1A-11a) and 250 mb (1A-11b), the westerlies advance equatorward. Jet stream activity is quite common at upper levels, as shown by the mean 200-mb position of the subtropical jet (STJ) during the winter of 1955–56 (1A-12a). An isotach maximum of over 150 kt is evident over the northern portion of the Arabian Peninsula. The NMC 200-mb analysis for 12 January 1980 (1A-12b) reveals that the STJ is near the mean position, while the polar front jet (PJS) lies to the north.

Generally, the northern Arabian Peninsula and the Persian Gulf are under the influence of a high pressure ridge that extends southward from the Asian anticyclone. The NMC surface streamline analysis for 3 January 1980 (1A-13b) is a typical example. On the 250-mb analysis (1A-13a), the STJ is shown passing over the northern Red Sea and the southern Persian Gulf. Strong horizontal speed shear is evident with winds over 100 kt decreasing to 70 kt and less south of the jet axis. Pronounced turbulence at upper levels is normally associated with such shear.

The presence of high pressure over the Arabian Peninsula results in light winds and nearly clear skies throughout the region, as shown on the DMSP visible picture for 3 January 1980 (1A-14a). The main cloudiness over Saudi Arabia is a band of cirrus associated with the STJ. Knowledge of the position of the STJ over Saudi Arabia during the winter season offers a useful clue regarding the location of the surface anticyclone which normally lies immediately south of this feature in the position as shown on the surface analysis (1A-13b). The transverse banding of the jet stream cirrus evident in the DMSP picture is indicative of horizontal speed shear and associated turbulence.

Northerly flow in the Persian Gulf on the east side of the surface high over the Arabian Peninsula is indicated on the DMSP picture (1A-14a) by the cloud line passing east of the Qatar Peninsula which broadens on its southward extremity, as cloudiness is advected onshore southeast of Qatar. Plotted wind reports on the surface analysis (1A-13b) verify the northerly flow condition over the gulf. There is also a mid-latitude disturbance observed to the north in the satellite picture (1A-14a). The disturbance is located over the Taurus Mountains of Turkey, with cirrus streaks associated with the PJS (1A-12b) sweeping over the Caspian Sea.

Reference

Krishnamurti, T. N., 1961: The subtropical jet stream of winter. *J. Meteor.*, **18**, 172–191.

Perrone, T. J., 1979: Winter shamal in the Persian Gulf. NAVENVPREDRSCHFAC Technical Report TR 79-06. Naval Environmental Prediction Research Facility, Monterey, Calif., 180 pp.

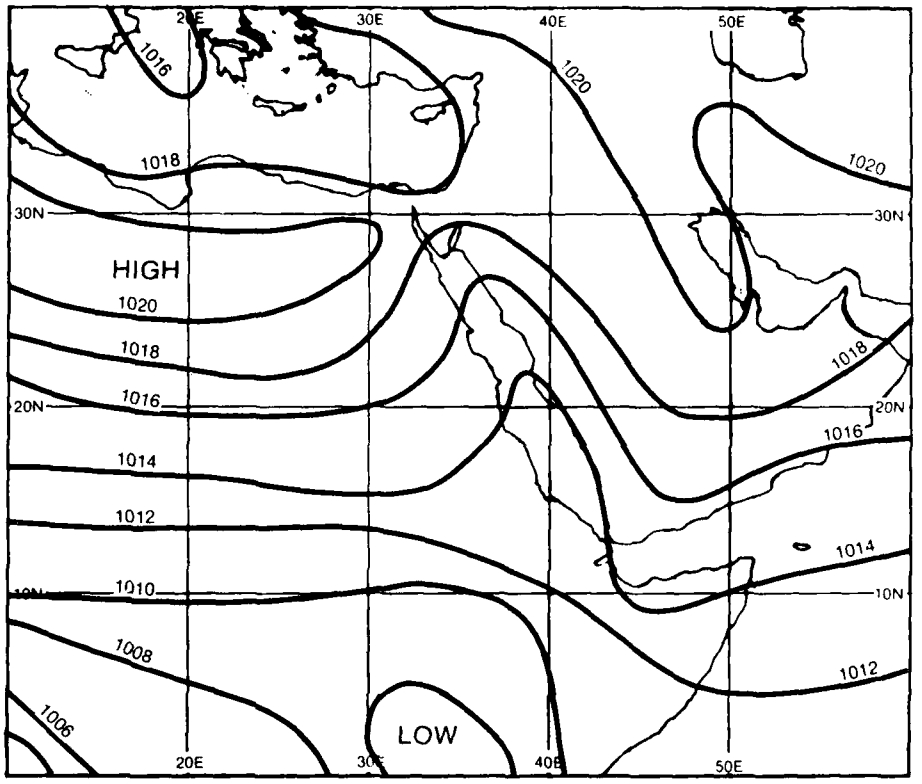

1A-8a. Approximate pressure (mb) at mean sea level for January.
(After NEPRF, 1980.)

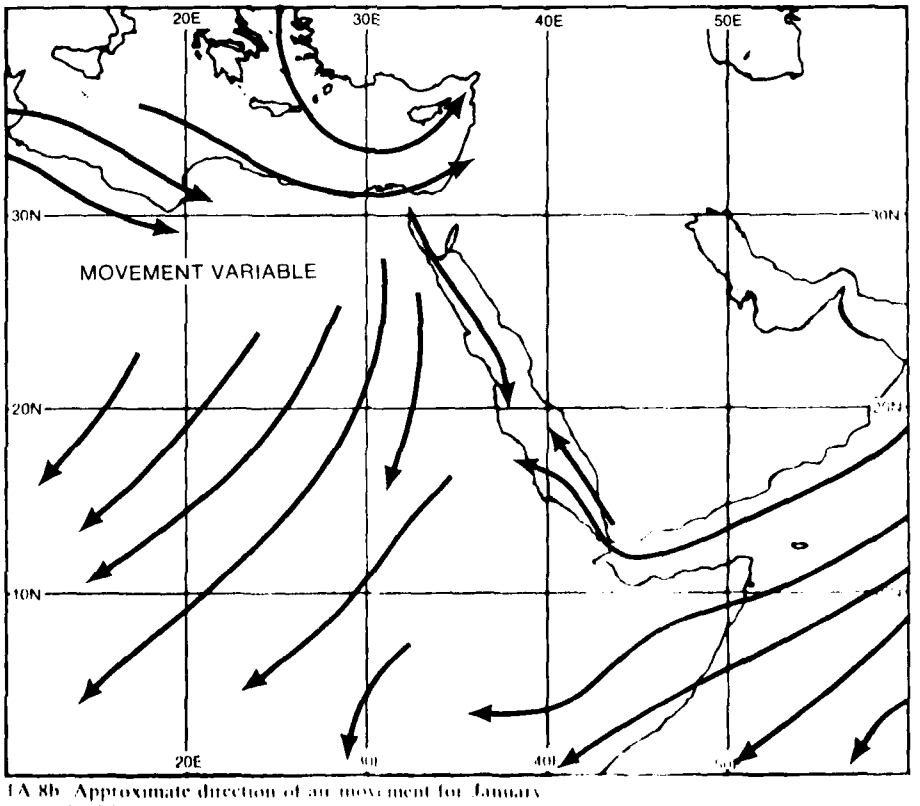

1A-8b. Approximate direction of air movement for January.
(After NEPRF, 1980.)

Red Sea/Persian Gulf

General Weather Patterns

Northeast Monsoon

IA-6a. GOES-Indian Ocean. Enlarged View. Visible Picture. 0630 GMT 26 October 1979.

surface

IA-6b. NMC Tropical Surface Streamline Analysis. 0000 GMT 26 October 1979.

Autumn Transition

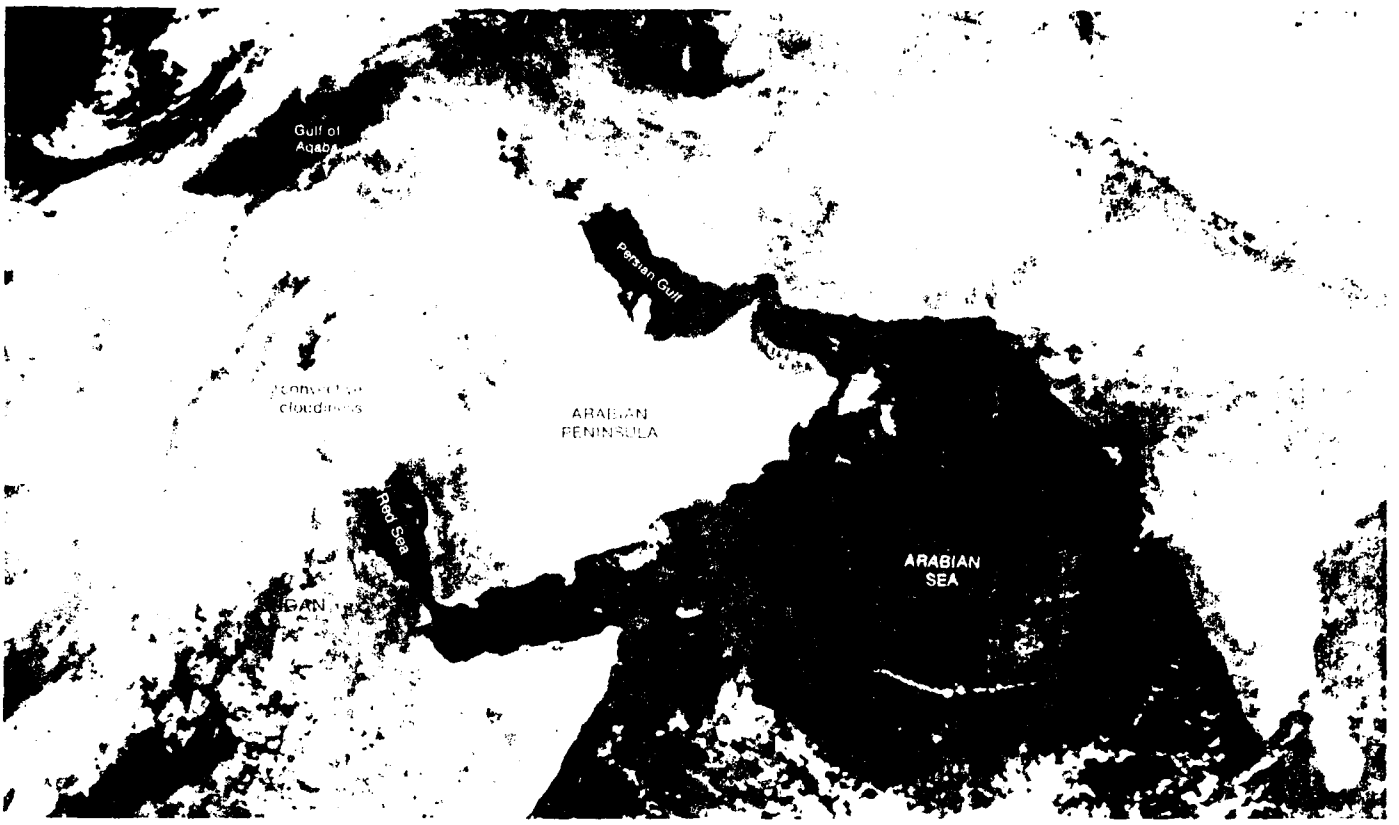

1A-5a. GOES-Indian Ocean. Enlarged View. Visible Picture. 0730 GMT 20 October 1979.

surface

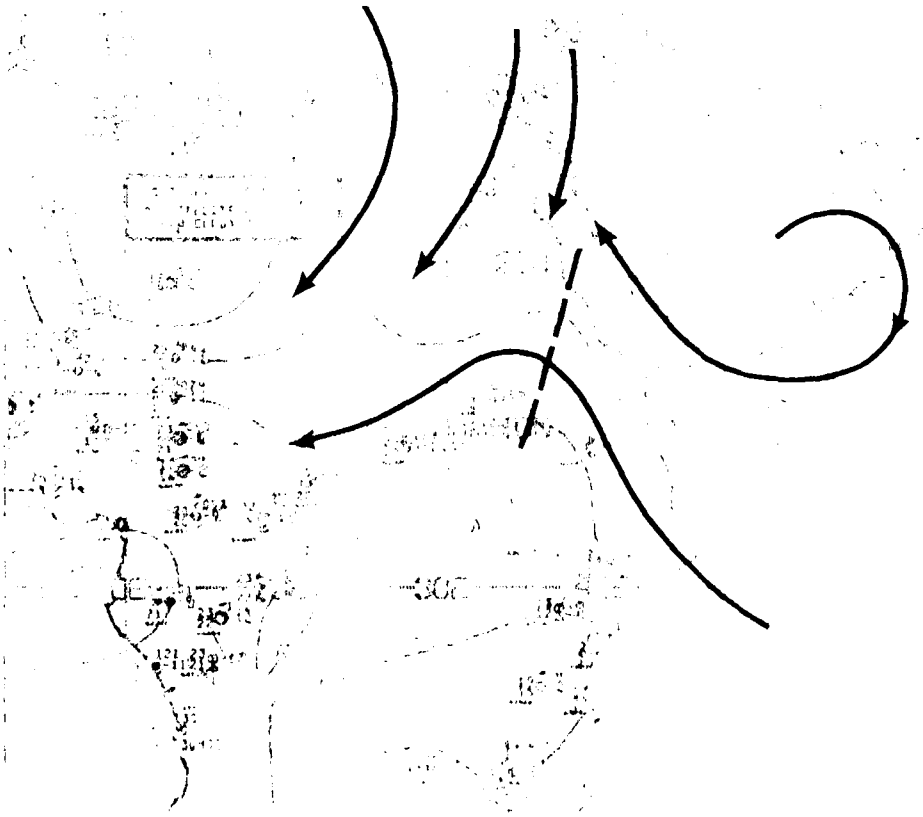

1A-5b. NMC Tropical Surface Streamline Analysis. 0600 GMT 20 October 1979.

850 mb

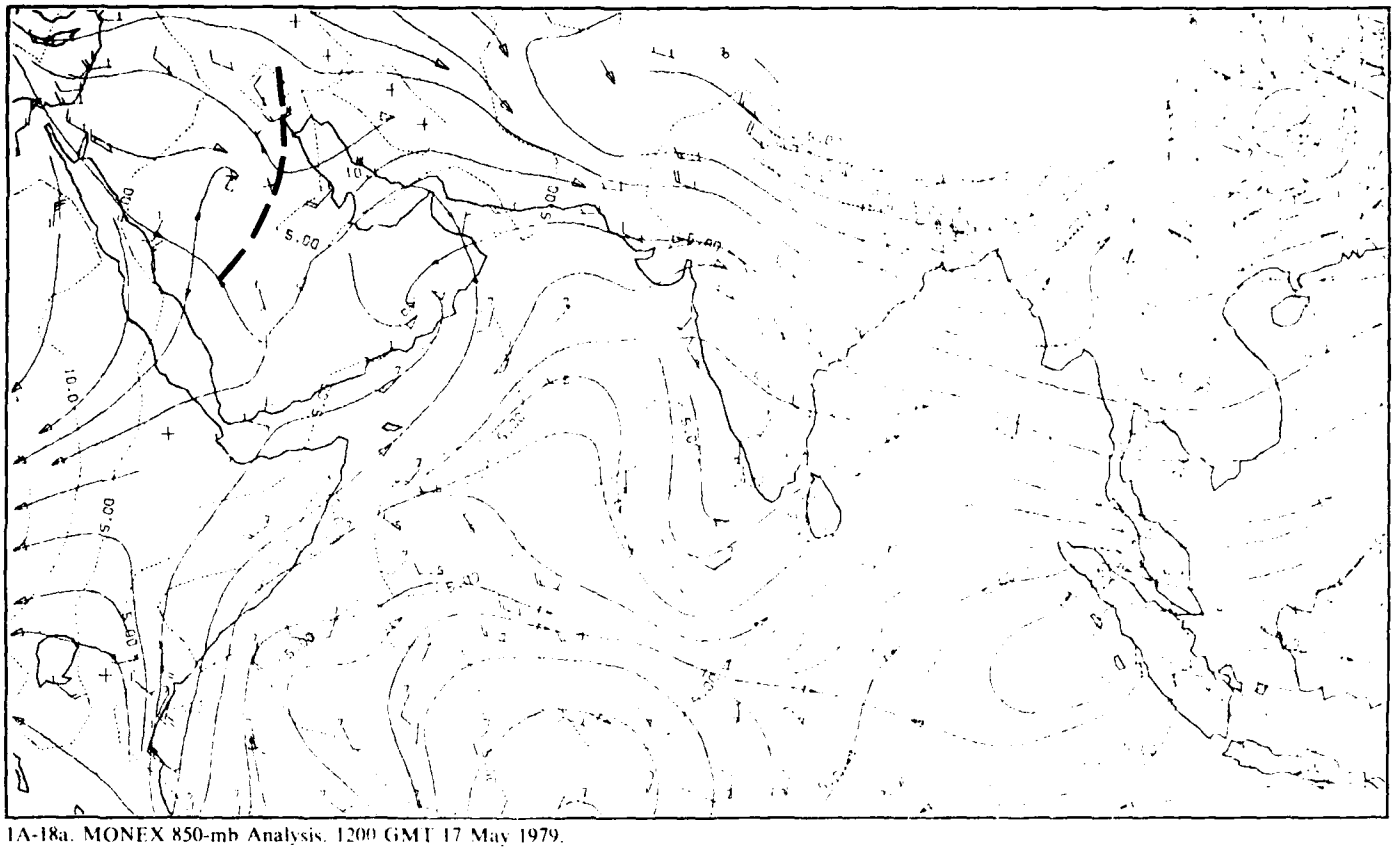

1A-18a. MONEX 850-mb Analysis. 1200 GMT 17 May 1979.

surface

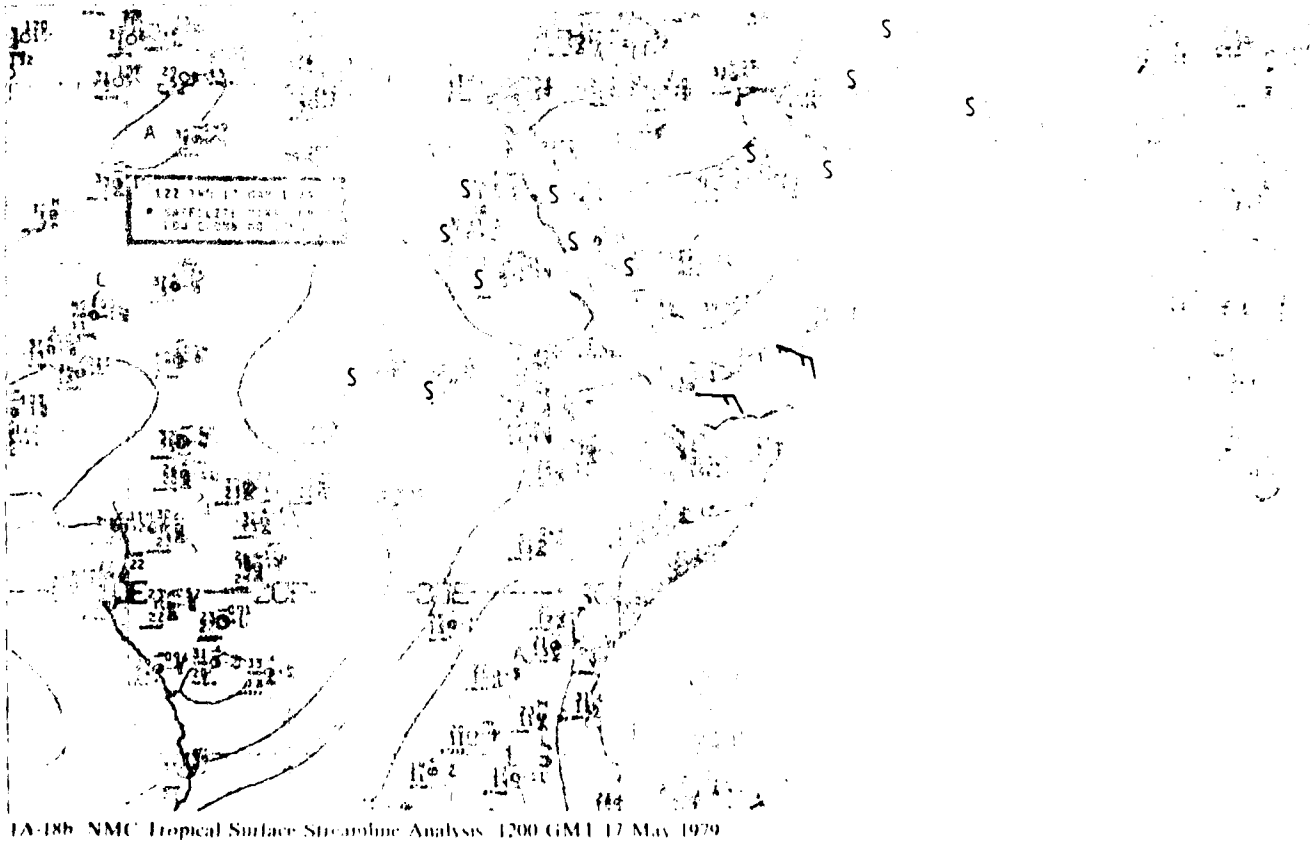

1A-18b. NMC Tropical Surface Streamline Analysis. 1200 GMT 17 May 1979.

Spring Transition: Late Phase (16 May–15 June)

During the late phase of the spring transition (16 May–15 June), southwest monsoon conditions become firmly established over Indo-China. However, the pattern over India remains less organized and still subject to effects of mid-latitude systems moving into the region. The Red Sea and Persian Gulf areas also are subject to incursions of the desert front moving southward through the region, pushed by strong northerly flow giving rise to duststorm episodes lasting for several days (see Sec. ID, Case 1).

The NMC surface streamline analysis for 17 May 1979 (1A-18b) depicts easterly flow in the Gulf of Aden implying southerly flow into the southern portion of the Red Sea. This type of flow is characteristic of the northeast monsoon and is a definite indicator that the southwest monsoon has not yet become established.

The low-pressure area over the Arabian Peninsula appears quite dry, judging from surrounding weather reports. Widespread observations of dust, however, are reported along a northeast southwest oriented band running through the low-pressure area, as defined by the cyclonic streamlines. This dust was raised by winds associated with the desert front which previously had moved into the area from the north, resulting in a modification of the thermal trough in the region.

The MONEX 850-mb flow field (1A-18a) shows a trough in the region of the desert front. Northerly winds over the Red Sea and Tigris Euphrates Valley align with the surface winds over those regions which enhances the tendency toward stronger low-level northerly flow.

On this day (17 May 1979), satellite imagery was not available over the region; however, the DMSP visible picture (1A-19a) of the Red Sea Persian Gulf region is shown for the previous day (16 May). Streamlines and surface observations superimposed on this image (1A-20a) reveal the desert front location which extends from the Persian Gulf, near Bahrain, to the southern portion of the Red Sea. Note especially the strong northerly winds in the Red Sea, the dust reports over Arabia, and the indication of dust over the northern Persian Gulf. (See Sec. ID, Case 1 for a discussion of the early development and movement of this desert frontal feature.)

The upper-tropospheric wind conditions, as shown at 250 mb (1A-21a), reveal a jet streak over the northern portion of the Red Sea Persian Gulf region. The mid-tropospheric wind conditions, as shown at 500 mb (1A-21b), are moderately strong from the west over the Red Sea Persian Gulf region while an anticyclone lies to the south in its typical position over southern Saudi Arabia. These winds turn in a typical manner, anticyclonically, producing strong northerly winds over the Persian Gulf.

The NMC surface streamline analysis over the Red Sea Persian Gulf region for 9 June 1979 (1A-22b) shows little change near the end of the pre-monsoon period. However, wind speeds to the south, near the coast of Somalia, have essentially doubled in strength indicating the near-term commencement of the southwest monsoon. The MONEX 850-mb flow field for 9 June (1A-22a), when compared to the 17 May, 850-mb flow field (1A-18a) emphasizes the surface depiction of a better organized southwest monsoon-type flow pattern.

Troughing at the 850- and 500-mb levels (1A-22a and 23b) over India appears to be the result of the penetration of a migratory mid-latitude trough into the region, and is responsible for enhanced cloudiness and convective activity over India, which cannot at this stage be attributed to a monsoonal influence. Modification of the thermal troughs over Pakistan and northern India by mid-latitude migratory systems is a characteristic feature of the pre-monsoon period. Such modification was also earlier noted over Saudi Arabia as the desert front moved southward across the Peninsula.

At upper levels, as shown on the NMC 250-mb analysis (1A-23a), easterlies now extend across the entire northern Indian Ocean except for a small region over the Red Sea and Persian Gulf north of 20° N. Such easterly flow is an essential ingredient of the southwest monsoon which was lacking in the early position of the pre-monsoon period.

The GOES-Indian Ocean visible picture (1A-24a) reveals the distinctive clear conditions over Saudi Arabia, Iran, Pakistan, and northern India, as is normal in the region of the thermal troughs.

Finally the MONEX 850-, 700-, and 200-mb mean flow fields for the period 16–31 May depict the fully-developed southwest monsoon. The 850-mb flow field (1A-24b) shows the anticyclone over central Saudi Arabia, with westerly flow to the north. At 700 mb (1A-25b), the southwesterly flow over the northern Arabian Sea continues to be over-run by northeasterly winds from a dominant high pressure cell in southern Saudi Arabia. The 200-mb analysis (1A-25a) continues to show two anticyclonic cells separated by a trough extending into the northern Arabian Sea. A jet streak is located over the northern Red Sea and Persian Gulf.

Spring Transition—Late Phase

FA 20a. [illegible] DMSP F8 Low Resolution Visible Imagery 0806 GMT 16 May 1979 (Note the position of the [illegible] of FA Puerto Rico) Surface Wind Reports and [illegible] Ocean Analysis 0000 GMT 16 May 1979

250 mb

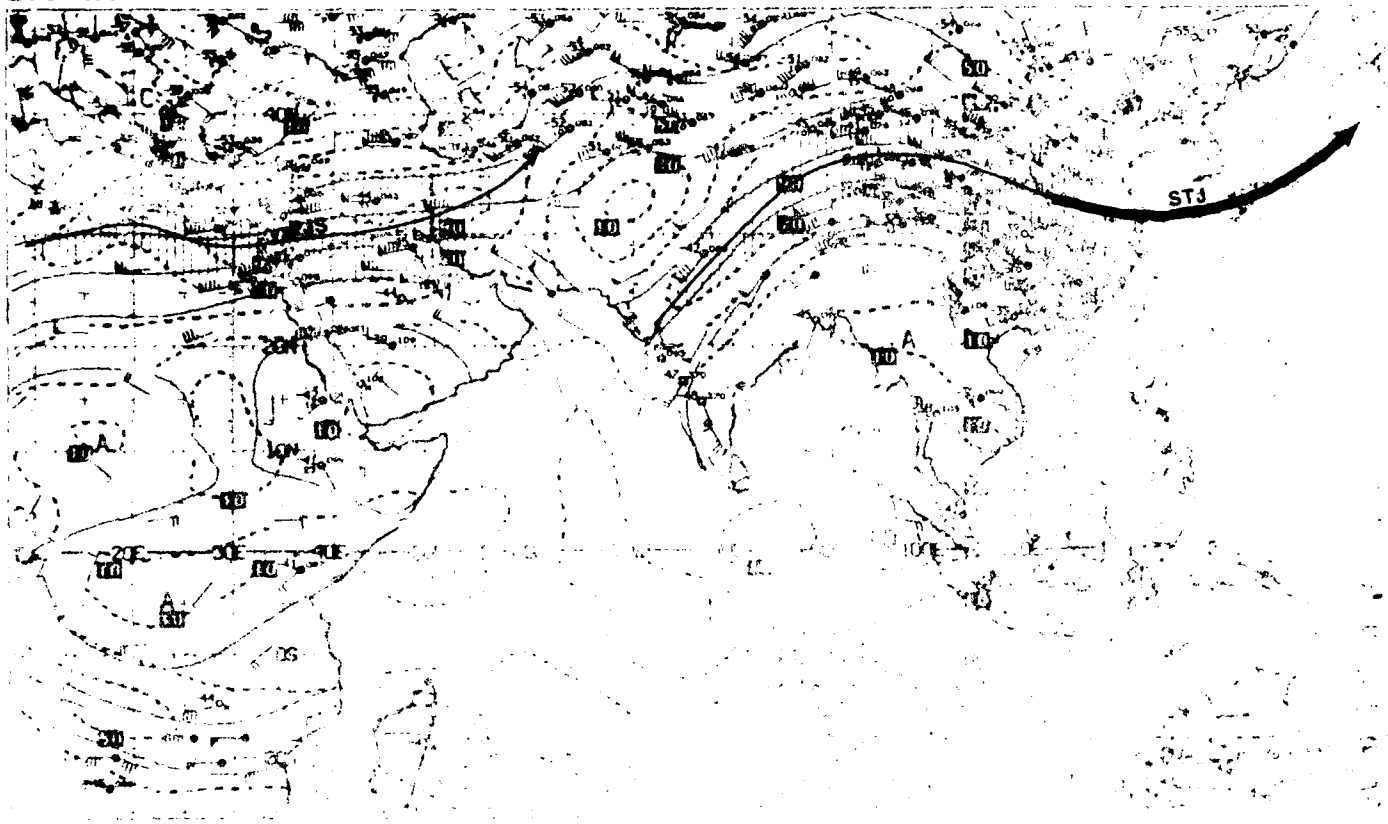

1A-21a. NMC Tropical 250-mb Streamline Analysis, 1200 GMT 17 May 1979.

500 mb

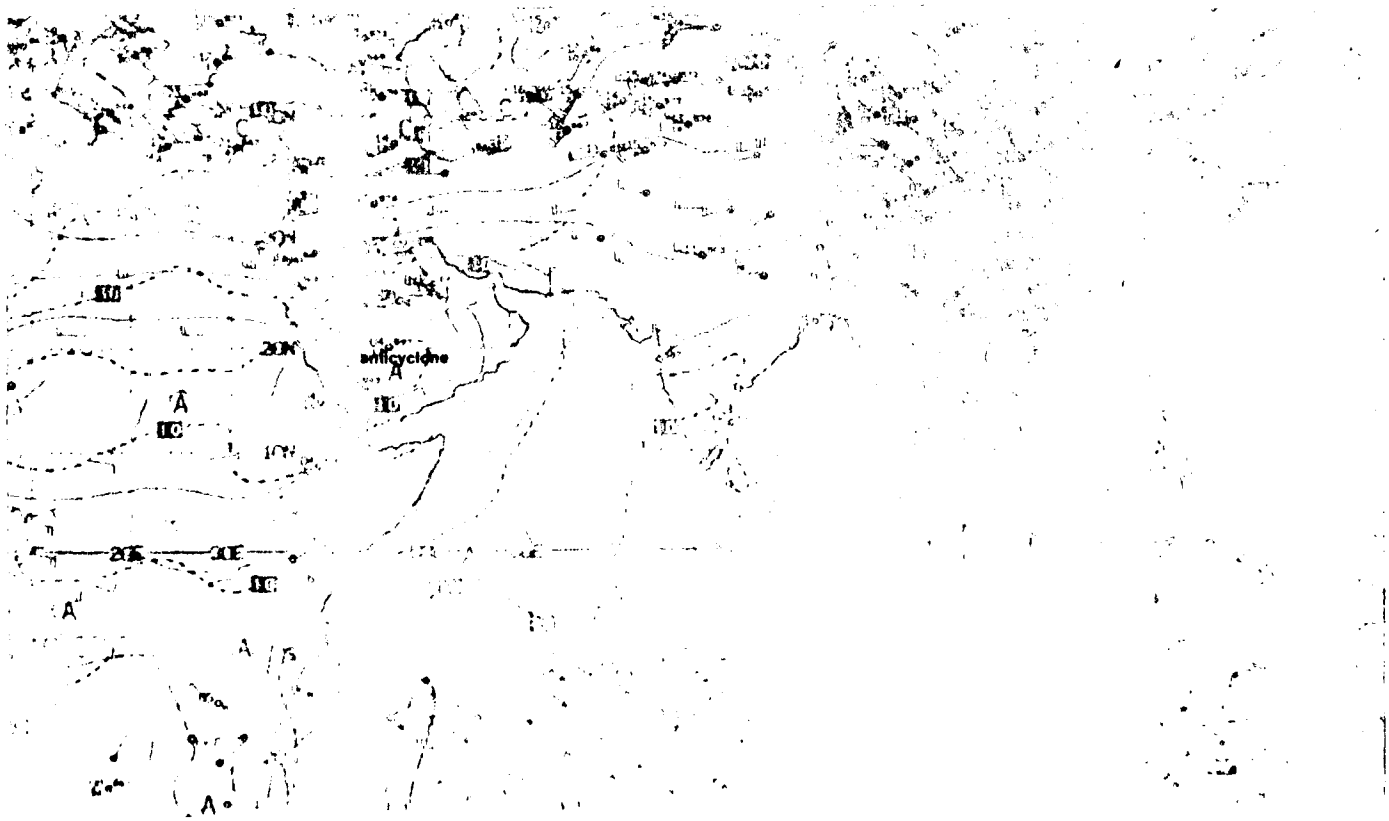

1A-21b. NMC Tropical 500-mb Streamline Analysis, 1200 GMT 17 May 1979.

850 mb

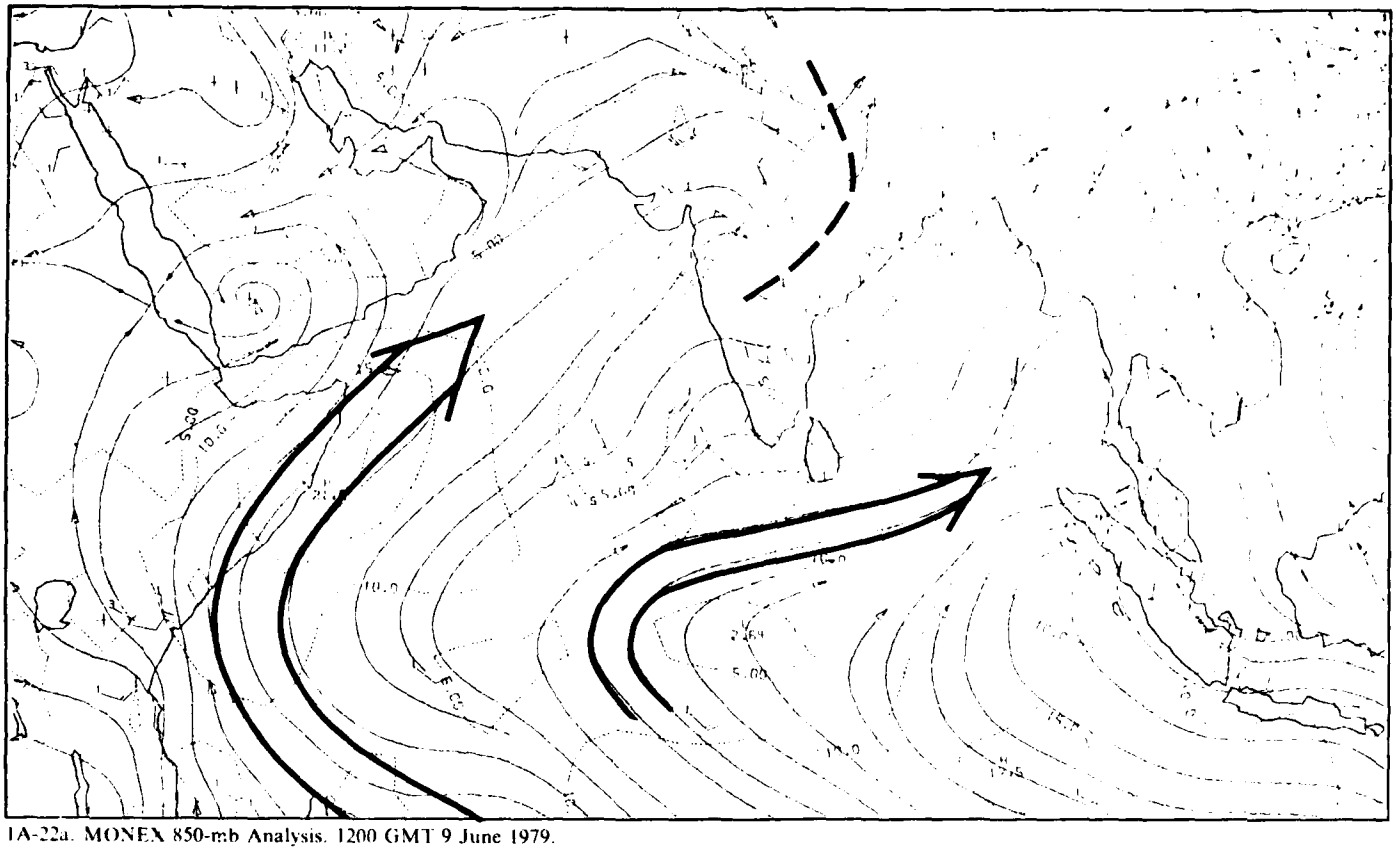

1A-22a. MONEX 850-mb Analysis, 1200 GMT 9 June 1979.

surface

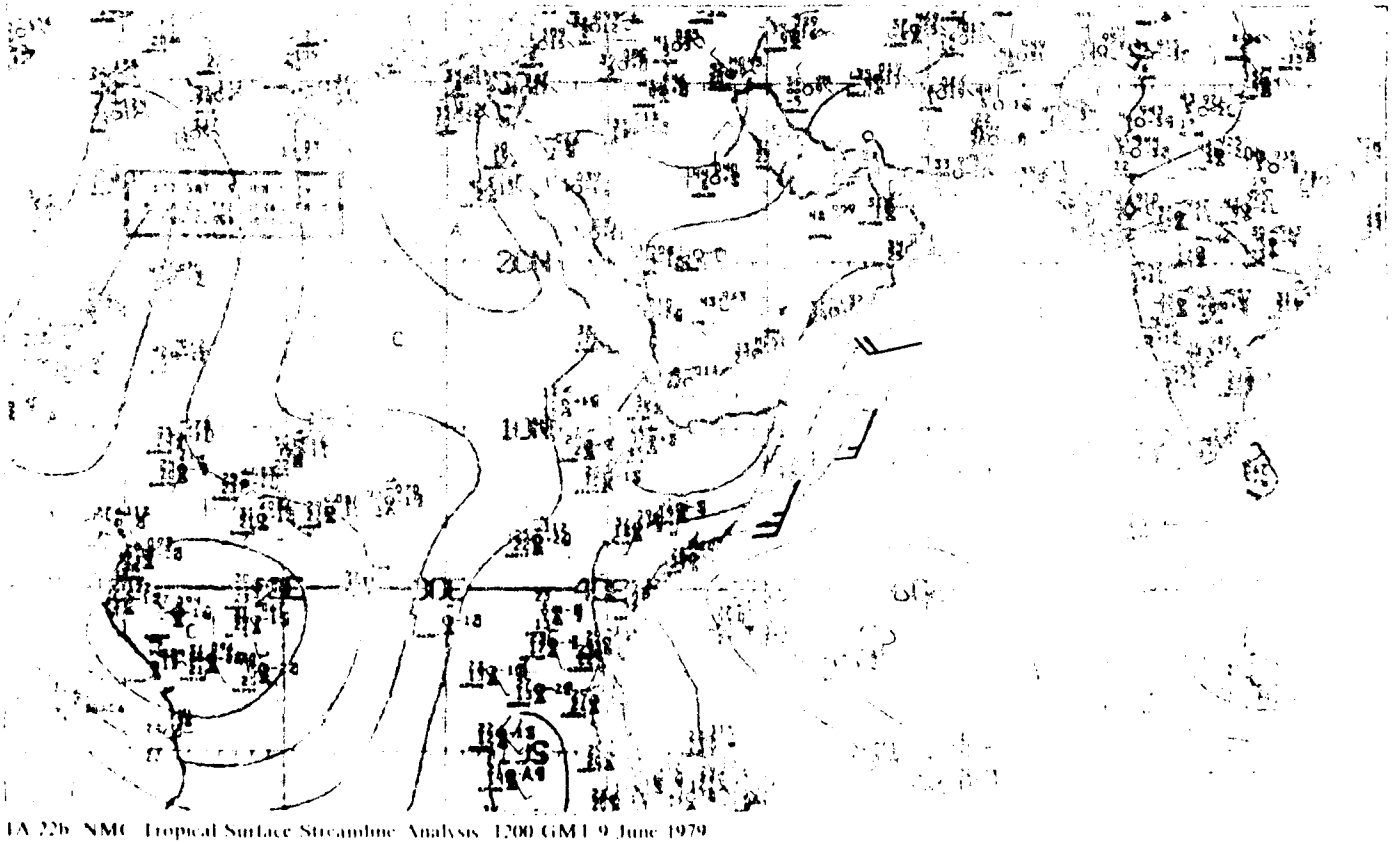

1A-22b. NMC Tropical Surface Streamline Analysis, 1200 GMT 9 June 1979.

250 mb

Spring Transition—Late Phase

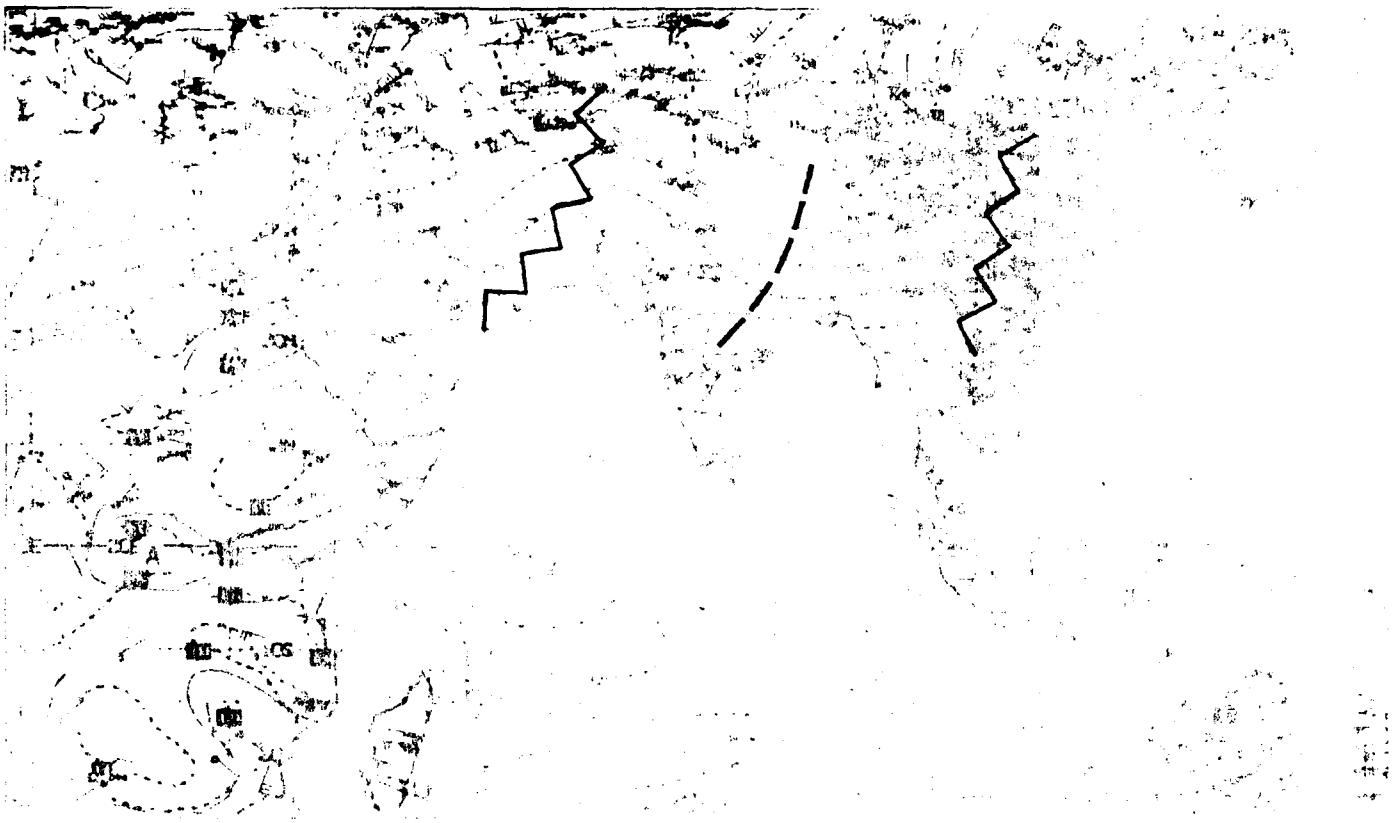

TA-23a. NMC Tropical 250-mb Streamline Analysis, 1200 GMT 9 June 1979.

500 mb

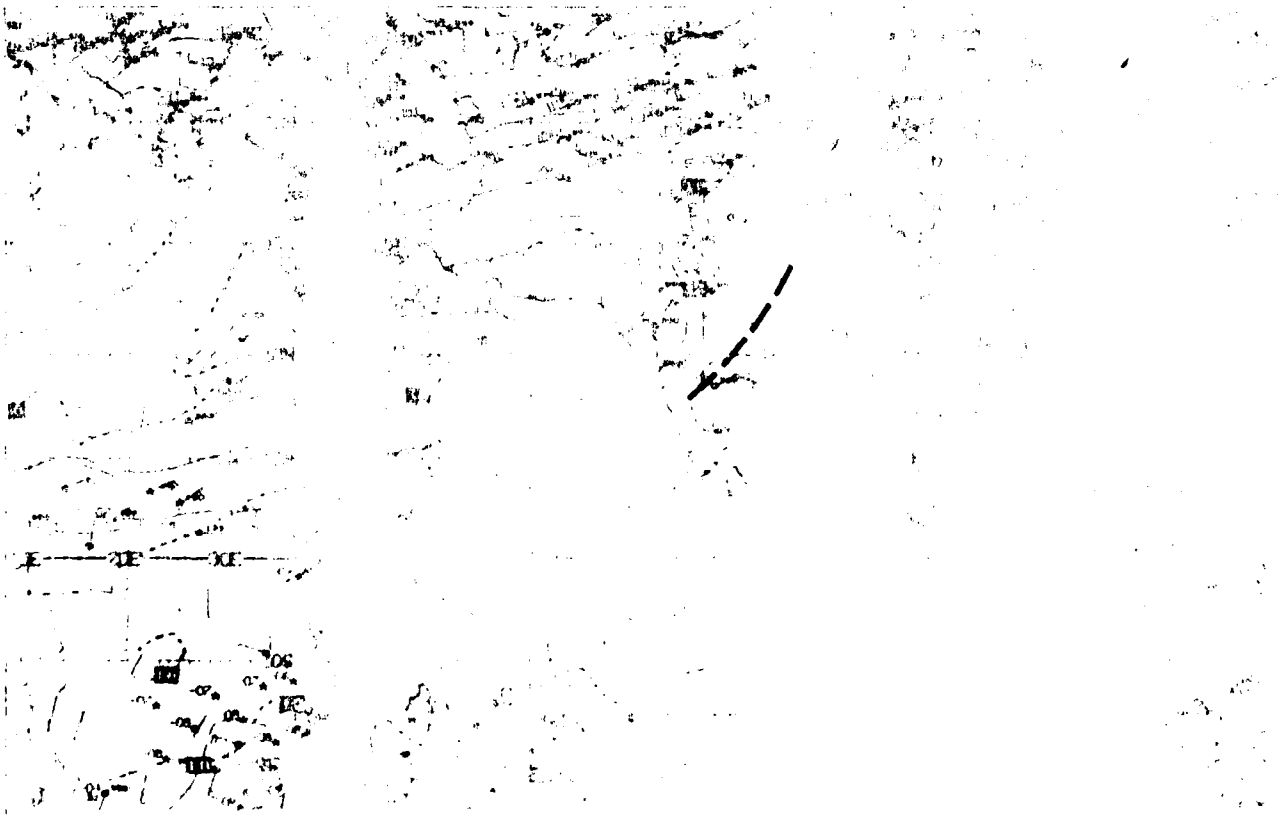

TA-23b. NMC Tropical 500-mb Streamline Analysis, 1200 GMT 9 June 1979.

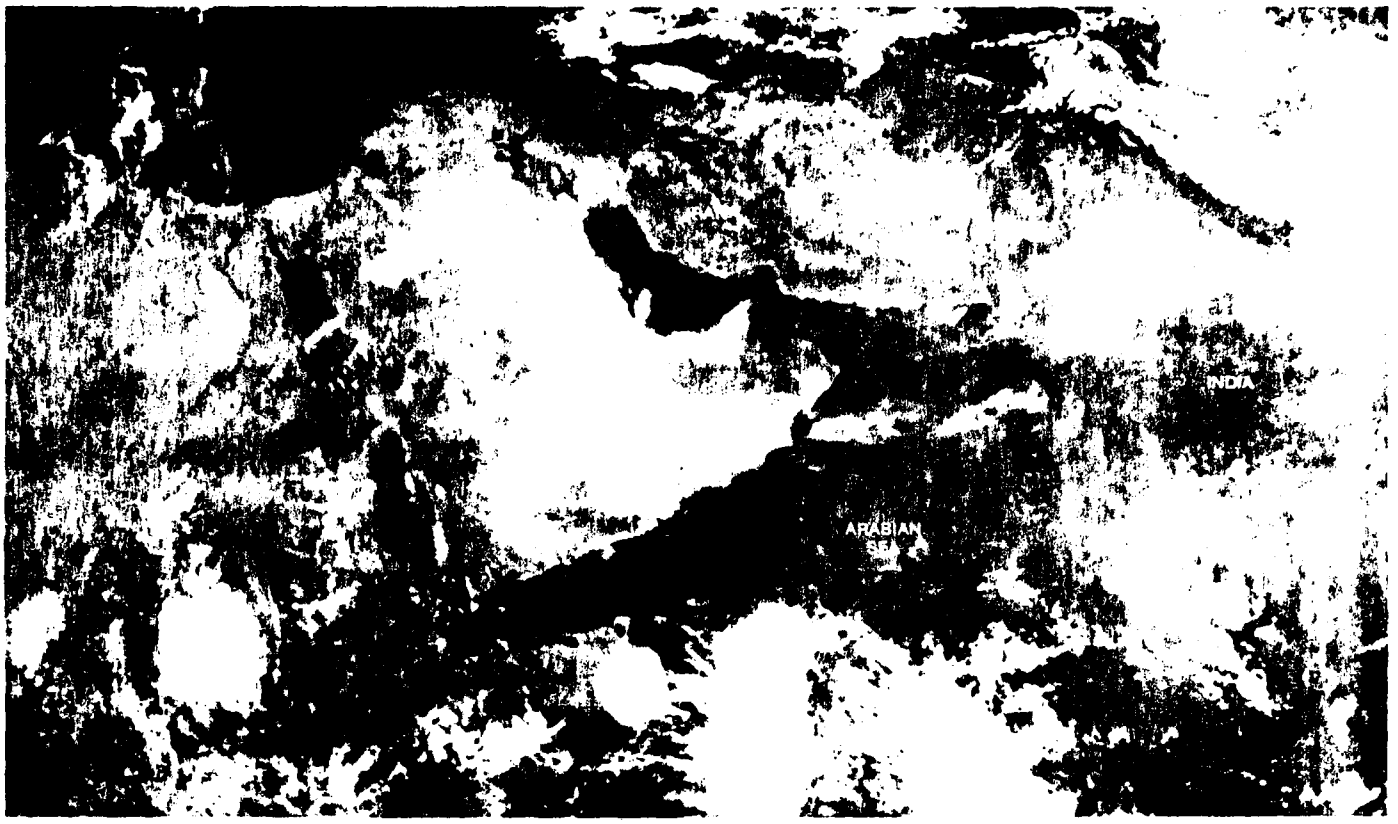

IA-24a. GOES-Indian Ocean. Enlarged View. Visible Picture. 0500 GMT 9 June 1979.

850 mb

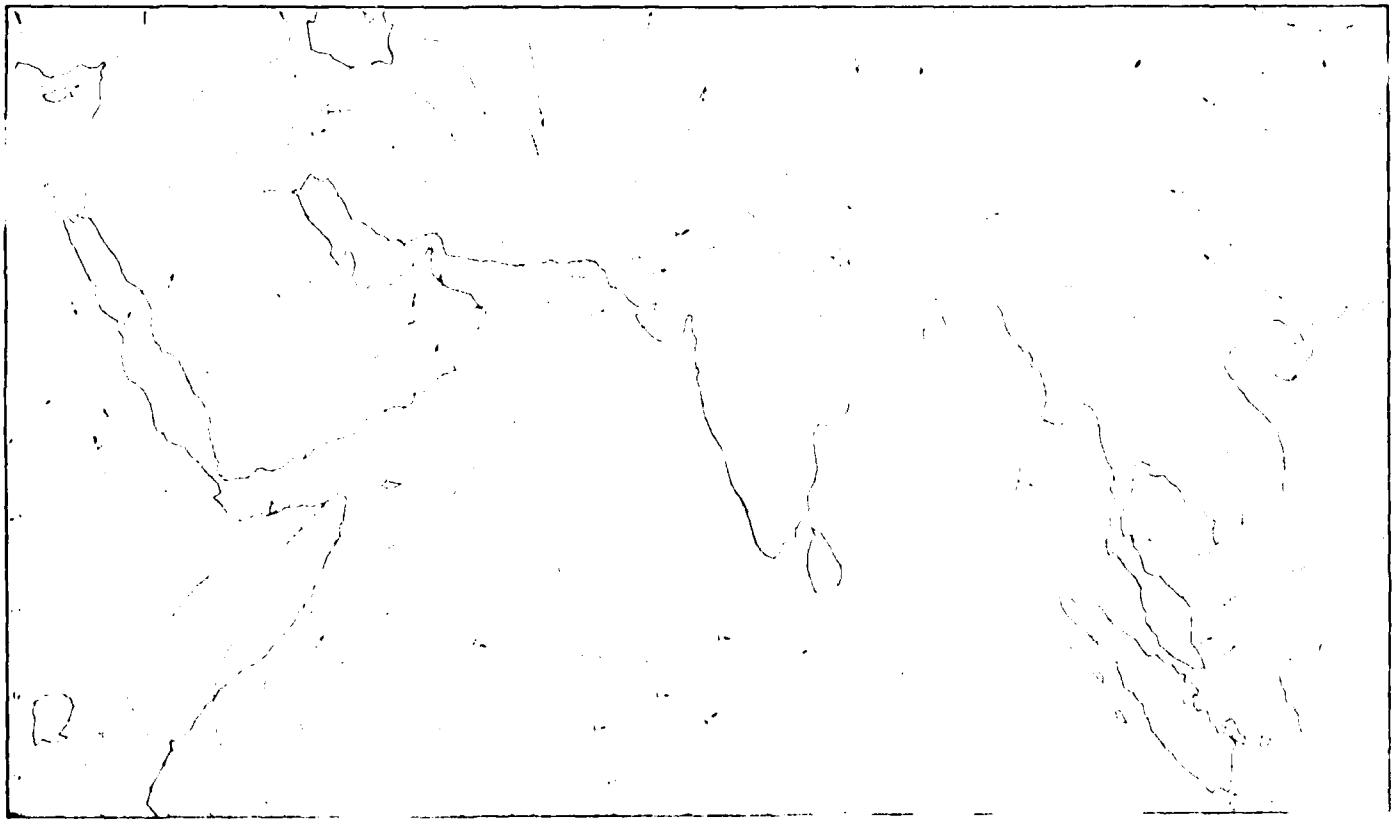

IA-24b. MONEX Mean 850 mb Analysis. 16-31 May 1979.

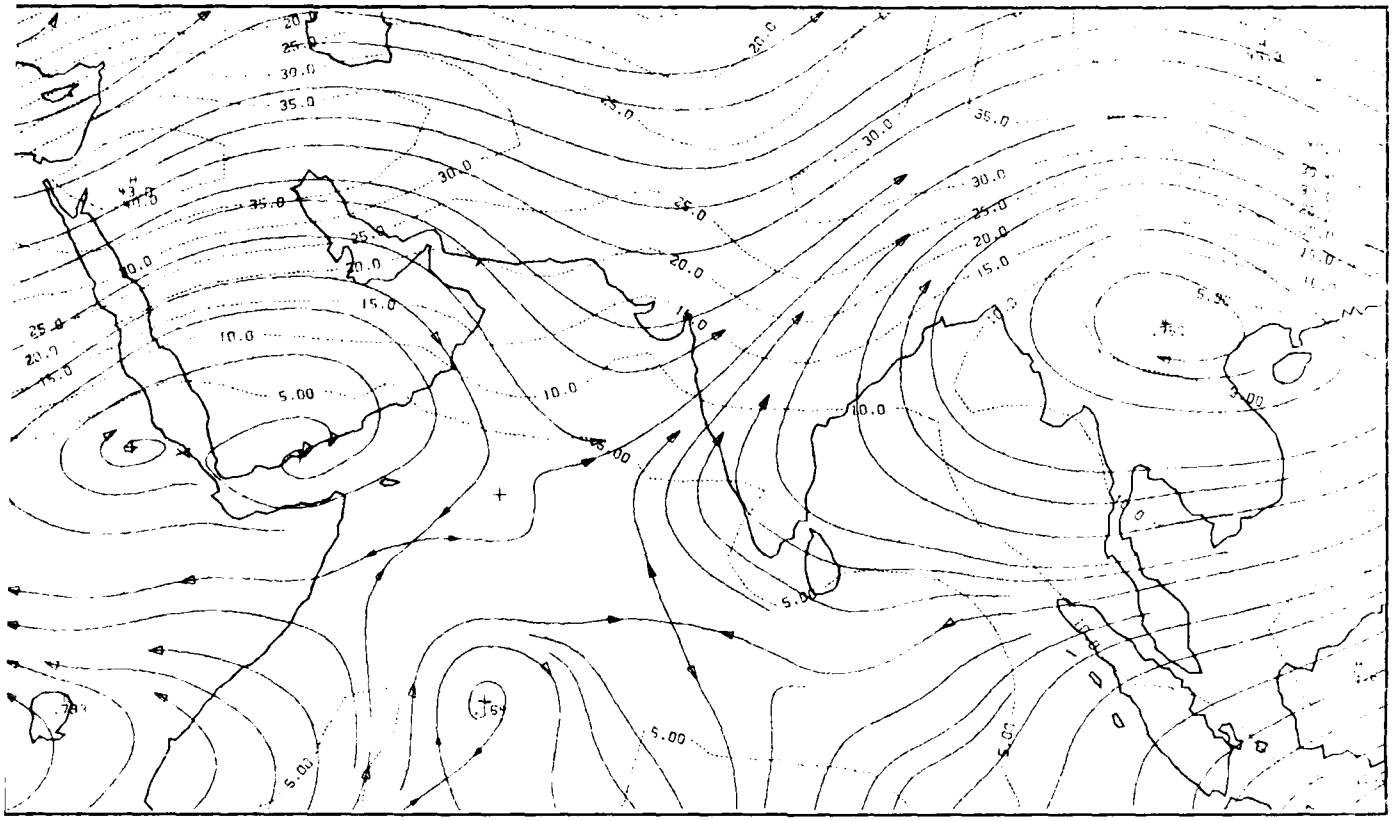

1A-25a. MONEX Mean 200-mb Analysis. 16-31 May 1979.

700 mb

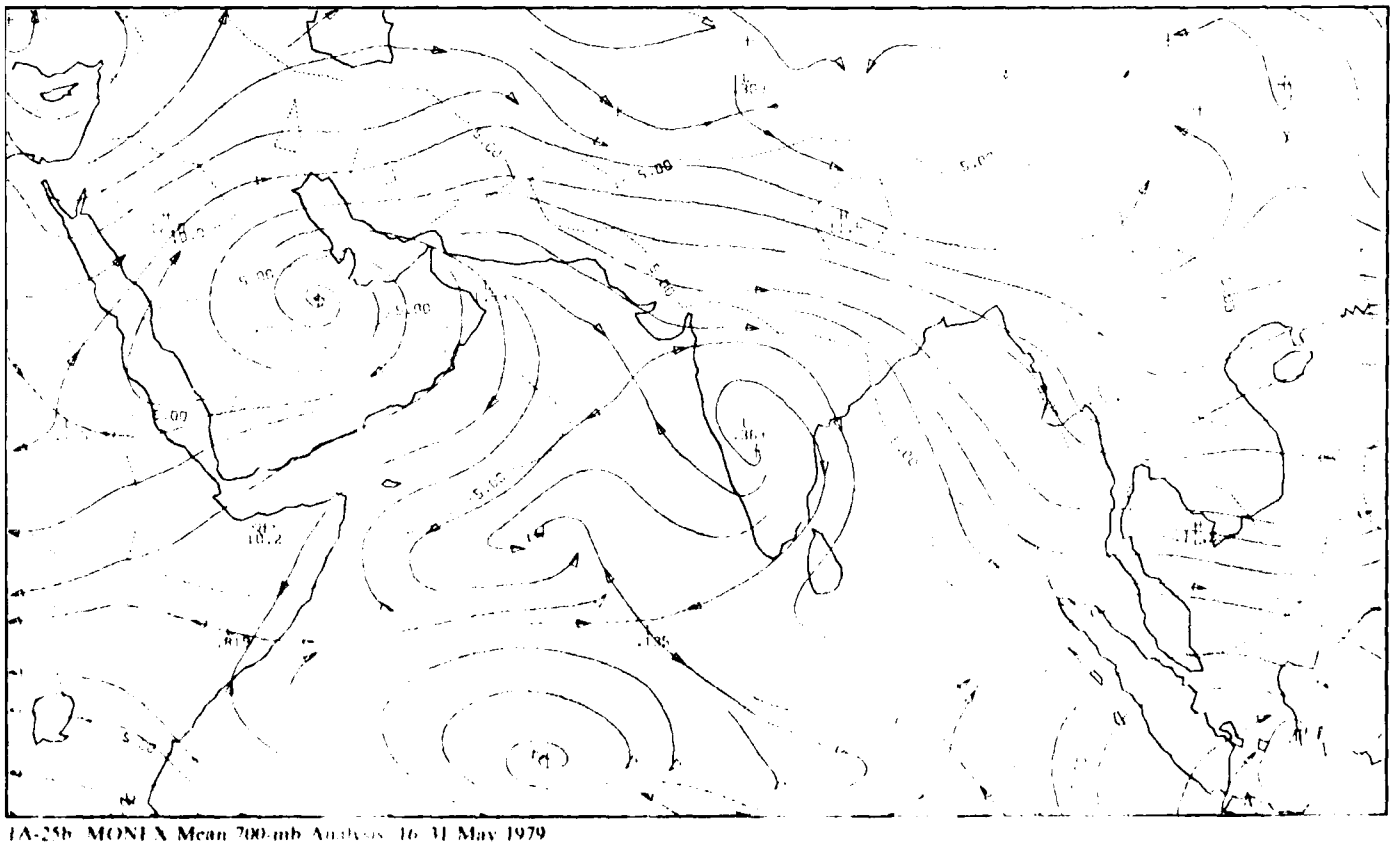

1A-25b. MONEX Mean 700-mb Analysis. 16-31 May 1979

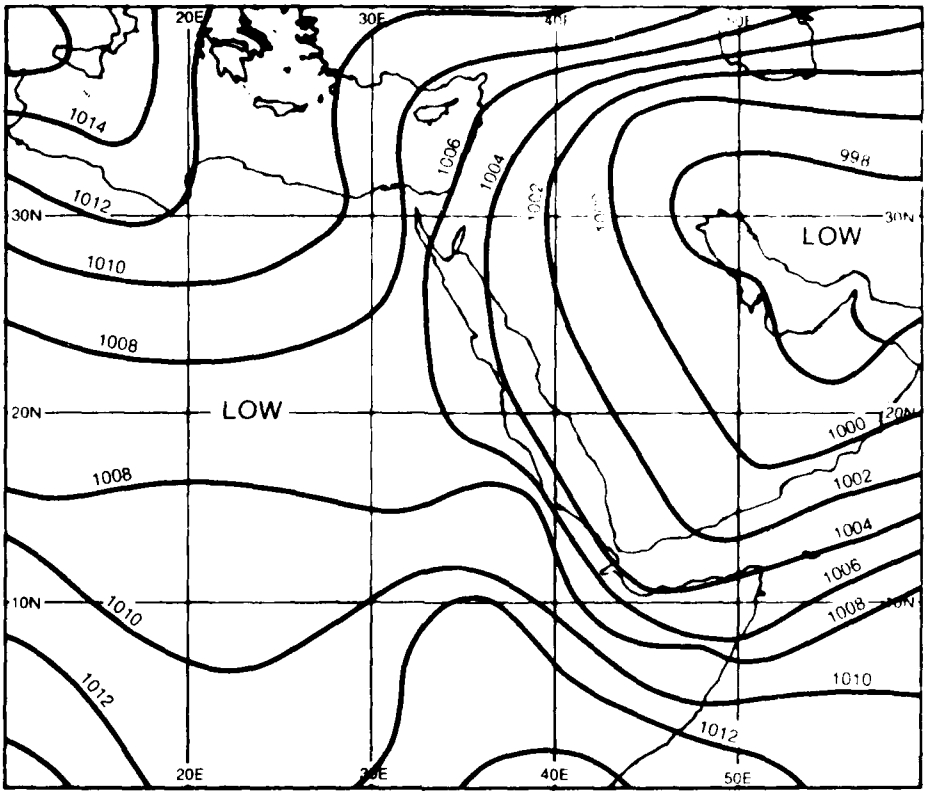

1A-26a. Approximate pressure (mb) at mean sea level for July.
(After NEPRF, 1980.)

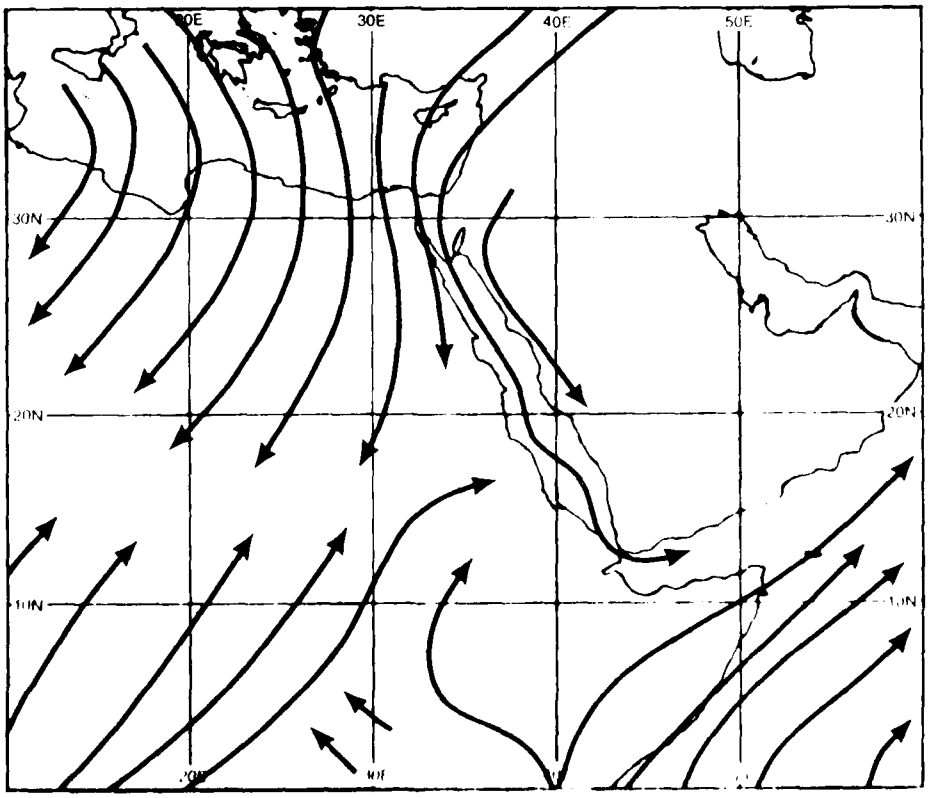

1A-26b. Approximate direction of air movement for July.
(After NEPRF, 1980.)

Southwest Monsoon (June–September)

The Red Sea Persian Gulf region does not participate in weather effects caused by the strong southwesterly flow across the Arabian Sea but rather is affected by weather conditions associated with the heat lows which cause the southwest monsoon. These lows and associated troughs develop over India, Pakistan, Afghanistan, Iran, and Saudi Arabia with extensions into the Sudan region of Africa.

Summer is a very hot and humid time over the region, especially in the south, while precipitation is negligible. In the shallow waters of the Persian Gulf, sea surface temperatures reach 96° F (35.6° C). Nighttime cooling effects as a result are slight over the water, and life aboard ship, without air conditioning, is somewhat difficult.

The typical surface pressure and direction of air movement in July (1A-26a and 26b) show northerly winds extending down the entire Red Sea (NEPRF, 1980). This is also the dominant direction in the Persian Gulf region except for the Gulf of Oman which is subject to a greater frequency of winds from the southeast.

Note that southwesterly flow across Africa extends through the Sudan towards the southern portion of the Red Sea. This frequently becomes strong enough to generate sand and duststorms which are then advected into the southern portion of the Red Sea (chiefly through the Tokar Gap; see Sec. 1E, Case 4). Dust raised by the cold down-rushing air of thunderstorms (haboobs) in the Khartoum region of Sudan is often caught in this current and carried out over the Red Sea near Tokar. The northern portion of the Red Sea is not subject to this effect and visibilities in that region are correspondingly much better.

The Persian Gulf is also subject to duststorms regularly raised during the summer months by strong northerly winds coming around the west side of low pressure over Iran Afghanistan. The northerly flow over the Persian Gulf, enhanced by a lee trough, and high pressure to the northeast, plus the topographical features of the area tend to enhance the northerly flow below 5,000 ft. This results in what is known as the 40-day shamal, or great shamal, most commonly occurring from 6 June to 16 July (see Sec. 1E, Case 5). Winds of up to 35 kt may blow for up to a week at a time during this period, though more commonly in 3 day intervals. The winds decrease during nighttime hours over land due to radiational cooling but remain quite strong aloft at low levels.

A common phenomenon is the development of a low-level nocturnal jet stream with a core near 1,2000 ft. This jet develops only under strong nocturnal low-level inversion conditions and can pose a hazard to aircraft on take-off or landing due to extreme wind shear attending the phenomenon.

Dust and sandstorm conditions brought on by the shamal characteristically reduce visibility to less than 3 n mi over the northern portion of the Persian Gulf and to less than ½ n mi in the source regions, such as near Basra, Iraq.

The heat lows disappear very rapidly with height and give way to high pressure routinely found aloft at 850 mb. This condition favors generally clear skies with little precipitation.

The GOES-Indian Ocean visible picture of the region on 15 June 1979 (1A-27a) shows the Nile River obscured in the northern Sudan. This indicates the presence of dust in the atmosphere a condition which is clearly revealed as a gray shade covering the southern half of the Red Sea in the GOES image. Other than a few clouds in the dust region and in southern Saudi Arabia, the rest of the land area affected by the heat lows is remarkably and typically clear.

The NMC surface streamline analysis (1A-27b) verifies features of flow similar to that of the mean conditions (1A-26b). Northerly flow extends down the entire length of the Red Sea turning to westerly in the Gulf of Aden. Southwesterly flow from Sudan converges with this flow near Tokar. Dust in suspension is reported at several stations in the Sudan with at least two locations reporting obscured skies. Note that winds are quite light in this morning analysis (0900 LST). The winds would be expected to increase as daytime heating is maximized in the early afternoon. Northerly flow is also in evidence over the Persian Gulf, responding to low pressure over Iran.

Reference

NEPRF, 1980: Weather in the Indian Ocean to Latitude 30° S and Longitude 95° E including the Red Sea and Persian Gulf. Vol. 2, Part 1. NAVENVPREDRSCHFAC Technical Bulletin 80-02, Naval Environmental Prediction Research Facility, Monterey, Calif., 83 pp

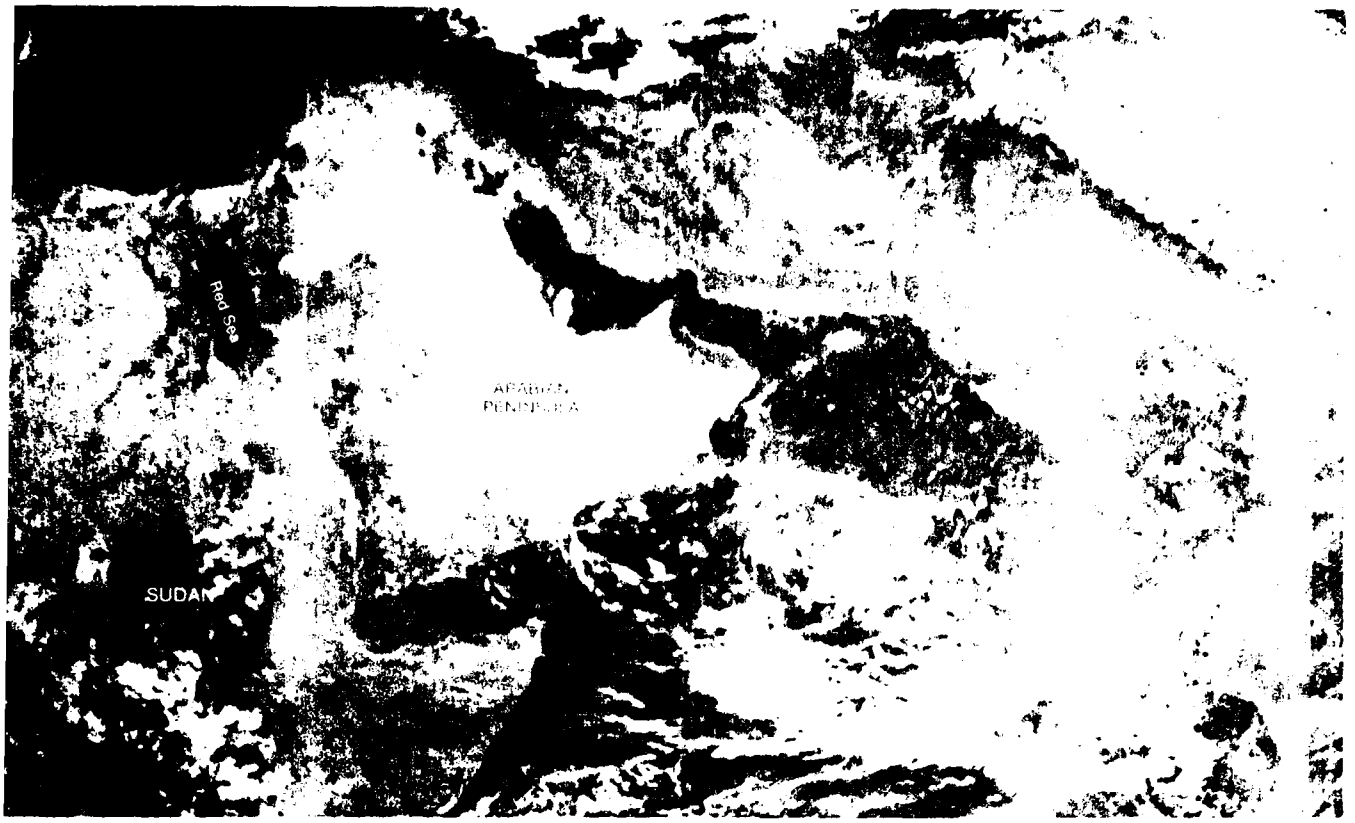

7a. GOES-Indian Ocean Enlarged View, Visible Picture, 0400 GMT 15 June 1979

rface

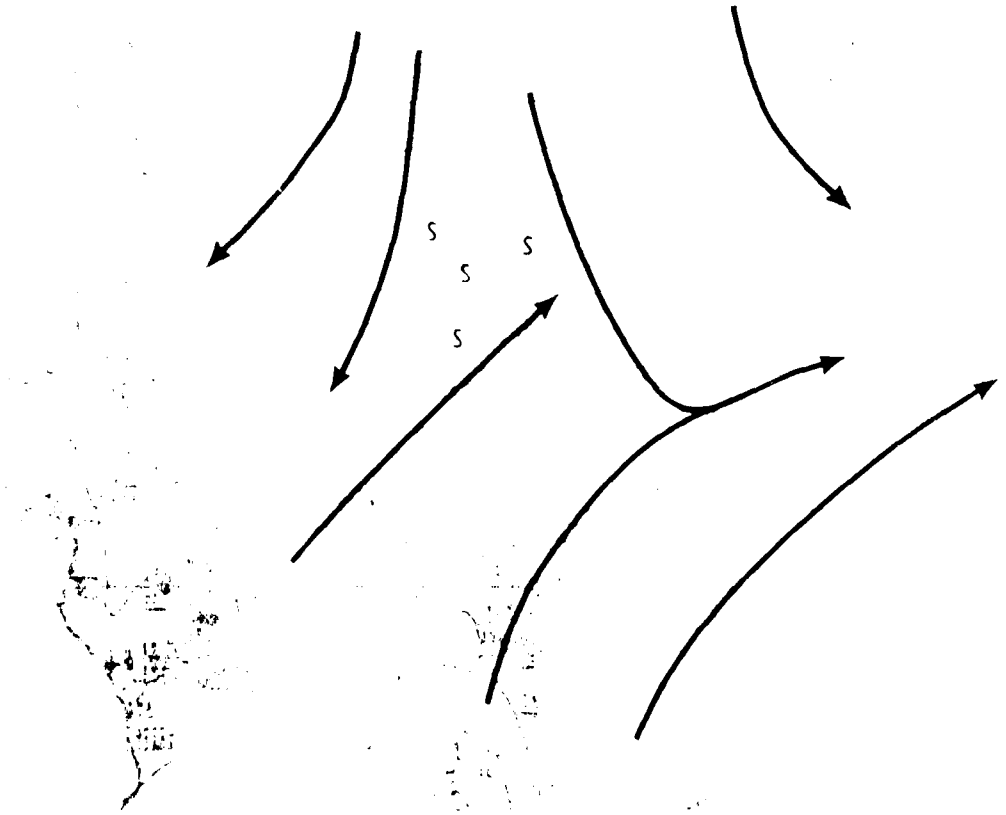

7b. NMC Tropical Surface Streamline Analysis, 0600 GMT 15 June 1979

Case 1 Red Sea/Persian Gulf— Autumn Transition

Convective Storms During the Autumn Transition

In general, the weather over the Red Sea and northern Arabian Peninsula has been characterized as very uniform with a minimum of low-level cloudiness, generally good visibility, light winds, and negligible rainfall (NEPRF, 1980).

This scenario, however, can be drastically altered during the fall transition to the northeast monsoon, whenever an upper-air, trough-ridge pattern, develops over east Africa and Saudi Arabia, respectively. Under this motion field, the Red Sea/western Saudi Arabian region is located under a cyclonic flow pattern favorable for deep convective developments. In particular, the southerly winds around the western border of the high pressure over Saudi Arabia and the southwesterly winds along the eastern edge of the low pressure over east Africa combine to channel southerly low-level flow from east Africa, across the Red Sea, and into the Arabian Peninsula. This southerly flow provides ample moisture for thunderstorm development, creating the potential for generally disturbed weather conditions.

Reference

NEPRF, 1980: Weather in the Indian Ocean to Latitude 30° S and Longitude 98° E including the Red Sea and Persian Gulf, Vol. 2, Part I, NAVENVPREDRSCHFAC Technical Bulletin 80-02, Naval Environmental Prediction Research Facility, Monterey, Calif., 83 pp.

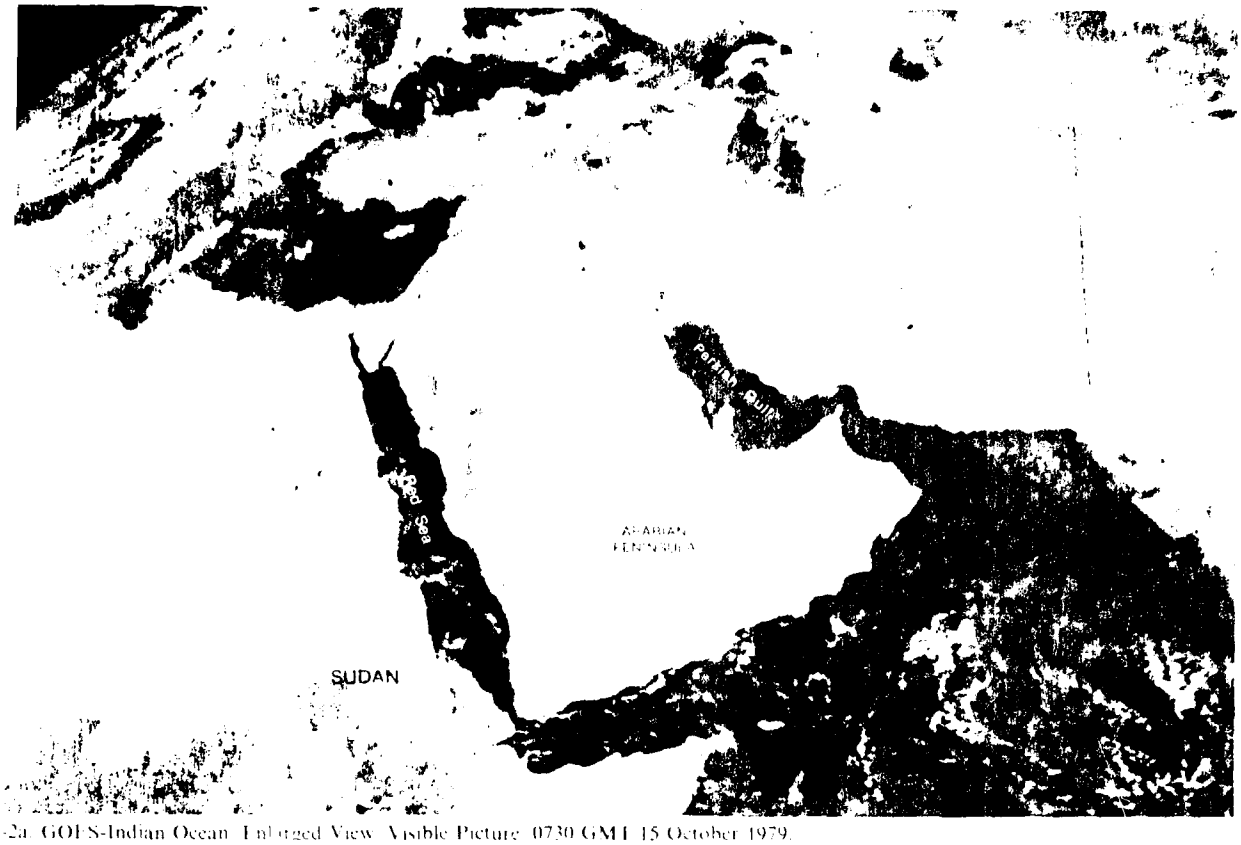

-2a. GOES-Indian Ocean Enlarged View Visible Picture 0730 GMT 15 October 1979.

ce

anticyclone

anticyclone

SUDAN
LOW

MC Tropical Surface Streamline Analysis 0600 GMT 15 October 1979

250 mb

Thunderstorm Outbreaks Associated with an Upper-level Divergence Pattern

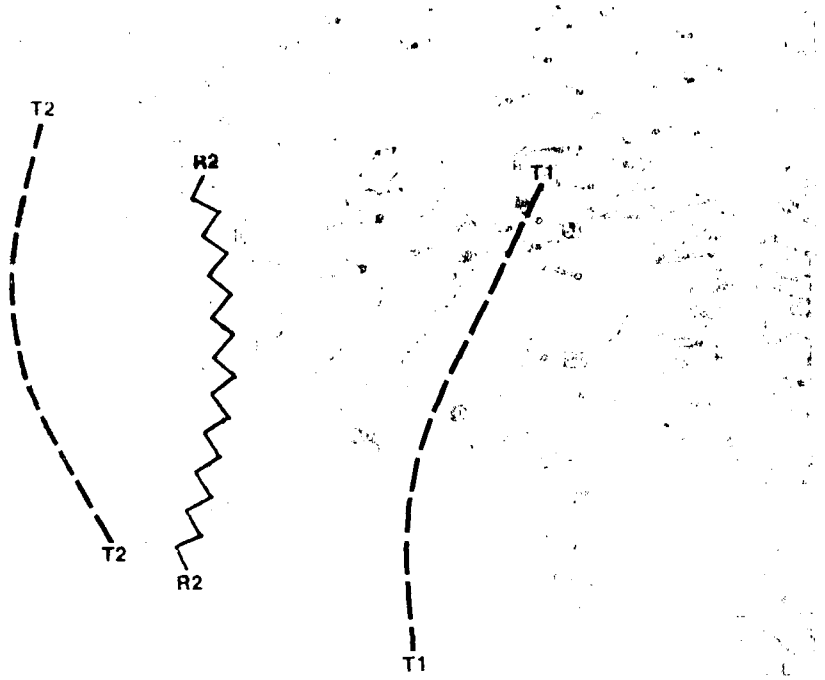

1B-11a NMC Tropical 250-mb Streamline Analysis, 1200 GMT 21 October 1979.

700 mb

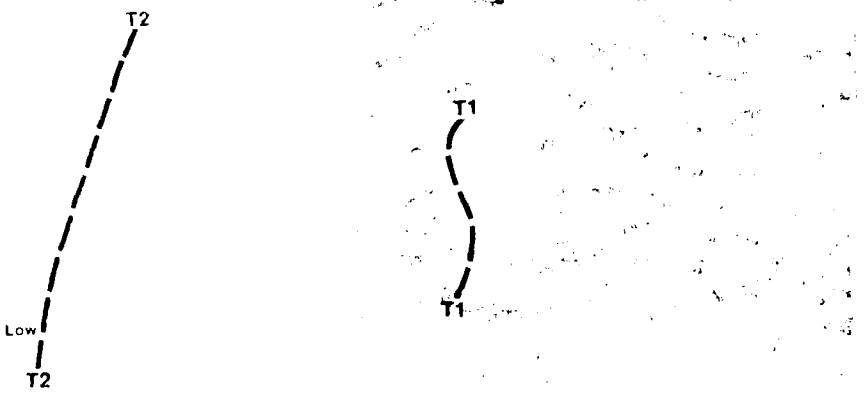

1B-11b NMC Tropical 700-mb Streamline Analysis, 1200 GMT 21 October 1979.

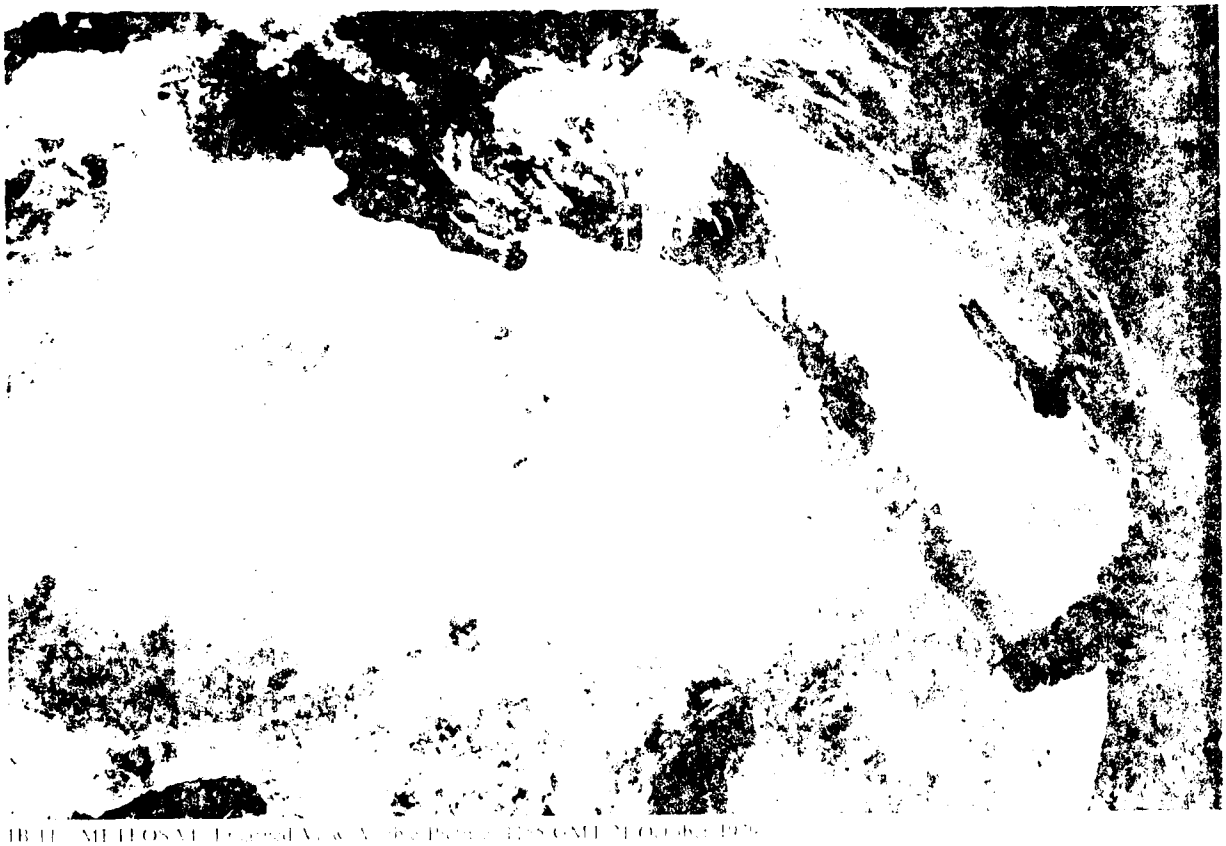

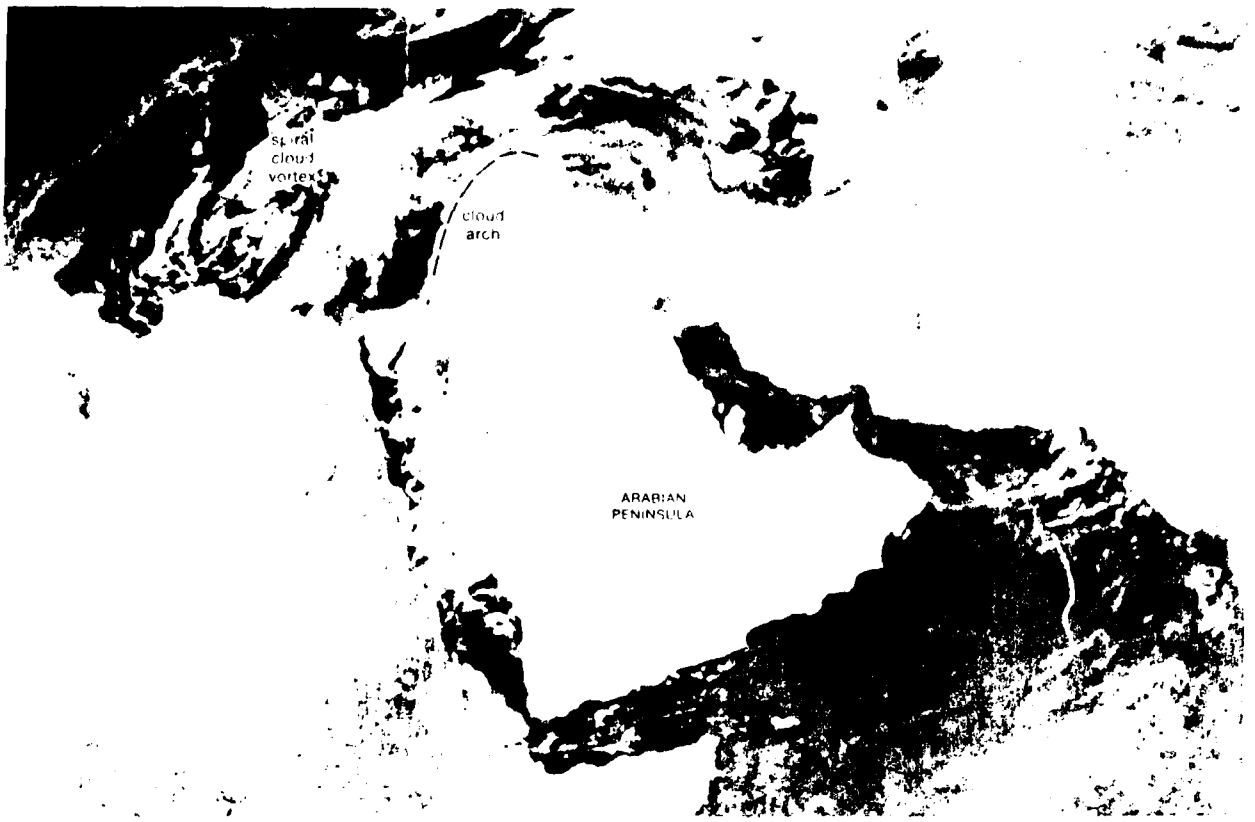

B-10a. GOES-Indian Ocean. Enlarged View. Visible Picture. 0700 GMT 21 October 1979.

ace

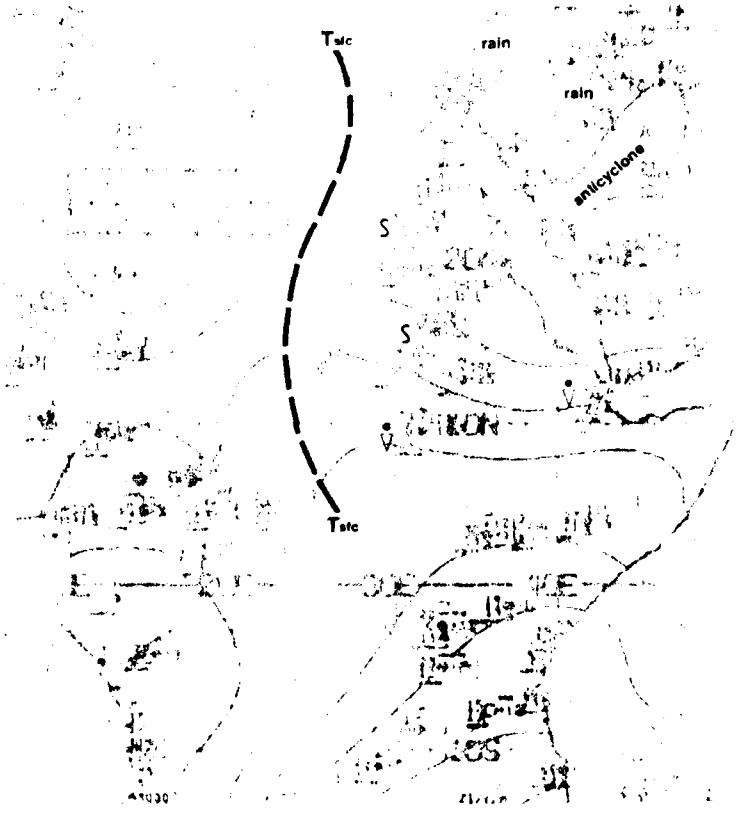

NMC. Tropical Surface Streamline Analysis. 0600 GMT 21 October 1979.

250 mb

Thunderstorm Outbreaks Associated with an Upper-level Divergence Pattern

1B-9a. NMC Tropical 250-mb Streamline Analysis, 1200 GMT 19 October 1979.

700 mb

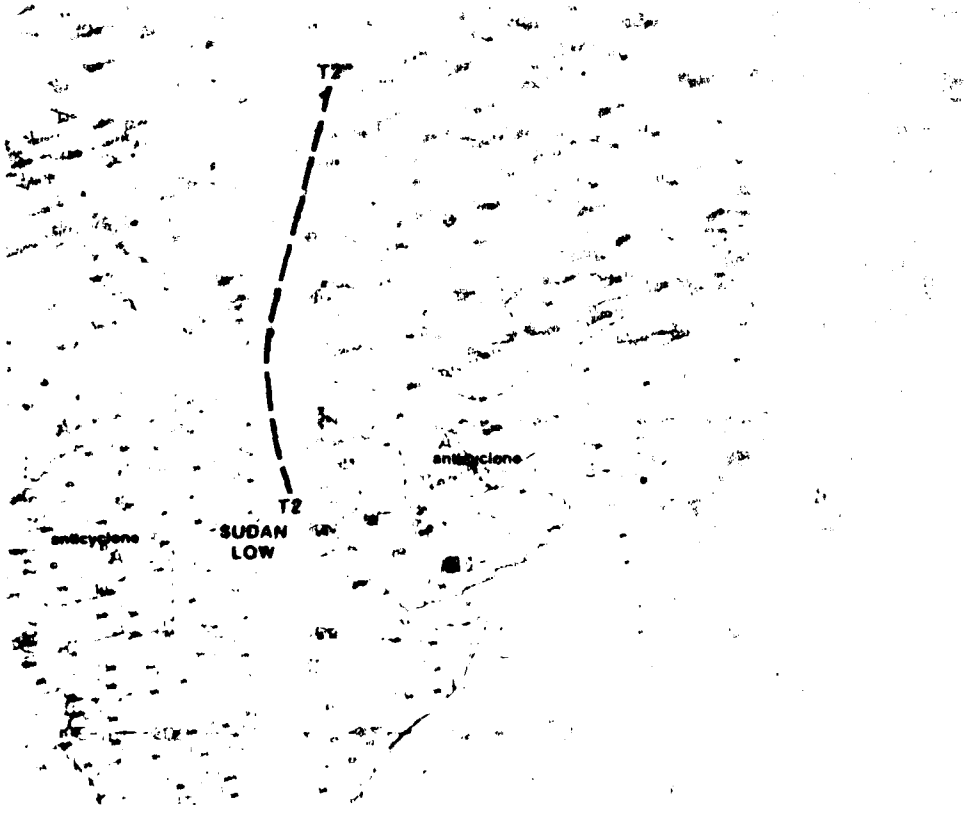

1B-9b. NMC Tropical 700-mb Streamline Analysis, 1200 GMT 19 October 1979.

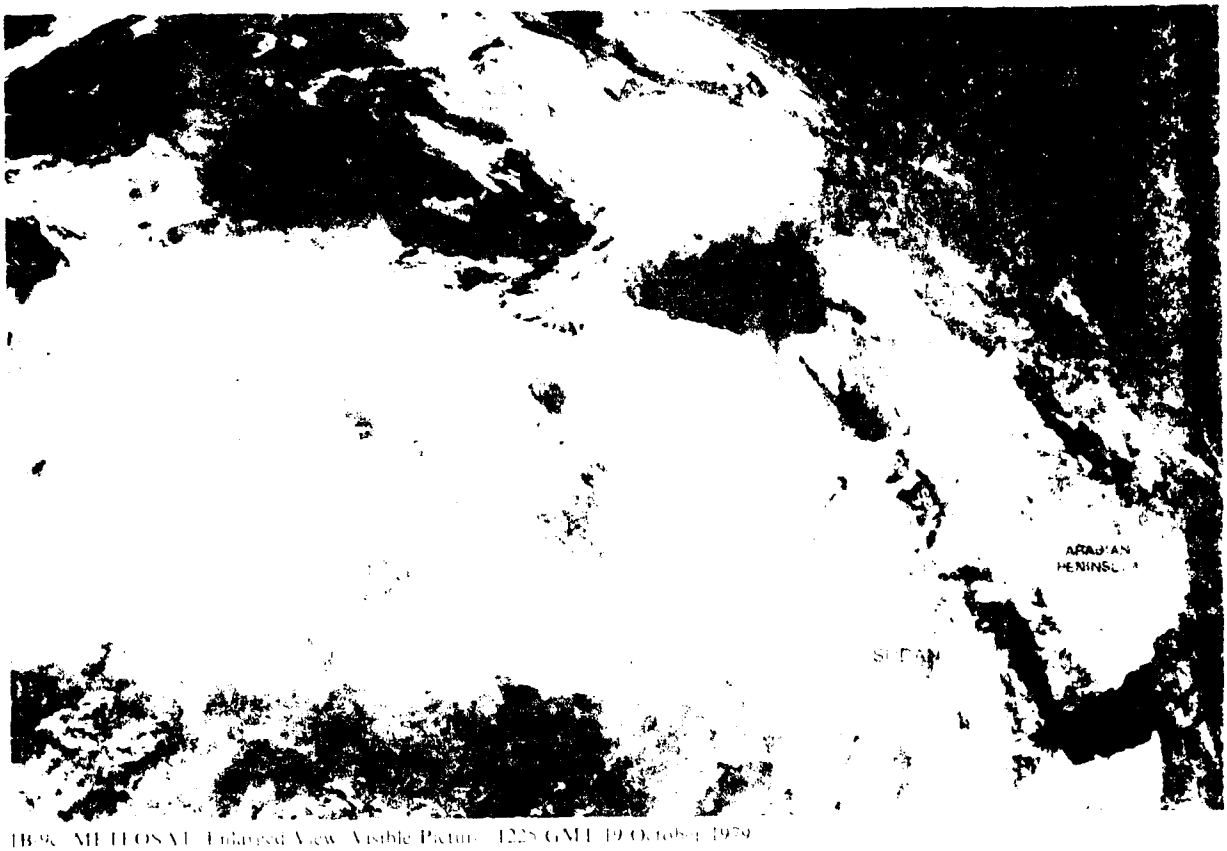

IB9c METEOSAT Enhanced View Visible Picture 1225 GMT 19 October 1979

IB9d METEOSAT Enhanced View Water Vapour Picture 1555 GMT 19 October 1979

19 October

The GOES Indian Ocean visible picture for 0730 GMT (1B-8a) shows that convective activity continues over the Red Sea region. The bands of cirrus debris from the deep convection curve anticyclonically over Saudi Arabia. This implies that there is an upper-level trough to the west over Africa. The surface streamline analysis for 0600 GMT (1B-8b) shows the inverted trough over the Sudan extending to the Mediterranean; however, it is weaker than before (see 1B-4b). There are reports of cumulus congestus, but no thunderstorms. Several stations indicate dust in suspension east of the inverted trough which may be related to convective activity in the region.

The 700-mb streamline analysis (1B-9b) shows a cyclonic center which identifies the Sudan low. Note that part of the eastern periphery of this circulation extends over the Red Sea. The mid-latitude trough **T2** extends southward toward the Red Sea and appears to be moving in phase with the Sudan low. High pressure cells (anticyclones) remain anchored to the east over Saudi Arabia and to the west over north Africa. The 250-mb streamline analysis (1B-9a) indicates that the southern portion of the trough **T1** has remained quasi-stationary over north Africa, while the northern portion has progressed slowly eastward. The new trough **T2** has moved eastward to a position over the central Mediterranean. As suggested in the GOES-Indian Ocean visible picture (1B-8a), the streamlines depict anticyclonic flow over the Red Sea and Saudi Arabia.

The METEOSAT visible picture at 1225 GMT (1B-9c) shows widely scattered convective activity over the Red Sea and adjacent land areas. The METEOSAT water vapor picture at 1355 GMT (1B-9d) again shows the position of the troughs **T1** and **T2** rather well, as well as the ridge **R1** over Saudi Arabia. An extratropical mid- to upper-level vortex is suggested by the water vapor data near the base of trough **T2** over the Balkans. The curved moisture band **M-M** near the northern portion of the trough **T1** suggests the presence of a vorticity center or cyclonic vortex in that region, and coincides with a cyclonic center at the 250-mb level (1B-9a).

21 October

In the GOES Indian Ocean visible picture acquired at 0700 GMT (1B-10a), heavy cloudiness is depicted over a broad area covering the central and northern Red Sea, and the northern half of Saudi Arabia. The extratropical spiral cloud vortex noted previously (1B-9d) over the Balkans is also now evident in the visible data near Crete. This cloud vortex configuration indicates an upper-level trough extending from the vortex southward over Africa, and suggests that there is a flow which turns around the base of the trough and over an upper-level ridge indicated by the nearly solid cloud cover arch over northern Saudi Arabia. Note that the main cloud development occurs ahead of the trough and along the western border of the ridge.

The surface streamline analysis (1B-10b) offers little evidence as to why the heavy cloudiness should be occurring over the northern Red Sea and northern Saudi Arabia. A high pressure cell (anticyclone) is depicted over central Saudi Arabia; the nearest trough is over north Africa, well to the west, and extends northward to the low over the Mediterranean. Surface reports over western and northern Saudi Arabia, however, do show some shower and rain activity, with broken to overcast skies as suggested by the satellite picture.

The 700-mb streamline analysis (1B-11b), similarly, is not helpful in providing a synoptic-scale circulation pattern responsible for the development of the cloudiness over the Red Sea and Saudi Arabia. Note, however, that the low associated with the spiral cloud vortex near Crete is well defined on the streamline analysis. Light anticyclonic flow typifies the synoptic pattern over the Red Sea and Saudi Arabia. The 250-mb streamline analysis (1B-11a) shows the trough **T2**/ridge **R2** configuration implied by the satellite picture. Cloudiness is located downstream of the trough **T2** and just to the west of the ridge **R2**.

Since there is no indication of a low-level disturbance to produce the cloudiness, it must be concluded that the cloudiness is an upper-level effect caused by divergence between the trough **T2** and the ridge **R2**. Moist tropical air is advected around the western periphery of the low-level anticyclone over Saudi Arabia. This combined with the upper-level flow as shown in the METEOSAT water vapor data provides a rich source of moisture for cloud production over the northern Red Sea and Saudi Arabia.

The METEOSAT visible picture at 1155 GMT (1B-11c) clearly depicts the spiral cloud vortex near Crete and the extensive convective activity over the northern Arabian Peninsula. The METEOSAT water vapor picture (1B-11d), depicts the trough **T2** ridge **R2** pattern very clearly. It can be seen that the brightest cloud forms, indicating deep convective developments, are located between the trough and the ridge.

continued on page 1B-13

IB-8a GOES Infrared Satellite Image

surface

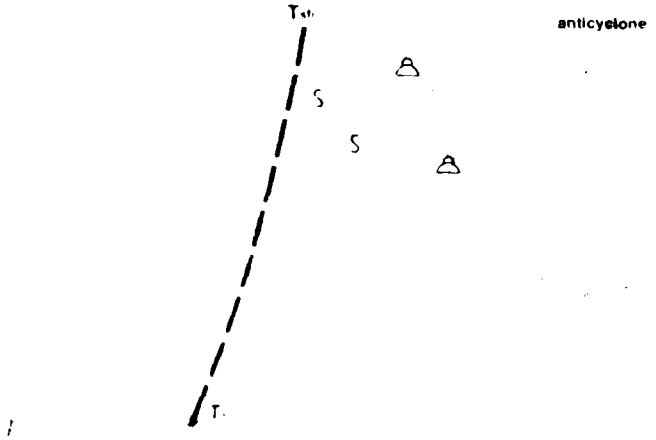

IB-8b NMC Tropical Surface Analysis

Case 1 continued

Red Sea/Persian Gulf Autumn Transition

Thunderstorm Outbreaks Associated with an Upper-level Divergence Pattern
Red Sea/Northern Arabian Peninsula
19–21 October 1979

250 mb

Thunderstorm Outbreaks Associated with an Upper-level Divergence Pattern

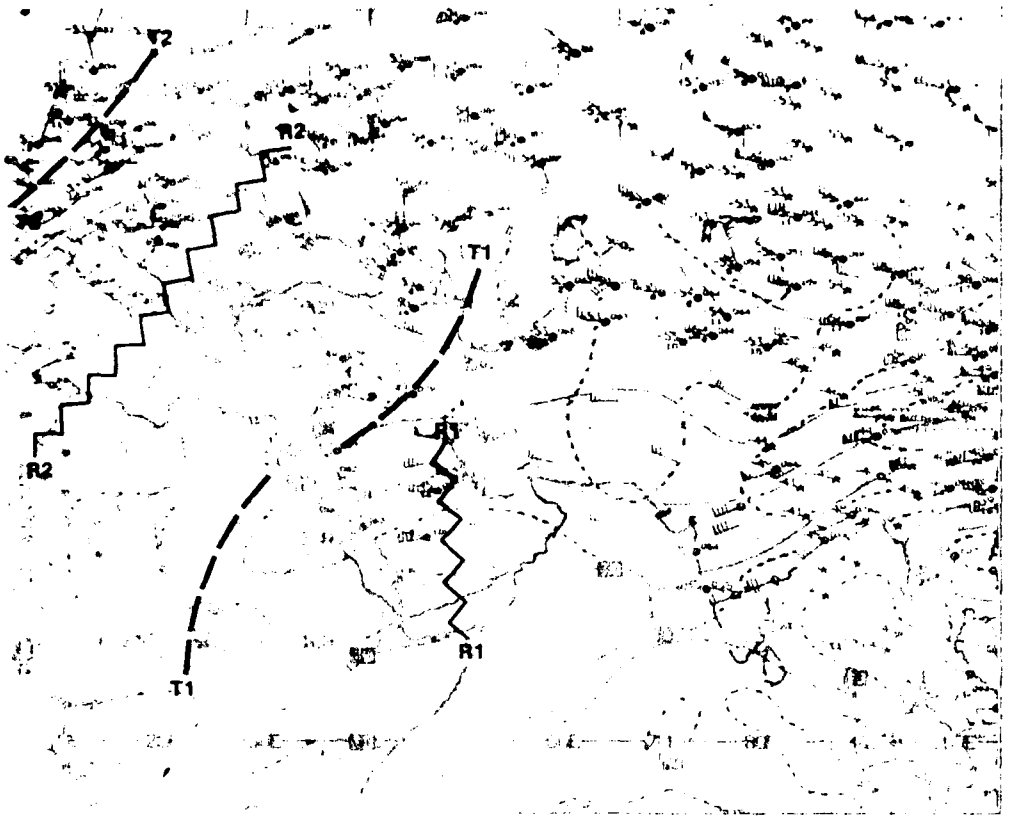

1B-5a. NMC Tropical 250-mb Streamline Analysis. 1200 GMT 17 October 1979.

700 mb

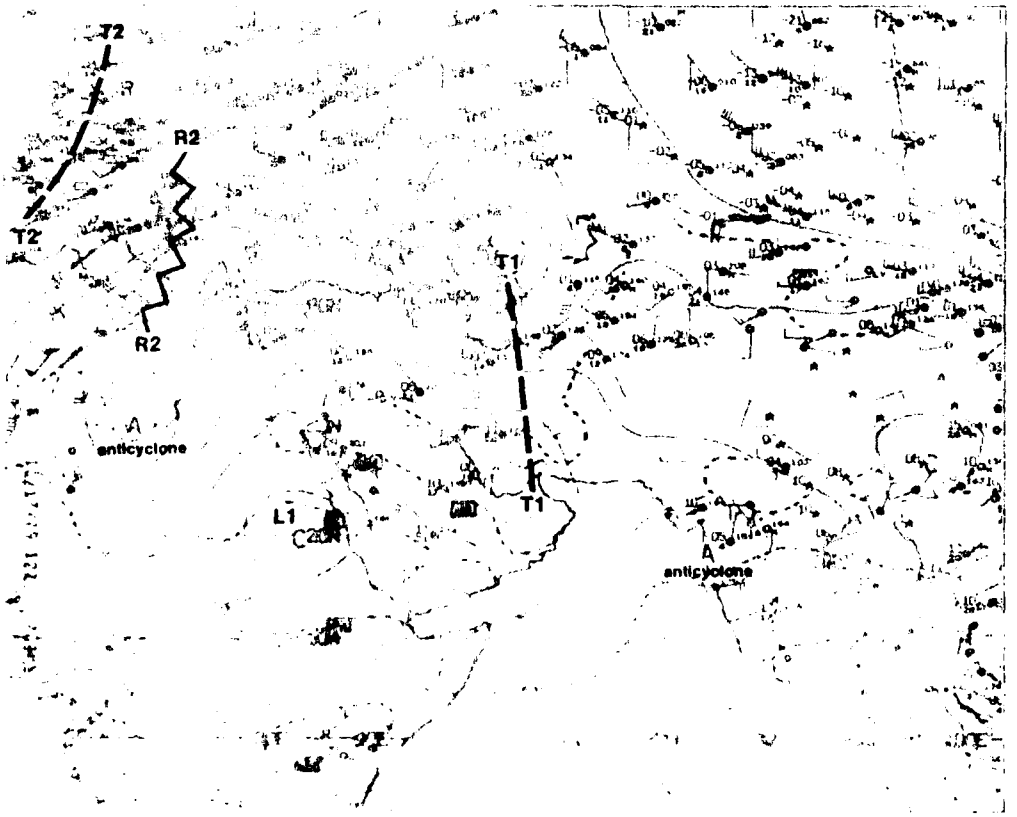

1B-5b. NMC Tropical 700-mb Streamline Analysis. 1200 GMT 17 October 1979.

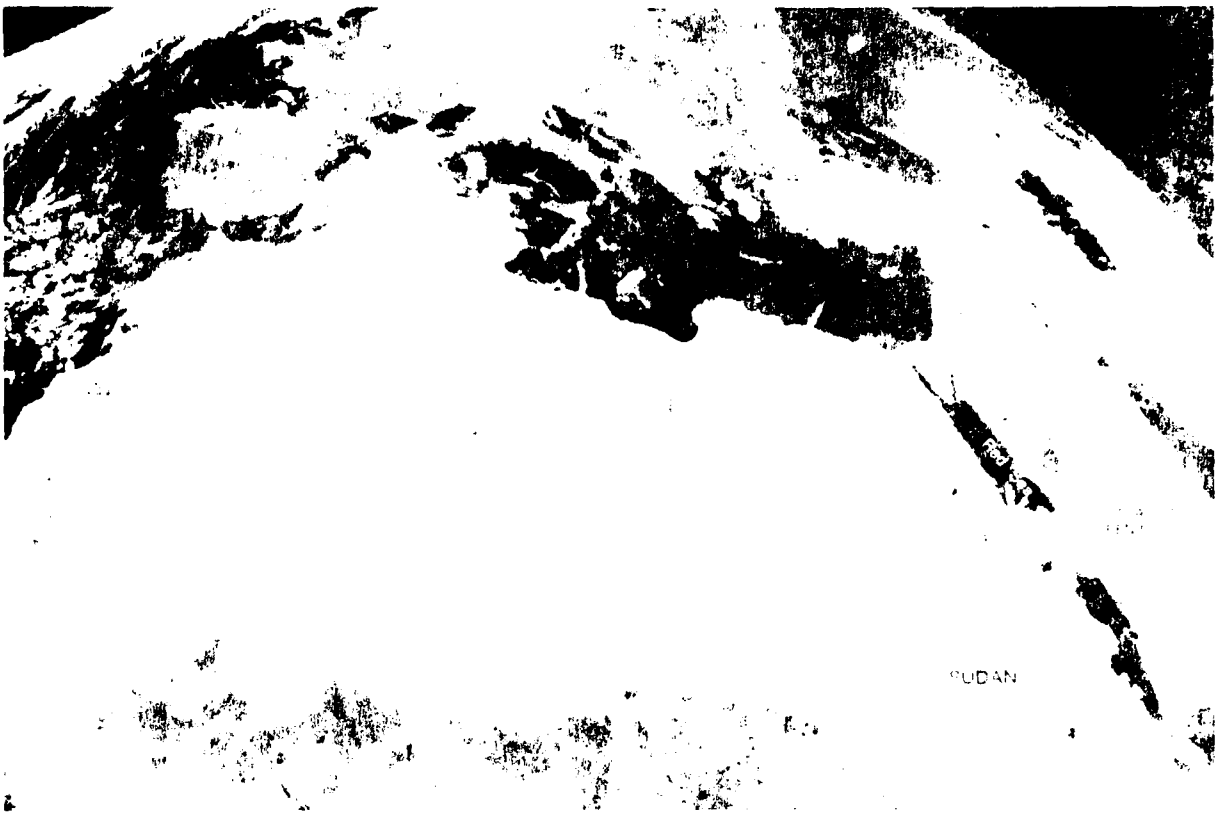

IB-5c. METEOSAT Enlarged View, Visible Picture, 1125 GMT 17 October 1979

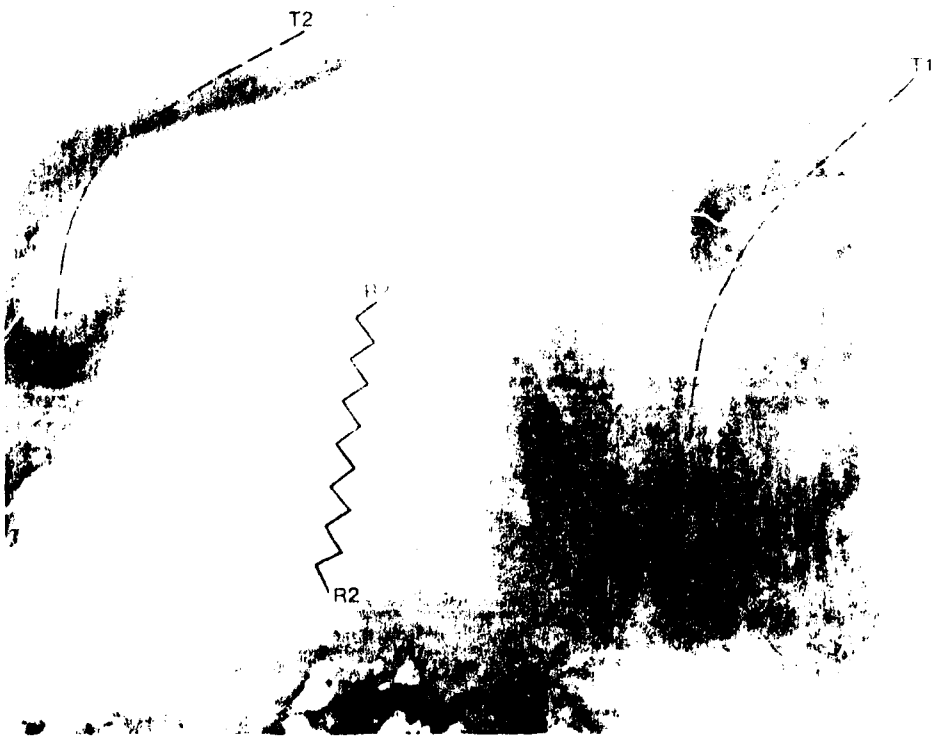

IB-5d. METEOSAT Enlarged View, Water Vapor Picture, 1655 GMT 17 October 1979

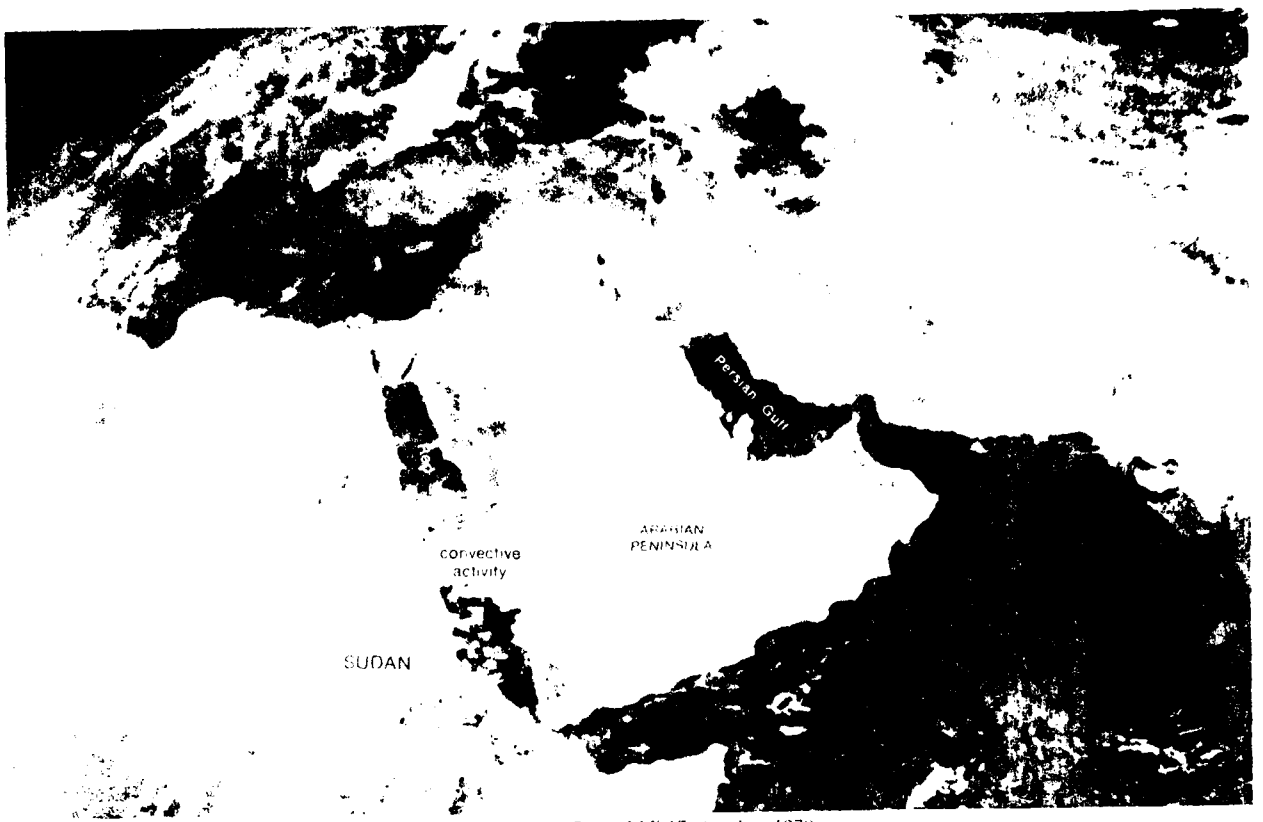

1B-4a. GOES-Indian Ocean Enlarged View, Visible Picture, 0700 GMT 17 October 1979.

surface

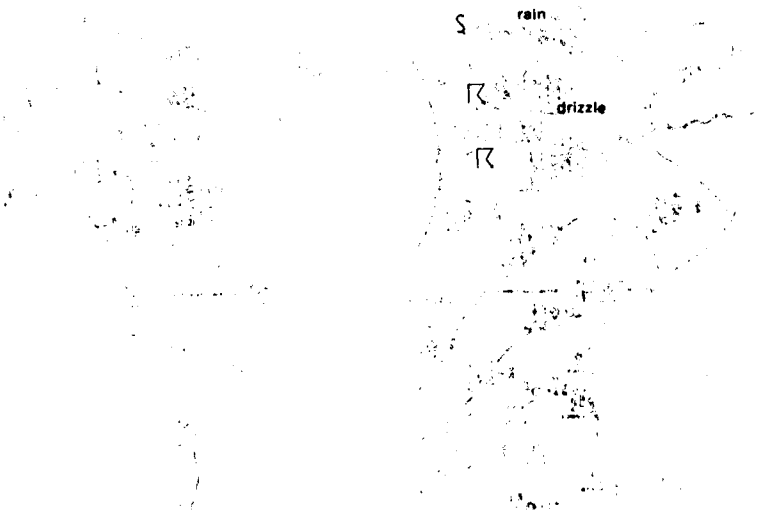

1B-4b. NMC Tropical Surface Streamline Analysis, 0600 GMT 17 October 1979.

250 mb

Thunderstorm Outbreaks Associated with an Upper-level Divergence Pattern

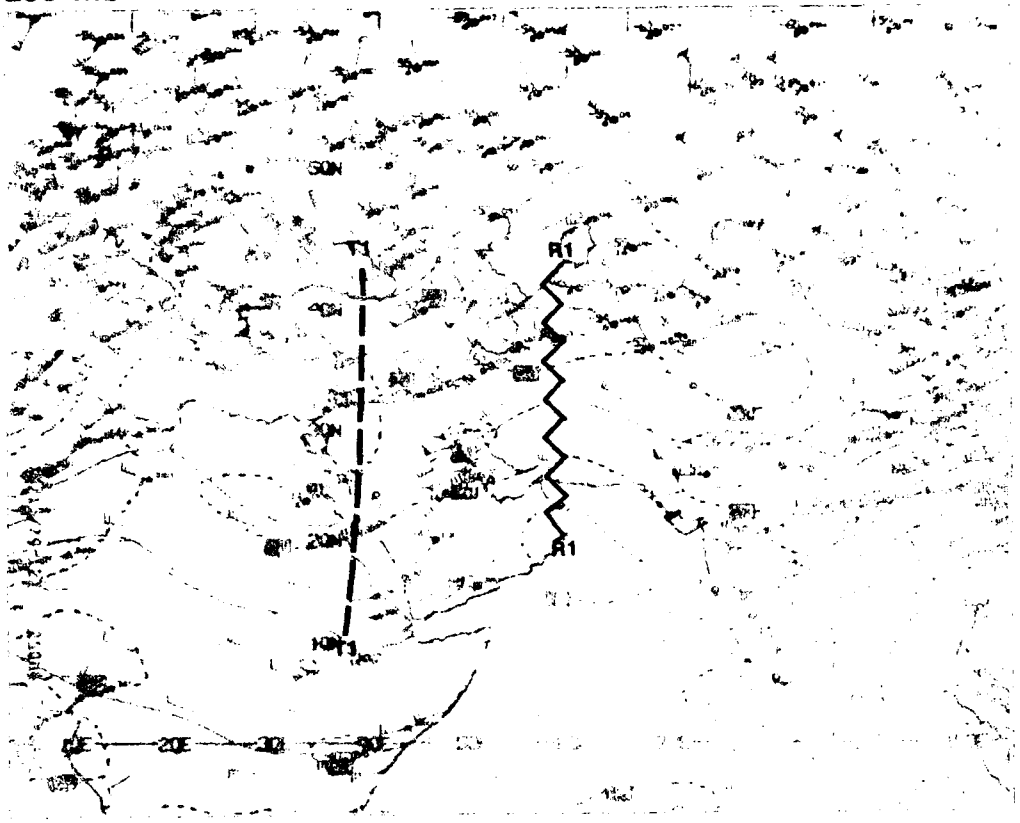

1B-3a. NMC Tropical 250-mb Streamline Analysis 1200 GMT 15 October 1979.

700 mb

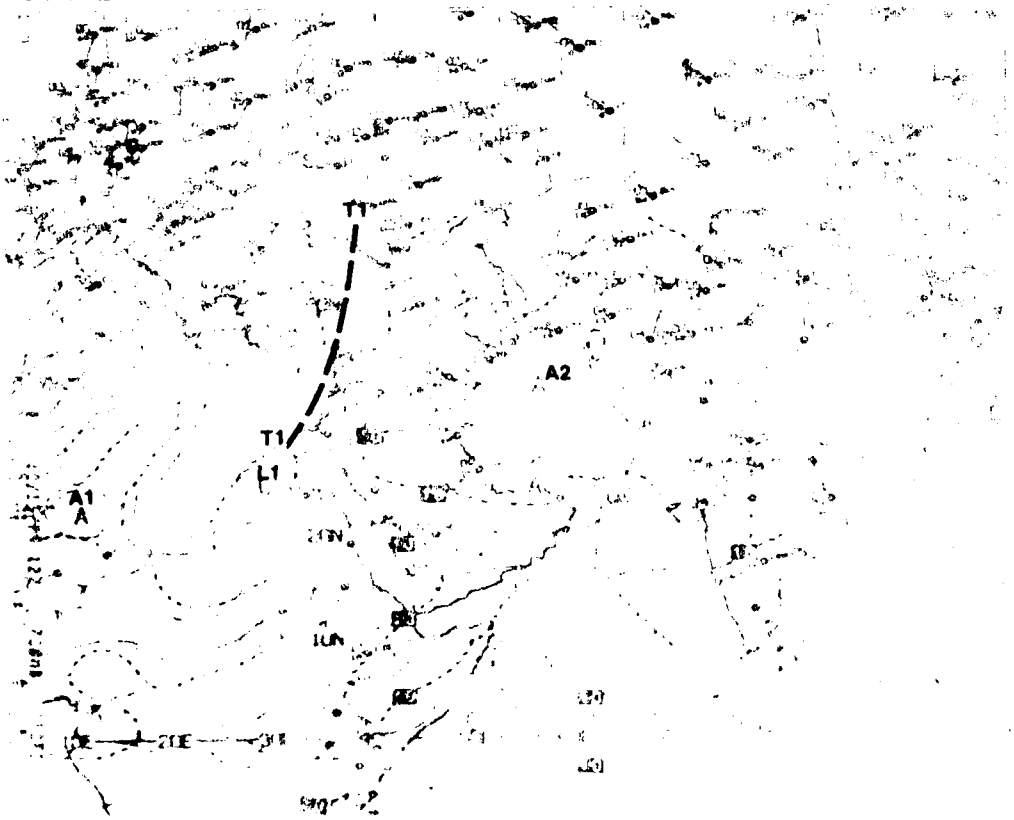

1B-3b. NMC Tropical 700-mb Streamline Analysis. 1200 GMT 15 October 1979.

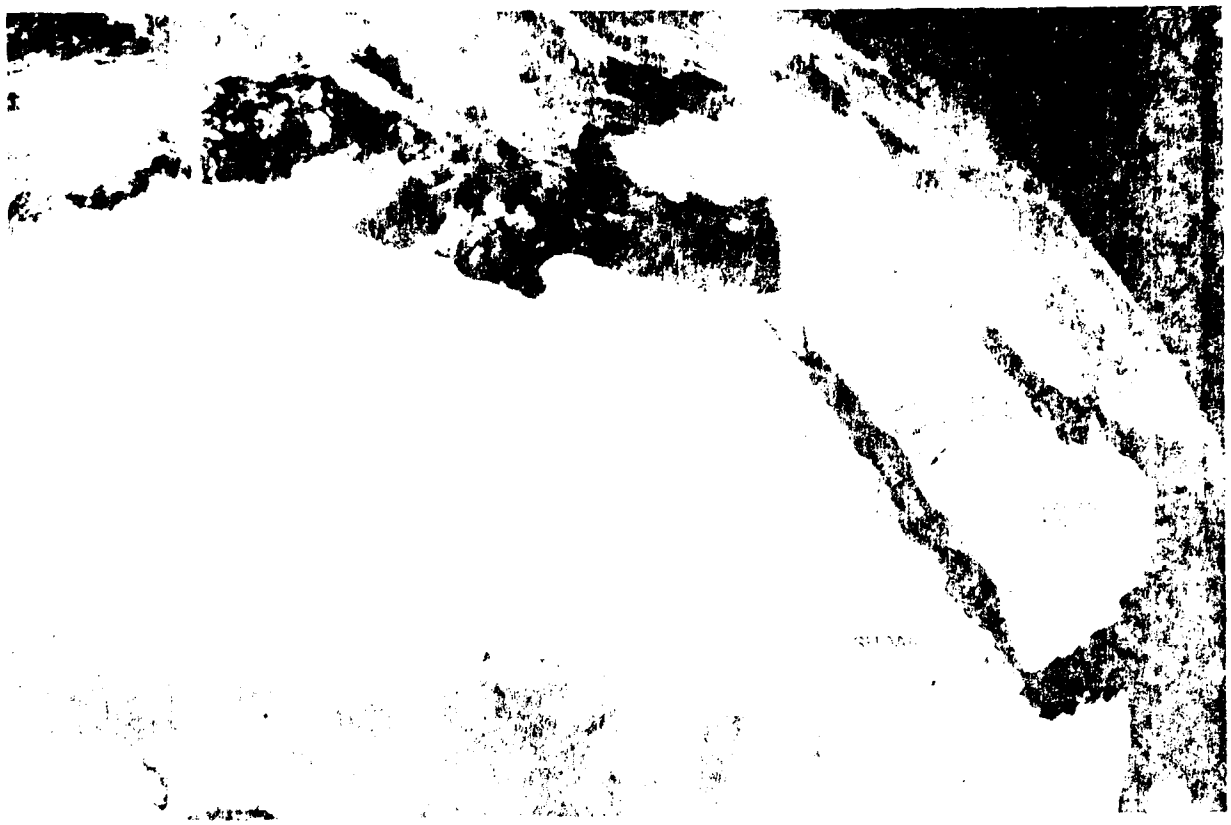

IR 3c. METEOSAT Enlarged View Visible Picture (ESS GMEL 15 Oct [illegible] 79)

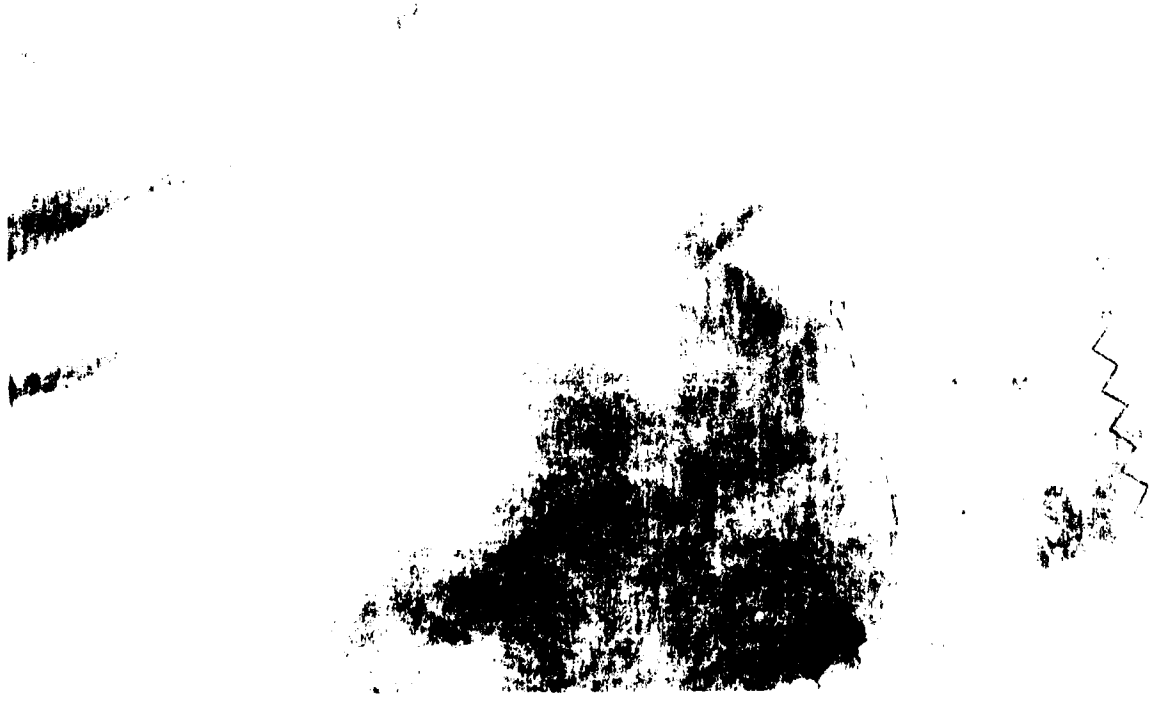

IR 3d. METEOSAT Enlarged View Water Vapor Picture (ESS GMEL 15 Oct [illegible] 79)

Thunderstorm Outbreaks Associated with an Upper-level Divergence Pattern
Red Sea/Northern Arabian Peninsula
October 1979

15 October

The early morning (0730 GMT) GOES Indian Ocean visible picture (1B-2a) shows isolated patches of cloudiness over the central and southern Red Sea. To the southwest, early morning convective activity has developed over the Sudan; however, it shows no organized pattern at this time. The surface streamline analysis for 0600 GMT (1B-2b) depicts generally clear conditions over the Red Sea and the northern Arabian Peninsula. The main circulation feature over east Africa is the Sudan low. There is a north south elongated anticyclonic circulation to the northwest of the Sudan low, weak anticyclonic flow over the southwestern Arabian Peninsula, and an east west oriented anticyclonic circulation over the northern Arabian Sea.

At upper levels, the 700-mb streamline analysis for 1200 GMT (1B-3b) shows a mid-latitude short-wave trough **T1** extending southward toward the Sudan, with a closed low circulation center **L1** over Egypt. Hhigh pressure cells (anticyclones **A1** and **A2**) are located upstream and downstream of the closed low. At 250 mb (1B-3a), the streamline analysis shows a well-defined short-wave trough **T1** which extends from mid-latitudes to the southern border of the Red Sea. Moderate wind speed divergence from the base of the trough to the downstream ridge **R1** is observed at this time. This is favorable for increased vertical motions at lower levels over the Sudan and southern Red Sea.

The METEOSAT visible picture (1B-3c) displays increased convective activity in advance of the upper-level trough **T1**, as evidenced by the sea breeze cloud line along the west coast of Saudi Arabia and the bright cluster of convective clouds over the Sudan near the base of the trough **T1** (for comparison, see the earlier satellite picture 1B-2a). The corresponding METEOSAT water vapor picture (1B-3d), showing moisture at mid to upper levels, reveals a broad band of moisture **M-M** extending across Saudi Arabia in advance of the trough **T1**; the downstream ridge **R1** is also depicted by the curved moisture band near the Persian Gulf. The cyclonically curved band in the moisture field near the base of the trough **T1** is the location of a vorticity maximum associated with the 700-mb low **L1** over Egypt (see 1B-3b).

17 October

The GOES Indian Ocean visible picture acquired at 0700 GMT (1B-4a) indicates that the convective activity has continued to develop over the central and southern Red Sea, and the Sudan region. The surface streamline analysis (1B-4b) confirms this convective activity with reports of thunderstorms, rain, and drizzle. The report of raised dust over the western Sudan is probably due to the gusty wind conditions associated with the thunderstorm activity in the area.

The upper level streamline analyses show that the trough extending from the Sudan to the northern Arabian Peninsula is persisting; however, some of the circulation features have changed. The 700-mb streamline analysis at 1200 GMT (1B-5b) indicates that the trough **T1** has progressed eastward, whereas the closed low circulation **L1** is displaced to the southeast, but remains over Egypt. Note that a new trough **T2** has moved into the region to the west of the area of interest. At 250 mb (1B-5a), the trough **T1** has split: the northern portion has advanced to the east and the southern portion has retrogressed from the southern Red Sea to over the western Sudan, with a corresponding retrogression of the ridge **R1** to a position over central Saudi Arabia. Speed divergence aloft from the trough **T1** to the ridge **R1** continues over the Red Sea so that conditions remain favorable for deep convective developments in the region.

The METEOSAT visible picture at 1125 GMT (1B-5c) shows numerous convective clusters covering the area from the central Red Sea to the Sudan. In the METEOSAT water vapor picture at 1655 GMT (1B-5d), the upper-level trough **T1** can be traced from its location near the Caspian Sea in the north to the small vortex near Crete, and then southward across Africa. The water vapor picture shows that the main thunderstorm activity lies between the trough **T1** over Africa and the ridge **R1** over Saudi Arabia. Convective activity appears to be restricted to the area along and immediately to the west of the ridge axis. Trough **T2** is well defined in the water vapor picture, as is the ridge line **R2**. It is of interest to note that the densest cloud cover, suggesting deep convective developments, also lies between the trough **T2** and the ridge line **R2**.

continued on page 1B-7

Case 1 continued

Red Sea/Persian Gulf Autumn Transition

Thunderstorm Outbreaks Associated with an Upper-level Divergence Pattern
Red Sea/Northern Arabian Peninsula
23 October 1979

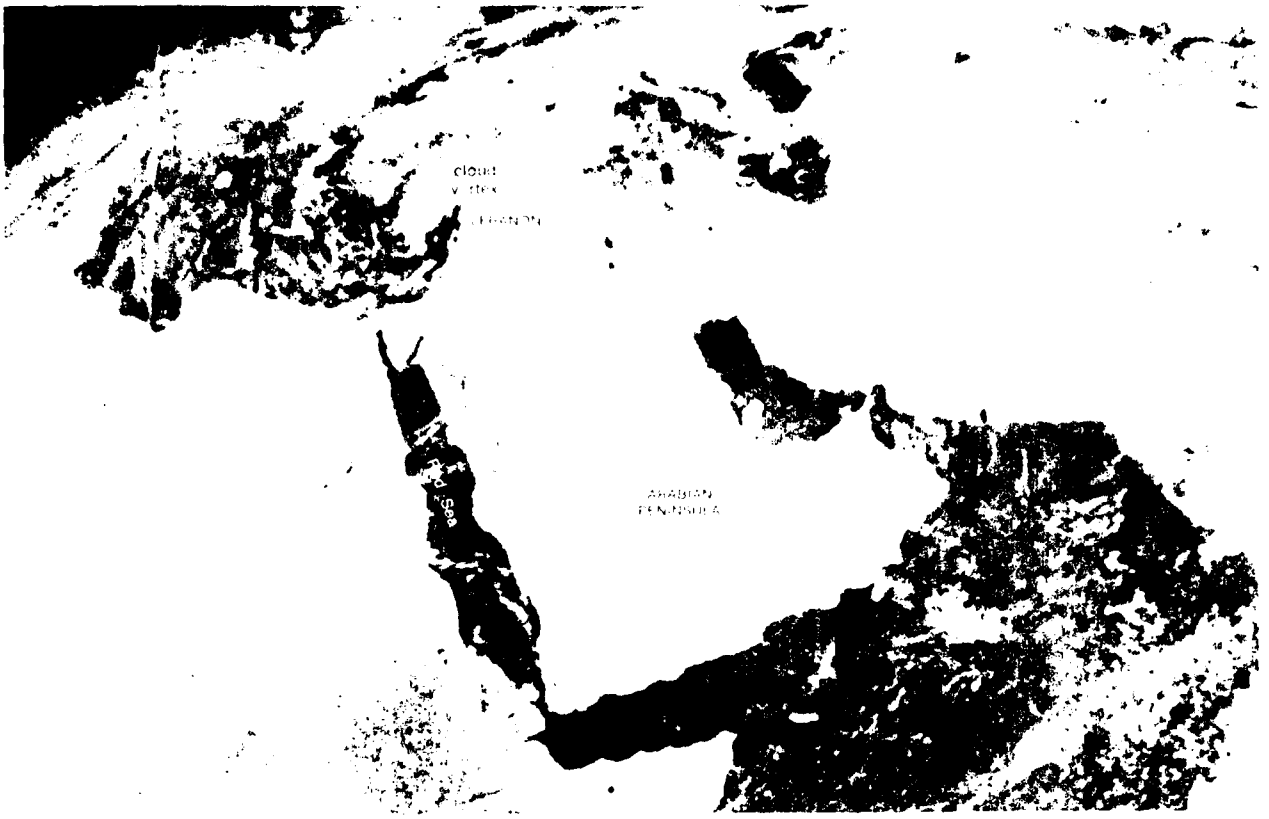

1B-14a. GOES-Indian Ocean. Enlarged View. Visible Picture. 0730 GMT 23 October 1979.

surface

SUDAN
LOW

1B-14b. NMC Tropical Surface Streamline Analysis. 0600 GMT 23 October 1979.

23 October

The GOES Indian Ocean visible picture at 0730 GMT (1B-14a) shows the vortex over the eastern Mediterranean, just off the coast of Lebanon. Cloudiness over the Red Sea and Saudi Arabia has largely dissipated with only a few indications of mainly high clouds. The surface streamline analysis (1B-14b) shows pronounced ridging across the northern Red Sea and Arabian Peninsula between the high pressure cells (anticyclones) over north Africa and the Persian Gulf. The Sudan low is near its normal position for this time of the year. Notice that there are no reports of rain or showers in the region.

On the 700-mb streamline analysis (1B-15b), high pressure cells (anticyclones) are also depicted over central Africa and southern Saudi Arabia with ridging across the Red Sea. The cyclonic circulation associated with the low near Lebanon also extends as a trough entering the northern Red Sea, but does not extend further south. The 250-mb streamline analysis (1B-15a), for the first time in this series, does not have a deep trough extending into Africa. The flow across the Red Sea and Saudi Arabia is westerly, turning slightly anticyclonically. Trough **T2**, associated with the low near Lebanon, is well to the north so that there is not the typical trough ridge pattern observed previously over this region during the deep convective developments.

The METEOSAT water vapor picture (1B-15d) shows the vortex near Lebanon. The moisture pattern indicates the trough **T3** associated with this disturbance does not extend very far to the south. Compare this picture with the previous water vapor picture (1B-15c), in which the moisture patterns depict a definite southward extension of the trough **T2** from the vortex. In the water vapor picture (1B-15d), anticyclonic flow is indicated just to the south of the vortex. The water vapor picture also shows that the next southward trough extension is located well to the east over eastern Saudi Arabia and the Persian Gulf.

Important Conclusions

1. Deep convective developments over the northern Red Sea and Saudi Arabia during the period of the autumn transition can be anticipated under the following conditions:
   a. Generally lower pressure over east Africa in the form of an inverted trough.
   b. Higher pressure over Saudi Arabia.
   c. An upper-level trough that extends from the Mediterranean southward over east Africa.
   d. An upper-level ridge over Saudi Arabia.

2. Under the above conditions, deep convective developments (thunderstorms) can be expected in the region between the upper level trough and just to the west of the ridge line.

3. In the absence of a low-level disturbance, thunderstorm activity is not likely to occur over the Red Sea Saudi Arabian region during the period of the autumn transition when upper-air flow is straight westerly and unperturbed.

4. METEOSAT water vapor pictures, or those from other satellites providing similar information, are useful for locating upper-level troughs and ridge lines. This information can be used to locate the most probable area for convective development, overcast skies, and generally disturbed weather conditions.

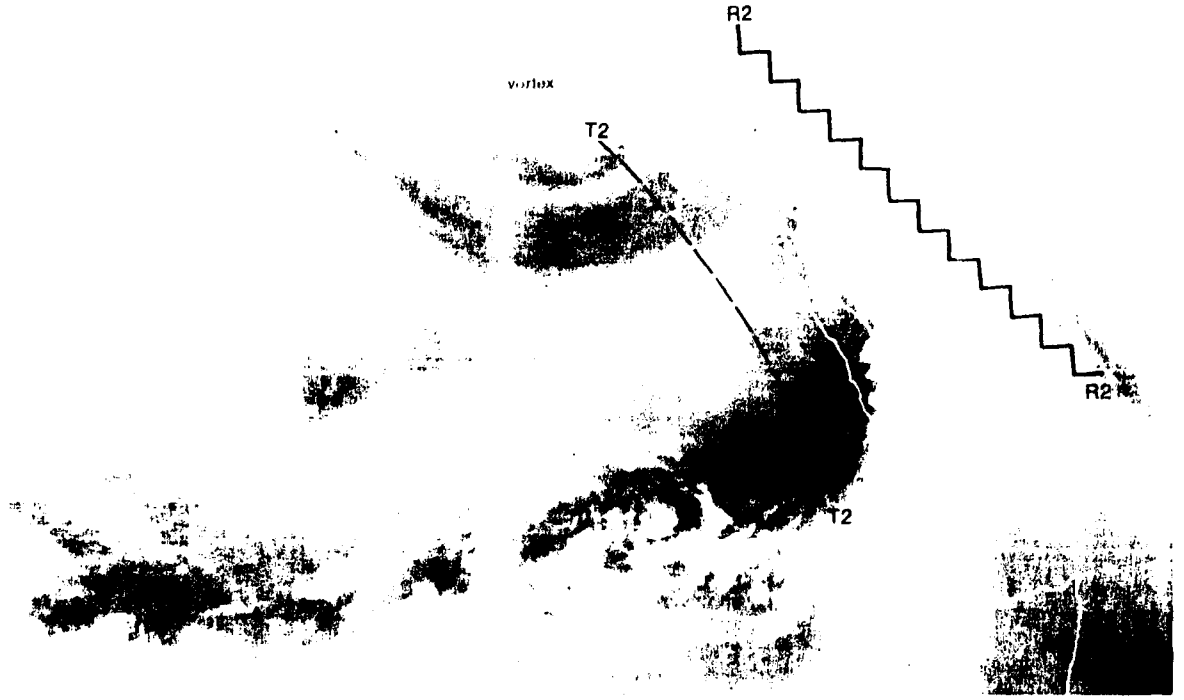

1B-15c. METEOSAT. Enlarged View. Water Vapor Picture. 0955 GMT 21 October 1979. (Note this picture is a repeat of 1B-11d.)

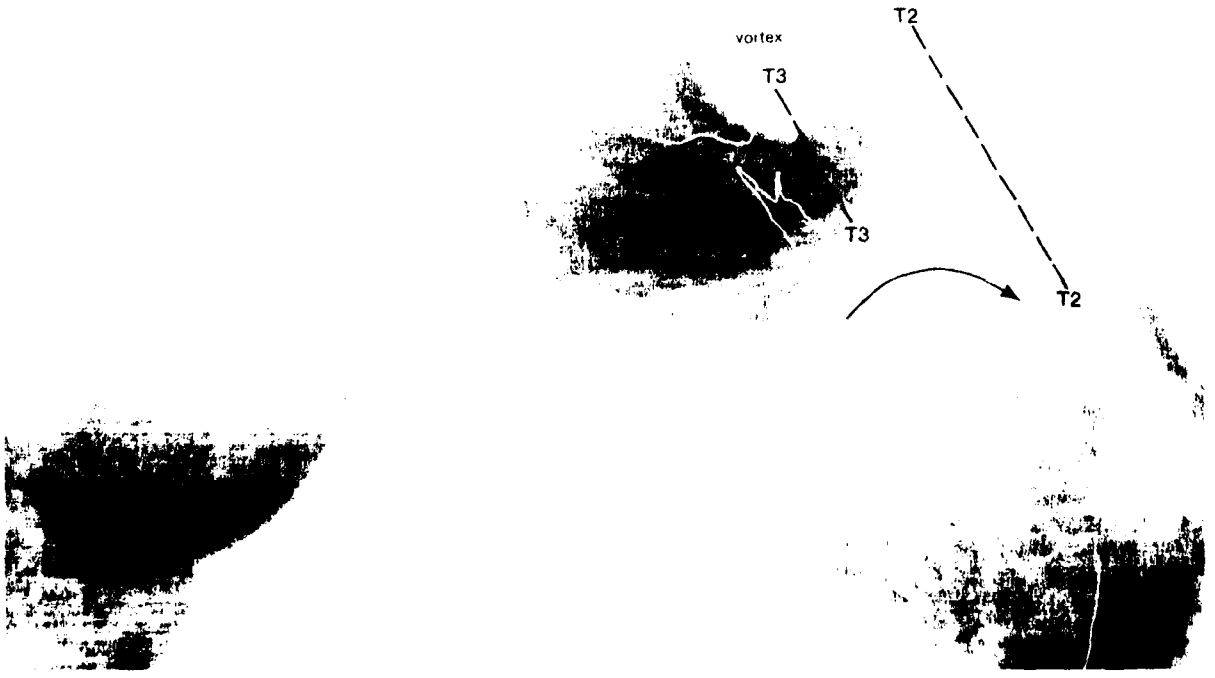

1B-15d. METEOSAT. Enlarged View. Water Vapor Picture. 1155 GMT 23 October 1979.

250 mb

Thunderstorm Outbreaks Associated with an Upper-level Divergence Pattern

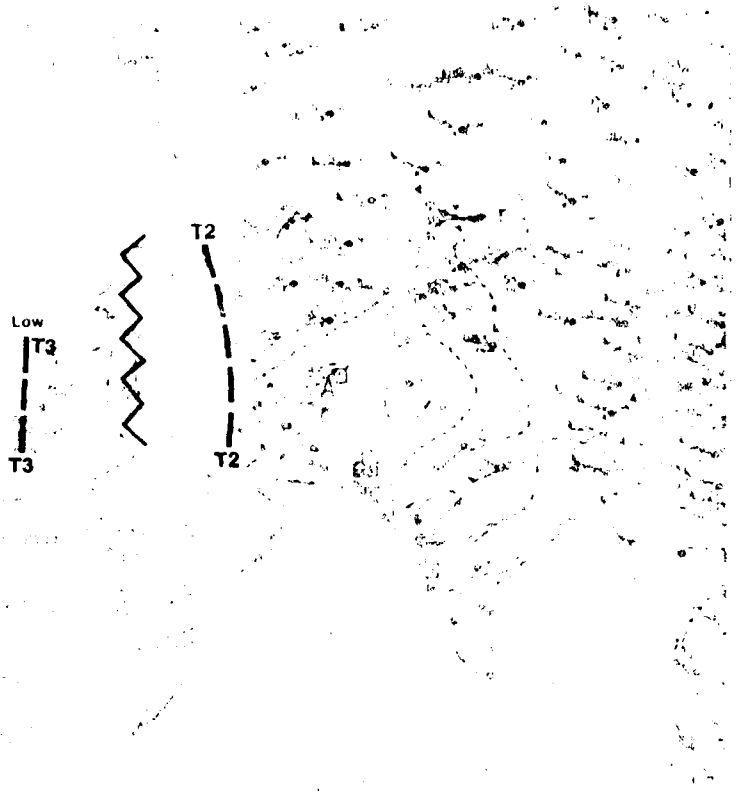

1B-15a. NMC Tropical 250-mb Streamline Analysis. 1200 GMT 23 October 1979.

700 mb

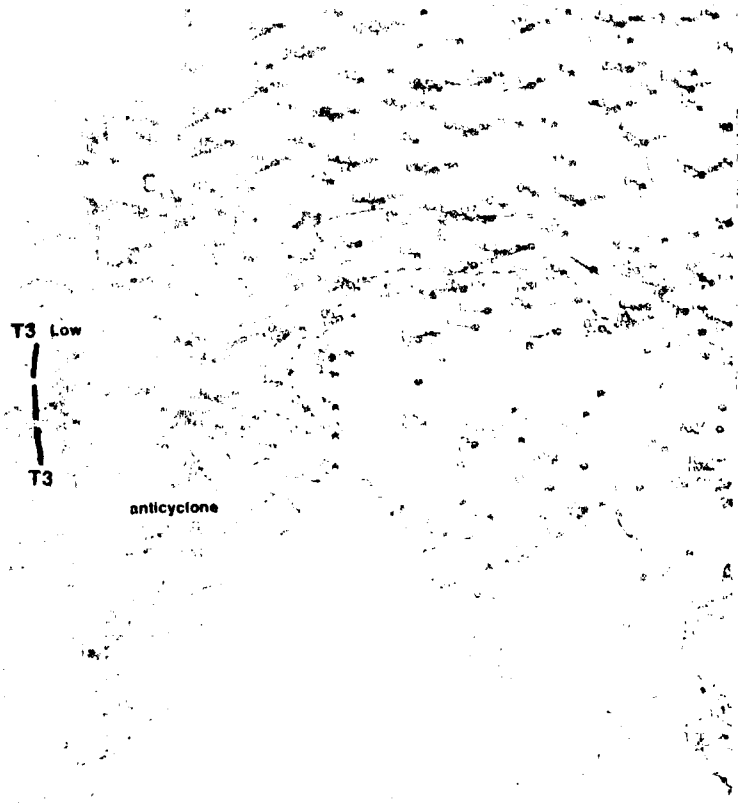

1B-15b. NMC Tropical 700-mb Streamline Analysis. 1200 GMT 23 October 1979.

Case 5 Red Sea/Persian Gulf—Winter

Jet Aircraft Generated Condensation Trails

A condensation trail (contrail) is a cloud-like streamer observed to form behind an aircraft flying in clear, cold, humid air (Huschke, 1959). Contrails form when the water vapor exhaust from the aircraft engine overbalances the heat added and brings the mixture of ambient air and exhaust to saturation. The relative humidity in the trail is dependent on the amount of heat and water added by the exhaust, the ratio of entrained environmental air to exhaust gas, and the initial pressure, temperature, and relative humidity of the environment.

Persistent contrails are often observed in satellite imagery. They are readily distinguished from clouds in visible imagery because they occur as thin, straight line segments, often in criss-cross formations where several aircraft have recently passed across the same area. Contrails are also observed in infrared imagery, where they appear as distinct white-tone (cold temperature) line segments. Sometimes contrails in visible imagery may degenerate to an anomalous gray shade, or not be apparent at all, but still be detectable in the infrared (see NTAG Vol. 1, Sec. 2B, Case 19).

Reference

Huschke, R. E. (Ed.), 1959: *Glossary of Meteorology*. American Meteorological Society, Boston, 638 pp.

Critical temperature graphs have been computed by Appleman (1953) for relative humidities with respect to water of 0, 60, 90, and 100 percent, for temperatures down to -80° C, and for ratios of entrainment of environmental to exhaust gas from 58:1 to 7000:1. From these graphs one can determine the point at which contrails will form and dissipate. If it is desired to know only whether or not a visible contrail will form, a much simpler graph (1C-47a) can be used. This graph can be replotted on a Skew T, Log P Diagram for making contrail forecasts.

To use the graph to evaluate potential contrail formation on a Skew T, Log P Diagram, the trace of the temperature curve on the diagram is related to the "yes", "possible", or "no" sectors of the graph. That portion of the temperature curve in the "yes" sector indicates that contrails will form; in the "no" sector, contrails will not form; and in the "possible" sector, formation will be determined by the relative humidity at the selected temperature vs. pressure level. A manual (AWS, 1960) is available for detailed guidance on contrail forecasting for jet aircraft.

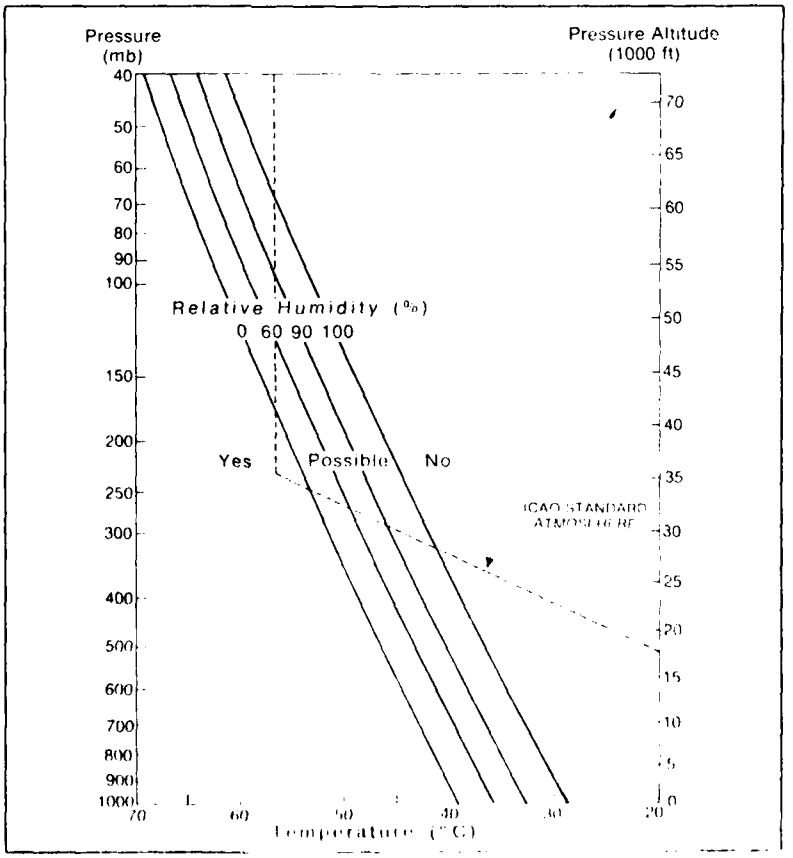

1C-47a Graph of relative humidity required for jet aircraft contrail formation as a function of pressure and temperature of the environment

References

Air Weather Service, 1960: Forecasting of aircraft condensation trails. Air Weather Service Manual AWSM 105-100 (Navy NAVAIR 50-1P-6), Air Weather Service, Scott AFB, Illinois, 21 pp.

Appleman, H., 1953: The formation of exhaust condensation trails by jet aircraft. *Bull. AMS*, 34, 14-20.

IC-48a I-2 DMSP FF Enhancement 0441 GMT 11 January 1980

Formation and Dissipation of a Contrail
Persian Gulf
January 1980

11 January

The DMSP visible picture at 0441 GMT (1C-48a) shows two linear anomalous cloud lines over the Persian Gulf. A close inspection of the cloud lines (1C-49a) identifies them as contrails. The northern cloud line extends over more than half the length of the Persian Gulf and displays an abrupt change in direction. This is atypical of clouds observed in the free atmosphere. The southern cloud line displays a shadow on the terrain below. The distance of the shadow from the cloud line at this time of the day is typical of that frequently observed of a cirrus cloud deck or cumulonimbus cirrus debris (cirrus spissatus) shadows in visible pictures, so that this cloud line is at high altitudes. These facts and a comparison of the location of the cloud lines and the high altitude jet routes over the area (1C-49b) show that they are definitely contrails.

The upper-air soundings for Dhahran, located on the western side of the Persian Gulf, for 0000 GMT (1C-50a) and 1200 GMT (1C-51a) can be analyzed for additional confirmation of the formation of contrails over the region. The contrail formation probability lines have been plotted on the diagrams, in accordance with the procedures described in the AWSM 105-100 publication (see reference, page 1C-47). On the 0000 GMT sounding (1C-50a), the temperature trace between about 235 mb and 188 mb, and above about 162 mb lies in the "yes" sector. This indicates that contrails will be formed by a jet aircraft flying at those levels. On the sounding at 1200 GMT (1C-51a), contrails would be expected at all levels above about 233 mb.

To determine the likelihood of contrail formation at levels where the temperature curve falls within the "possible" sector, the relative humidity values are required. The line on the Skew T, Log P Diagram separating the "yes" and "possible" sectors represents the 0% ambient relative humidity (RH), and the line separating the "possible" and "no" sectors represents the 100% ambient relative humidity. These RH values are the minimum ambient RH required at a particular pressure temperature level for contrails to form. Using Appleman's technique (see reference, page 1C-47), the "possible" sector can be linearly scaled by the 60% and 90% RH lines. The procedure is then to calculate the RH from the plotted temperature and dew point values at a given pressure level and compare the RH obtained to the RH scale in the possible sector. If the calculated RH is greater than the scale RH for that level, contrail formation can be expected.

The DMSP visible picture at 0610 GMT (1C-53b) shows a faint, linear cloud feature along the eastern shore of the Persian Gulf, which extends to the northwest and becomes indiscernable over the land. The contrail observed earlier has almost dissipated. This time frame of dissipation of less than 1.5 hours is typical of contrails. The NMC 250-mb analyses for 0000 GMT (1C-52a) and 1200 GMT (1C-52b) indicate that the displacement of about 60 n mi of the contrail between the successive pictures is in reasonable agreement with the upper-level winds over the region.

Important Conclusions

1. Contrails appear in satellite imagery as distinct linear cloud lines.

2. Evaluation of upper-air soundings, using standard contrail formation procedures, can provide guidance on contrail formation. This information can be used to define potential areas on satellite imagery where contrails are most likely to be observed.

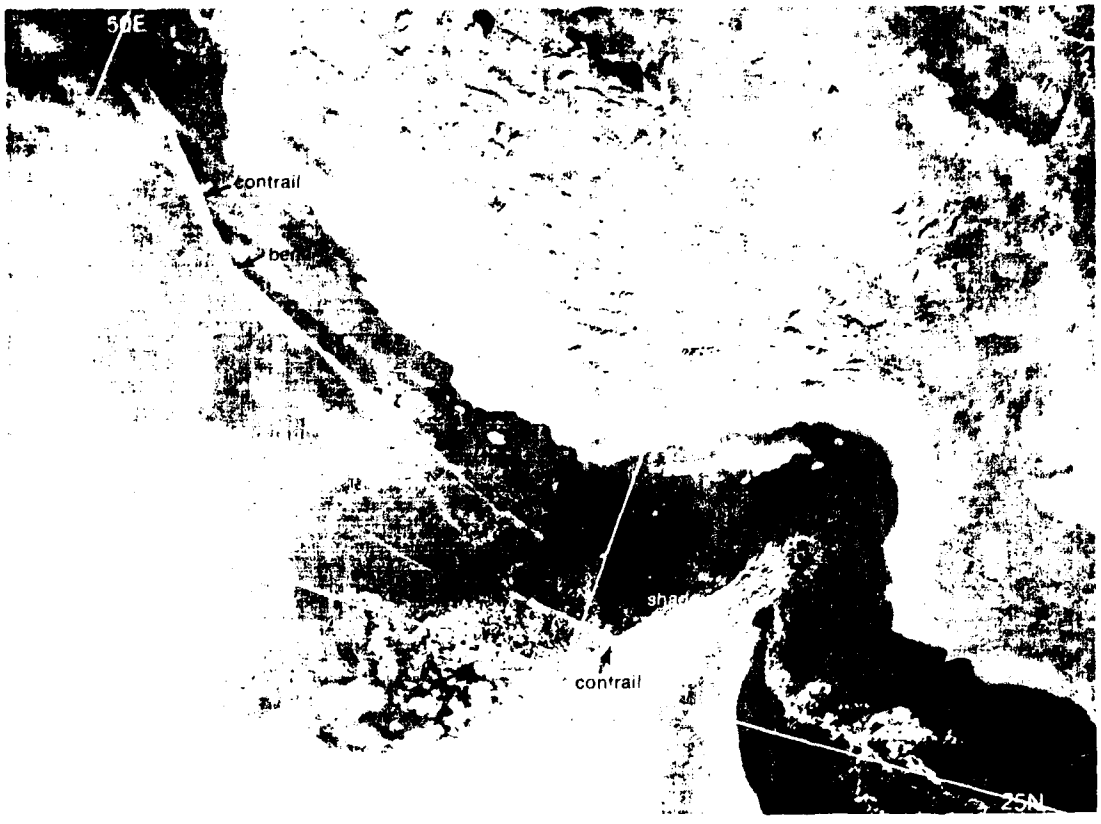

IC-49a. F-2. Enlarged View. DMSP LF Log Enhancement. 0441 GMT 11 January 1980.

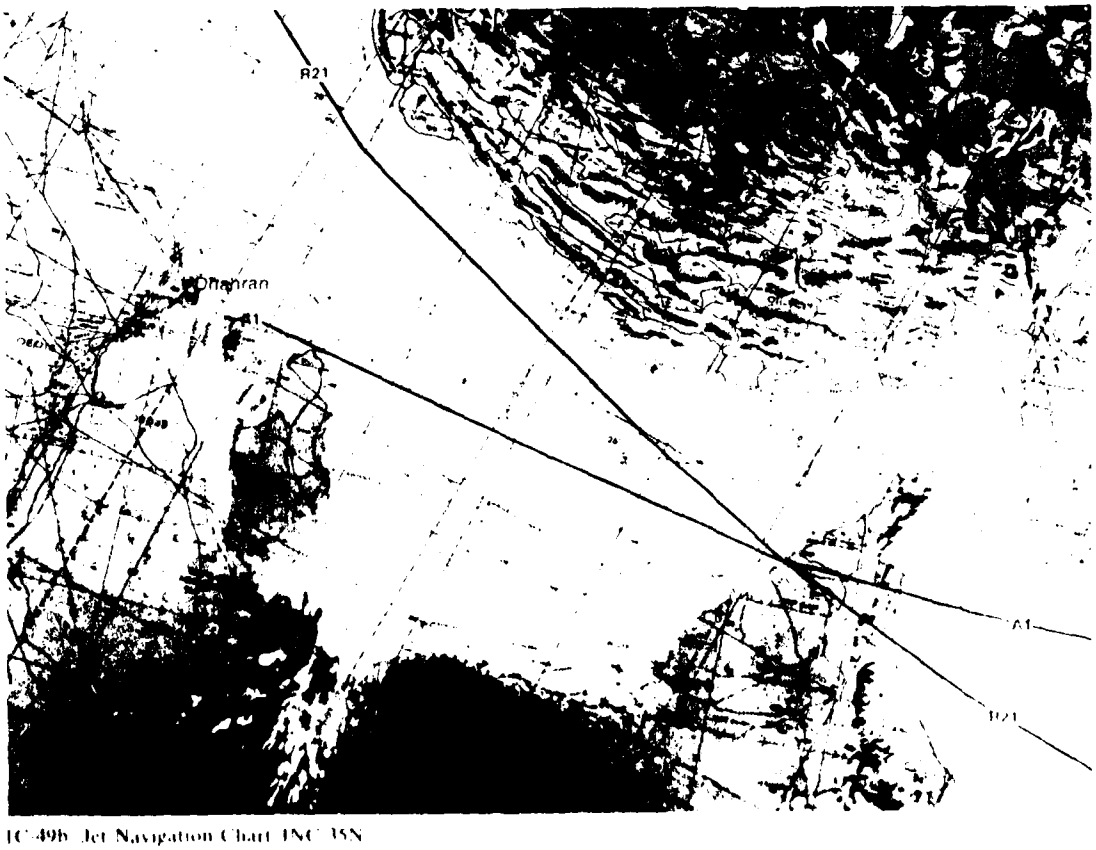

IC-49b. Jet Navigation Chart JNC 35N

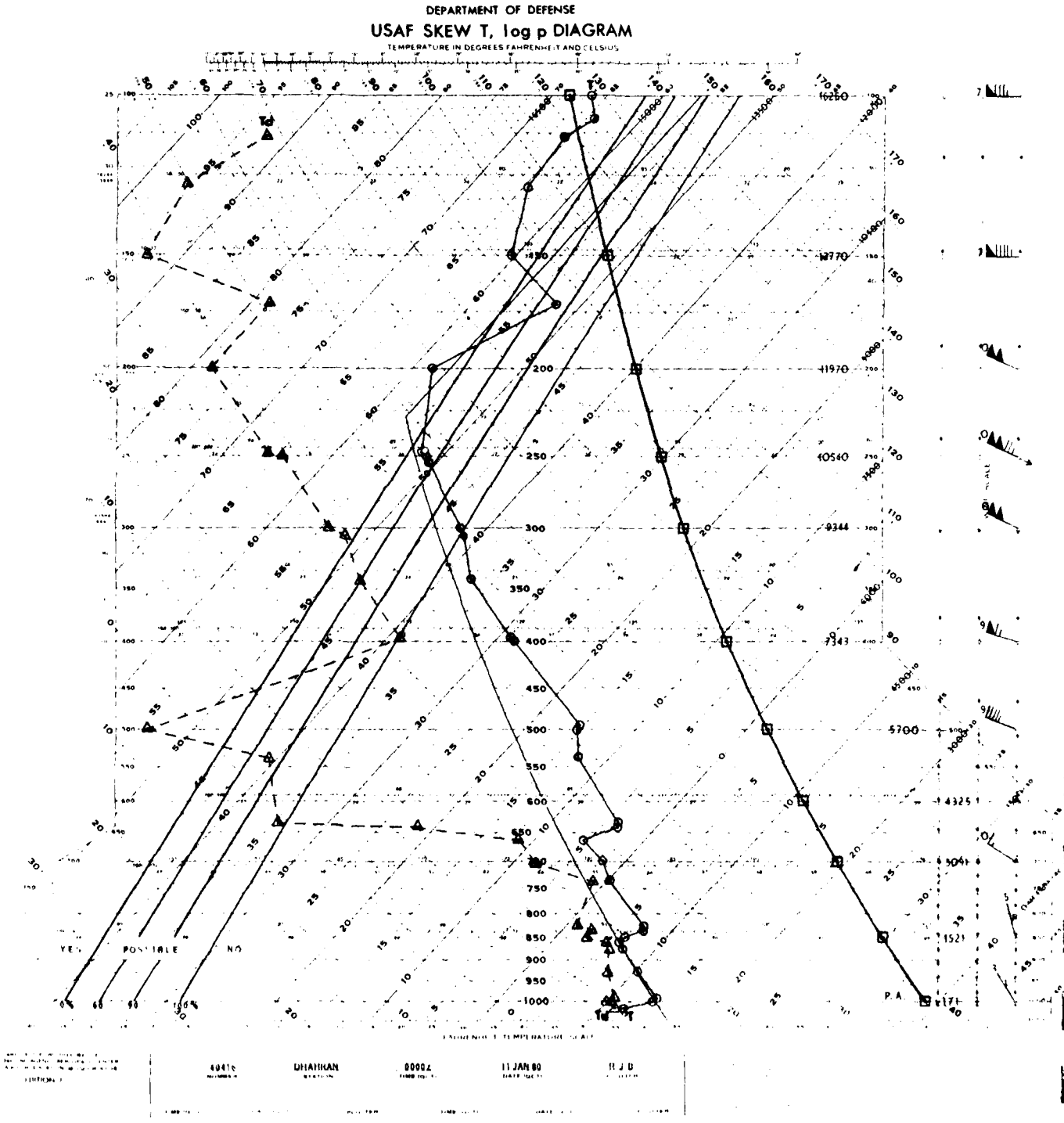

Dhahran Sounding 0000 GMT 11 January 1980

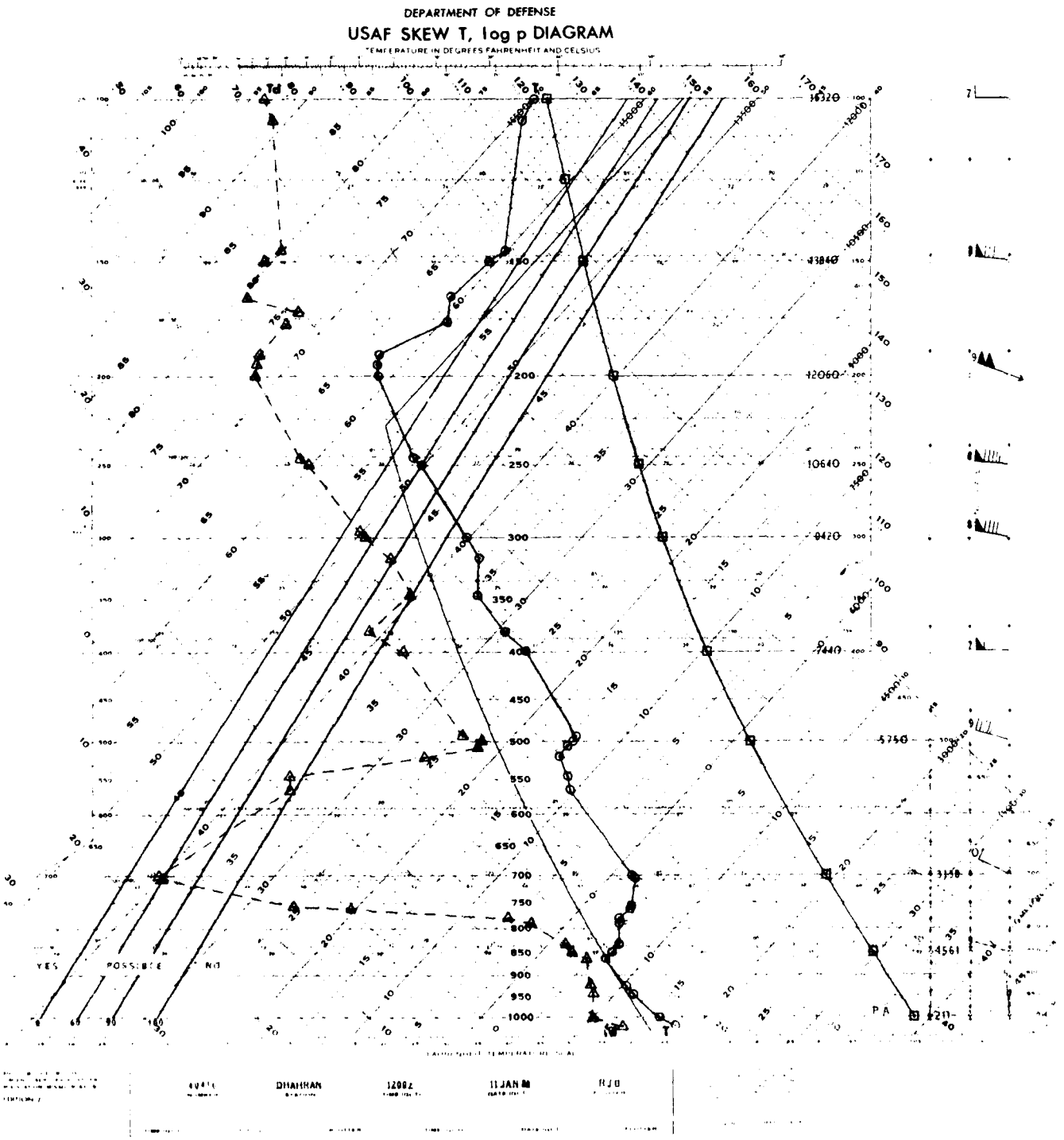

Dhahran Sounding 1200 GMT 11 January 1980

b

NMC 250-mb Analysis 0000 GMT 11 January 1980

nb

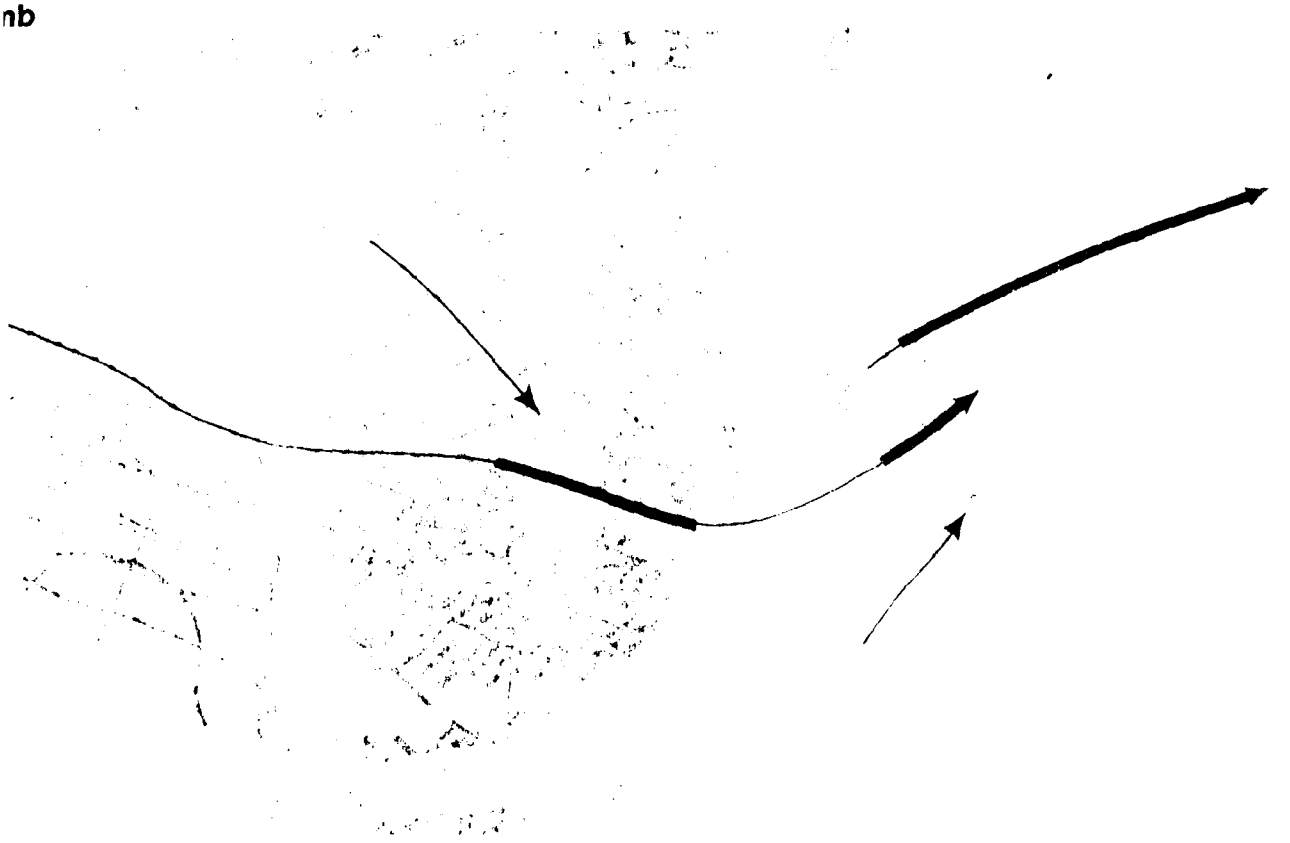

NMC 250 mb Analysis 1200 GMT 11 January 1980

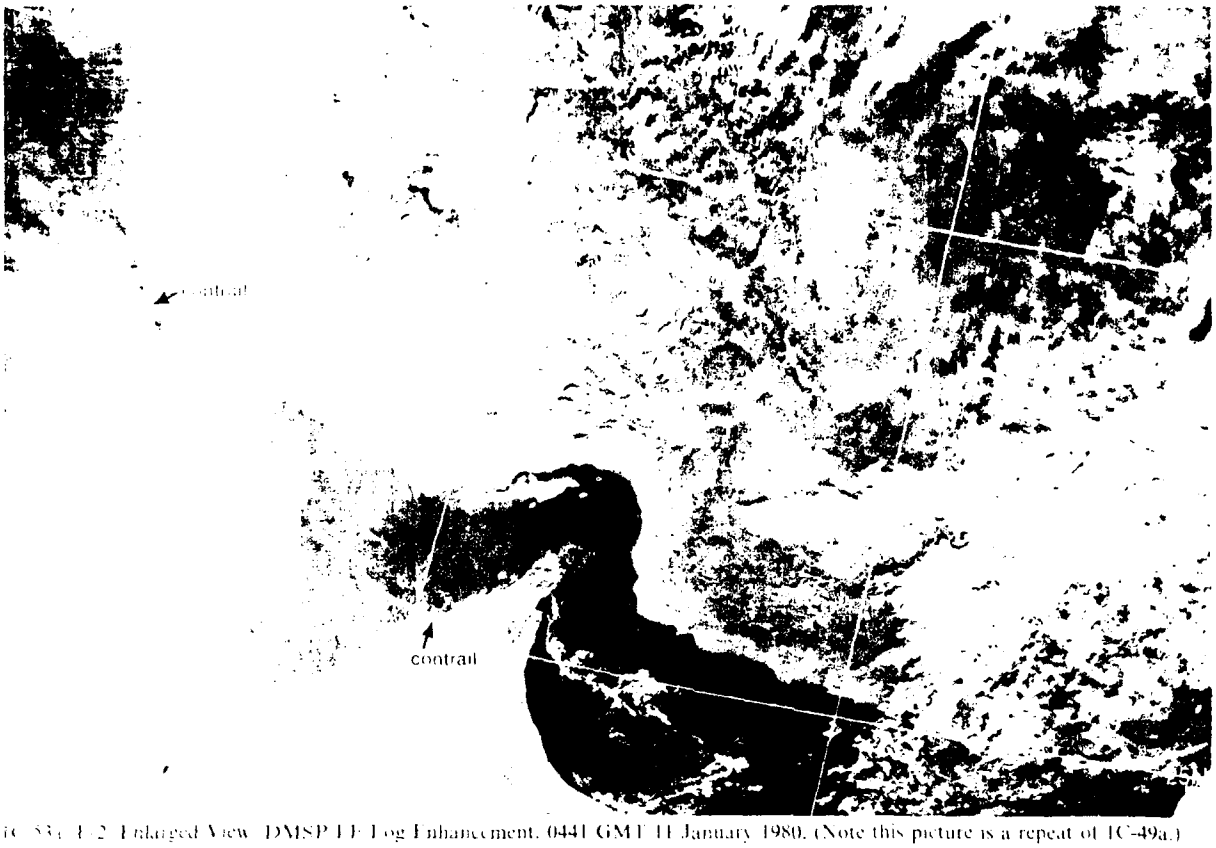

IC-53a, Fig. 2. Enlarged View. DMSP FE Log Enhancement. 0441 GMT 11 January 1980. (Note this picture is a repeat of IC-49a.)

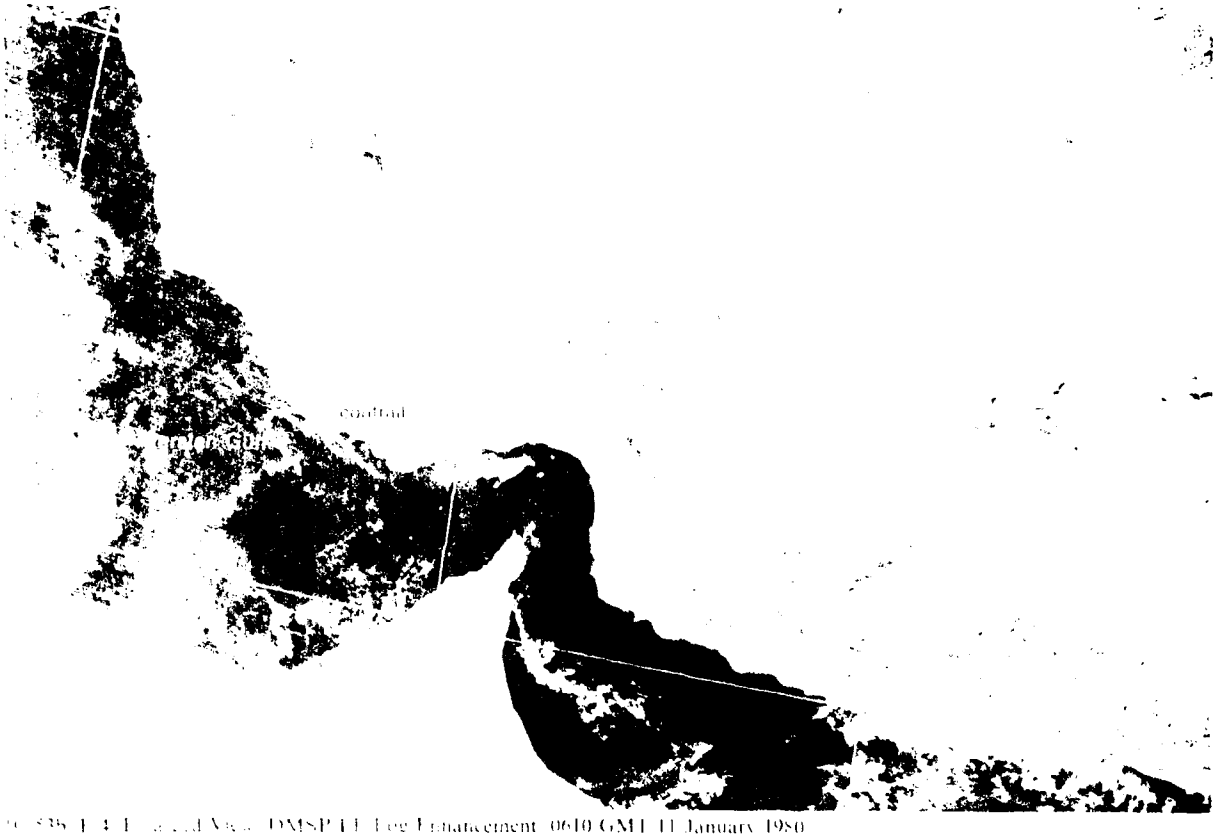

IC-53b, Fig. 3. Enlarged View. DMSP FE Log Enhancement. 0610 GMT 11 January 1980.

Case 1 Red Sea/Persian Gulf—Spring Transition

Desert Front

During winter and early spring, the polar front, referred to in the literature (NEPRF, 1980) as the desert front, is located over the northern Red Sea region. The desert front is frequently semi-stationary over this region during blocking periods over Western Europe. During such situations, meridional lows to the west and east of the block also tend to remain stationary. Under these conditions, the desert front may be strengthened periodically, as northerly flow around the low over the Balkans on the east side of the block directs surges of polar air southward into north Africa and the Middle East.

An intensification of the Balkan low or a movement of the low eastward can result in the desert front being pushed southward across the Red Sea, Arabian Peninsula, and the Persian Gulf region. Since merged polar and subtropical jet-force winds are often found through a deep layer on the southern portion of the polar low and in the baroclinic zone above the desert front, severe duststorm conditions may be spawned by terrain-induced turbulence produced by the jet-force winds coupling with the low-level polar surge flow.

Reference

NEPRF, 1980: Weather in the Indian Ocean to Latitude 30° S and Longitude 95° E including the Red Sea and Persian Gulf, Vol. 2, Part 1, NAVENVPREDRSCHFAC Technical Bulletin 80-02, Naval Environmental Prediction Research Facility, Monterey, Calif., 83 pp.

Red Sea/Persian Gulf
Spring Transition Case I

mb

Eaststorms Generated by the Desert Front

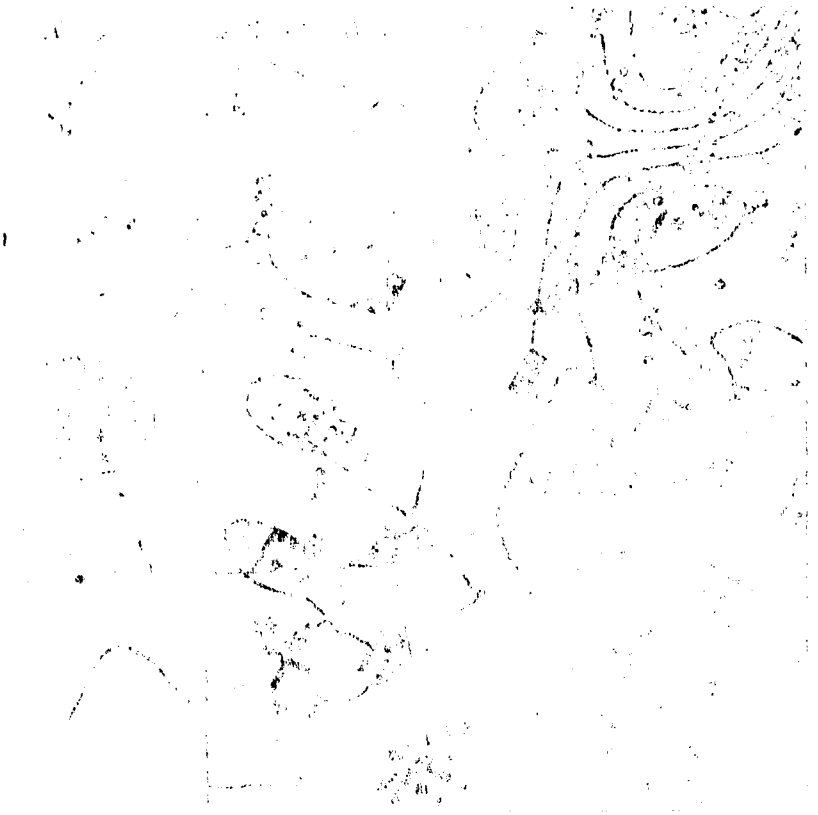

NMC 850 mb Analysis 1200 GMT 14 May 1979

mb

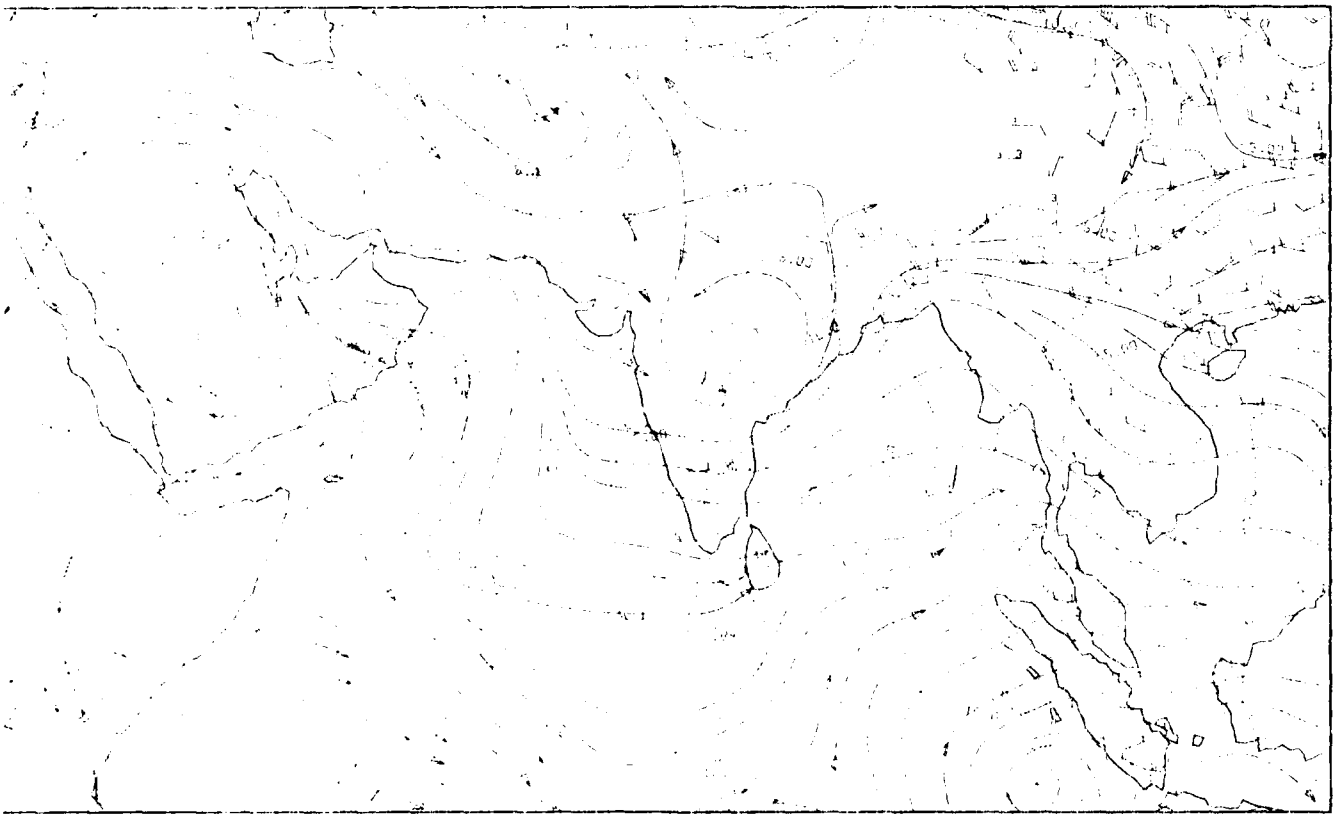

b MONEX 700 mb Analysis 1200 GMT 14 May 1979

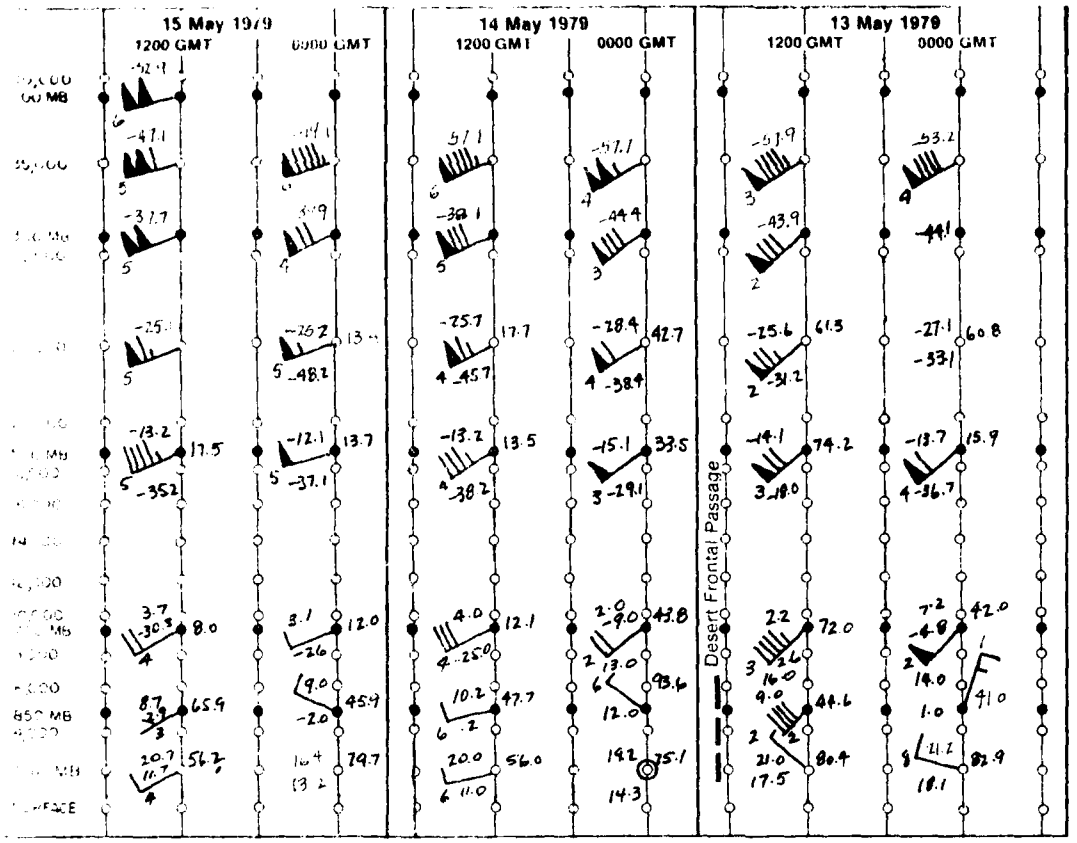

1D Etc. Time Section, Beirut, Lebanon.

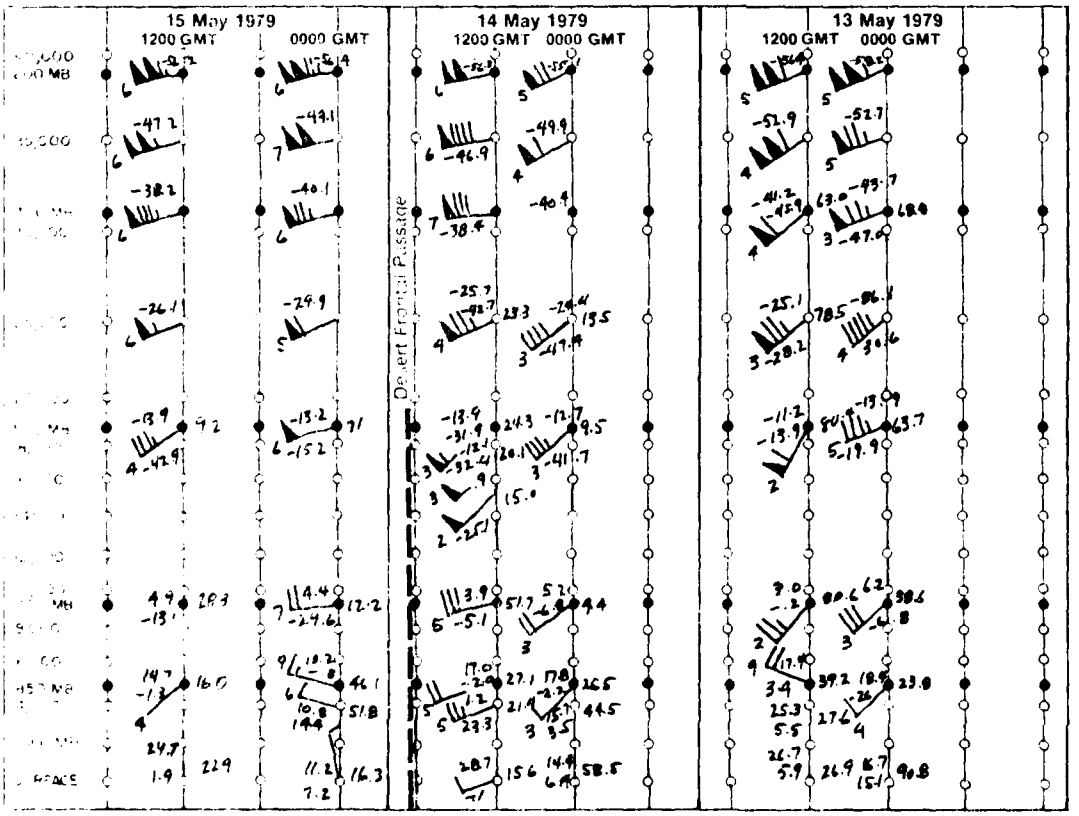

1D Std. Time Section, Damascus, Syria.

Red Sea, Persian Gulf
Spring Transition Case I

14 May

The NMC surface analysis for 1200 GMT (1D-10a) shows continued northerly flow in the eastern Mediterranean around the west side of the surface low **L1** over Turkey, which has remained essentially stationary and has intensified slightly from the previous day. In the Israel, Lebanon, Jordan, Syria region, northwesterly flow of 10-15 kt is reported, with several stations indicating suspended dust and haze in the area. The corresponding NMC surface streamline analysis (1D-10b) reveals suspended dust down to the northern region of the Persian Gulf, with some stations reporting obscured skies (dust). Freshening northerly flow is also shown west of the Red Sea, with numerous reports of suspended dust. An anticyclonic center is still indicated over Arabia, just west of the northern portion of the Persian Gulf. A couple of stations just north of this center are indicating light southeasterly flow, implying that the desert front is still to the north of this area.

The time section for Beirut, Lebanon (1D-11c) provides evidence of the desert front apparently passing this location. Passage of the front is suggested at Beirut between 1200 GMT 13 May and 0000 GMT 14 May. Passage at Damascus, Syria, as indicated in the time section for this station (1D-11d) occurred approximately 24 hours later.

The NMC 850-mb analysis (1D-11a) continues to show a low pressure center **L** over the Balkan region with a high pressure cell over Saudi Arabia. A packing of the isotherms over the Sinai Peninsula, and to the northeast and southwest of this region is still apparent. Air circulating around the base of the Balkan low then turns anticyclonically into the Persian Gulf. The nature of the anticyclonic circulation over Saudi Arabia is revealed on the MONEX 700 mb flow field (1D-11b), which shows strong winds entering the area from the eastern Mediterranean and turning anticyclonically into the Persian Gulf.

At 300 mb (1D-12a), a jet streak with winds over 100 kt is shown passing just north of the Sinai Peninsula. Conditions are favorable for duststorm generation by turbulent transfer of winds from upper levels to lower levels.

The METEOSAT visible picture (1D-12b) reveals that the cloud band associated with the desert front has moved southward, and extends from the southern Sinai Peninsula, across Saudi Arabia into northern Iraq. The front has broken up considerably in terms of total cloudiness, and not much weather of consequence is apparent in the visible picture over northern Saudi Arabia. However, the corresponding METEOSAT infrared picture (1D-13a) reveals cooler temperatures extending as a halo effect around the visible cloud forms. These cooler temperatures reflect the presence of raised dust in the frontal region. Note that the IR data does not suggest such cool temperatures over Egypt and Sudan where dust was also reported in the surface observations (1D-10b). This indicates that the dust in those areas was not widespread, or developed as that associated with the desert front.

Correlating the infrared METEOSAT data with the Damascus time section (1D-11d) shows that the winds at lower levels have increased in speed prior to frontal passage (14 May after 1200 GMT), due to transfer of momentum from aloft.

The METEOSAT water vapor data picture (1D-13b) reveals the broad westerly flow associated with the **STJ**, delineated by the dark (dry) slot on the northern edge of the **STJ**, and the region of convergence of this feature with the **PJS**. The position of the dry slot is shown on the 300-mb analysis (1D-12a), which also shows the jet stream convergence in that region.

14 May, continued on page 1D-14

ace

a. NMC Surface Analysis, 1200 GMT 14 May 1979.

ace

NMC Tropical Surface Streamline Analysis, 1200 GMT 14 May 1979

500 mb

Duststorms Generated by the Desert Front

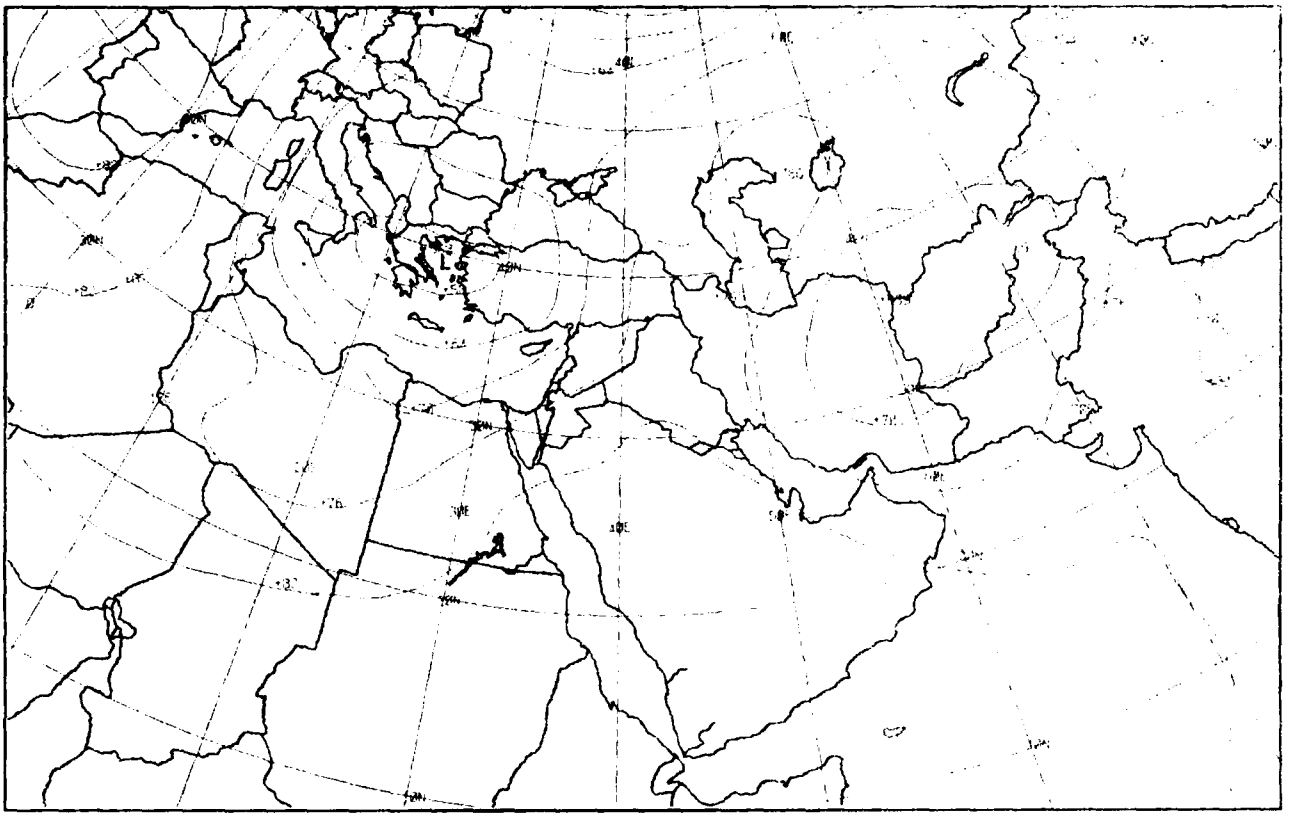

TD-9a. FNOC PE Initial 500-mb Analysis. 0000 GMT 13 May 1979.

500 mb

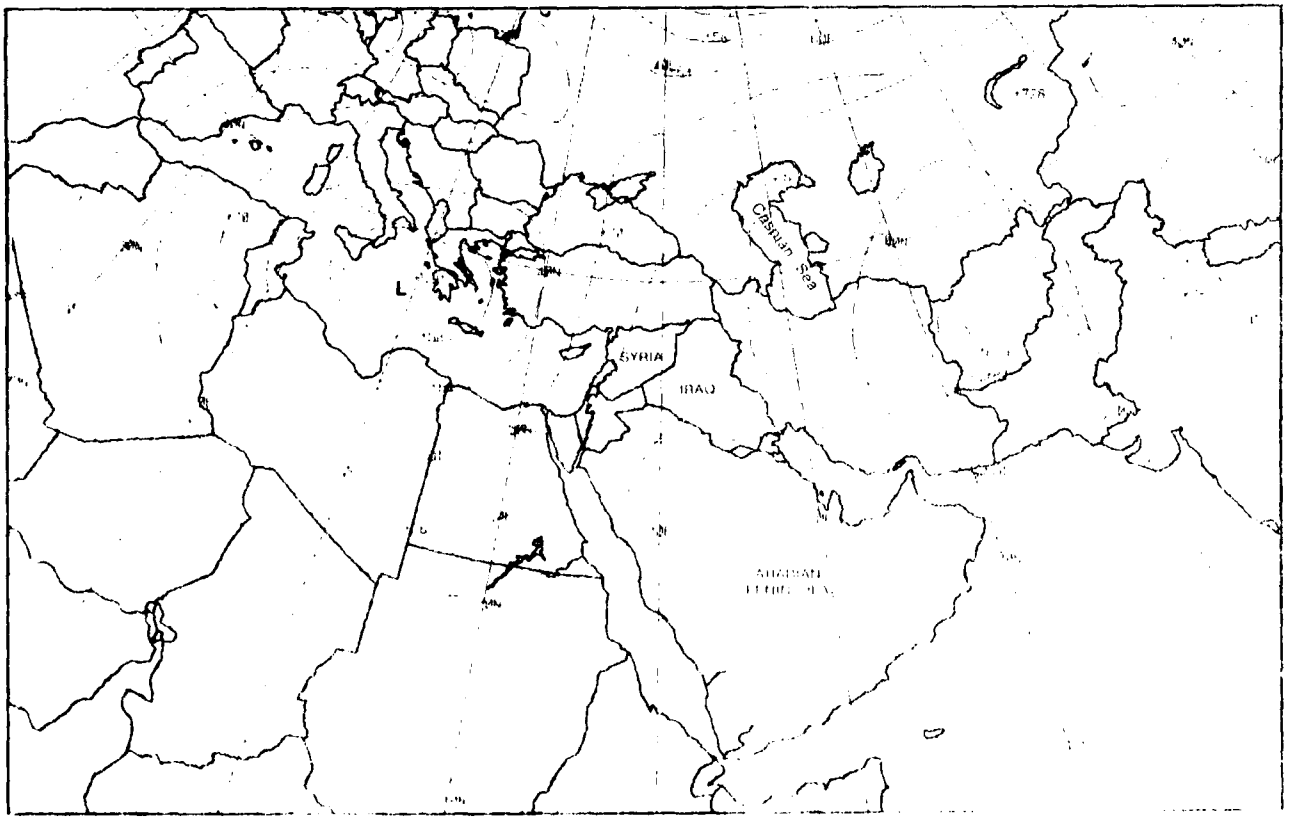

TD-9b. FNOC PE 36-hr 500-mb Prognosis. Valid 1200 GMT 14 May 1979.

surface

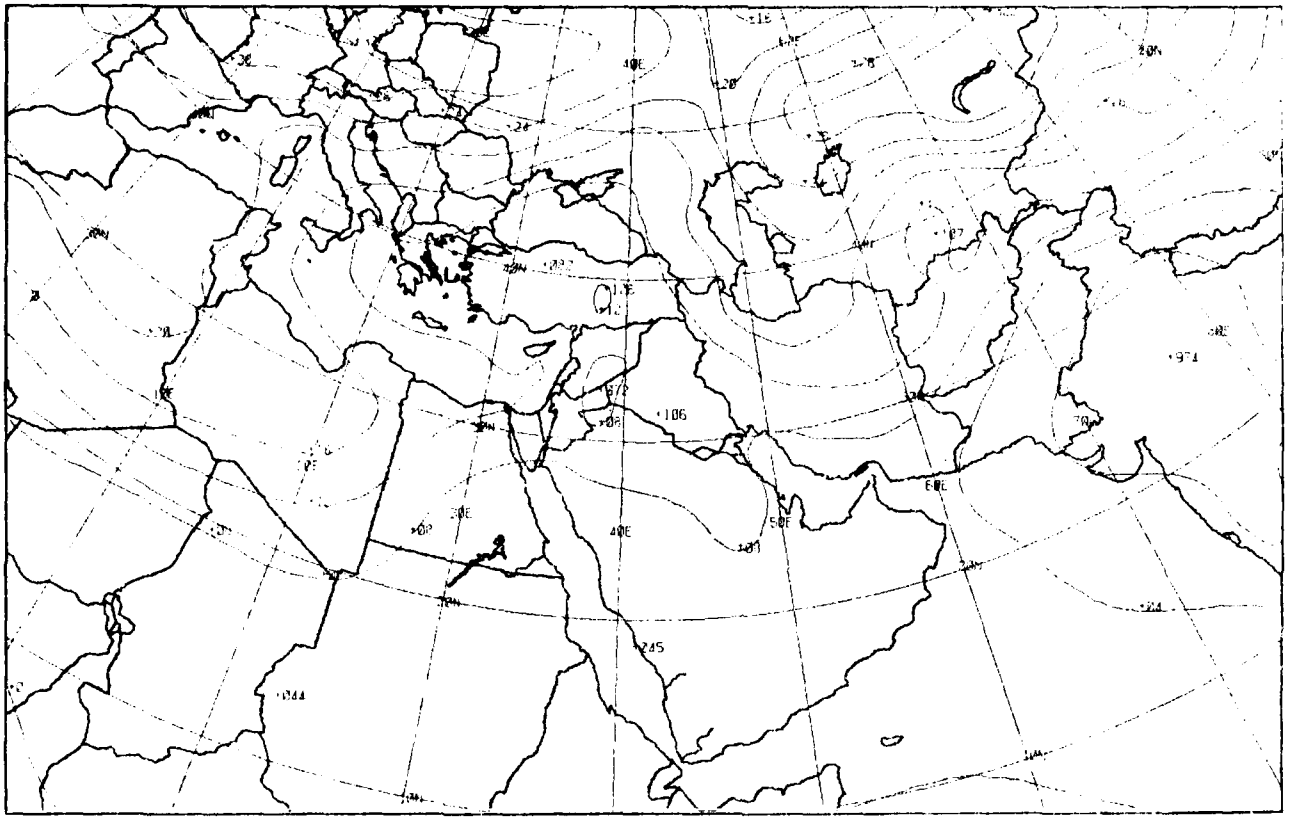

1D-8a. ENOC PE Initial Surface Analysis. 0000 GMT 13 May 1979.

surface

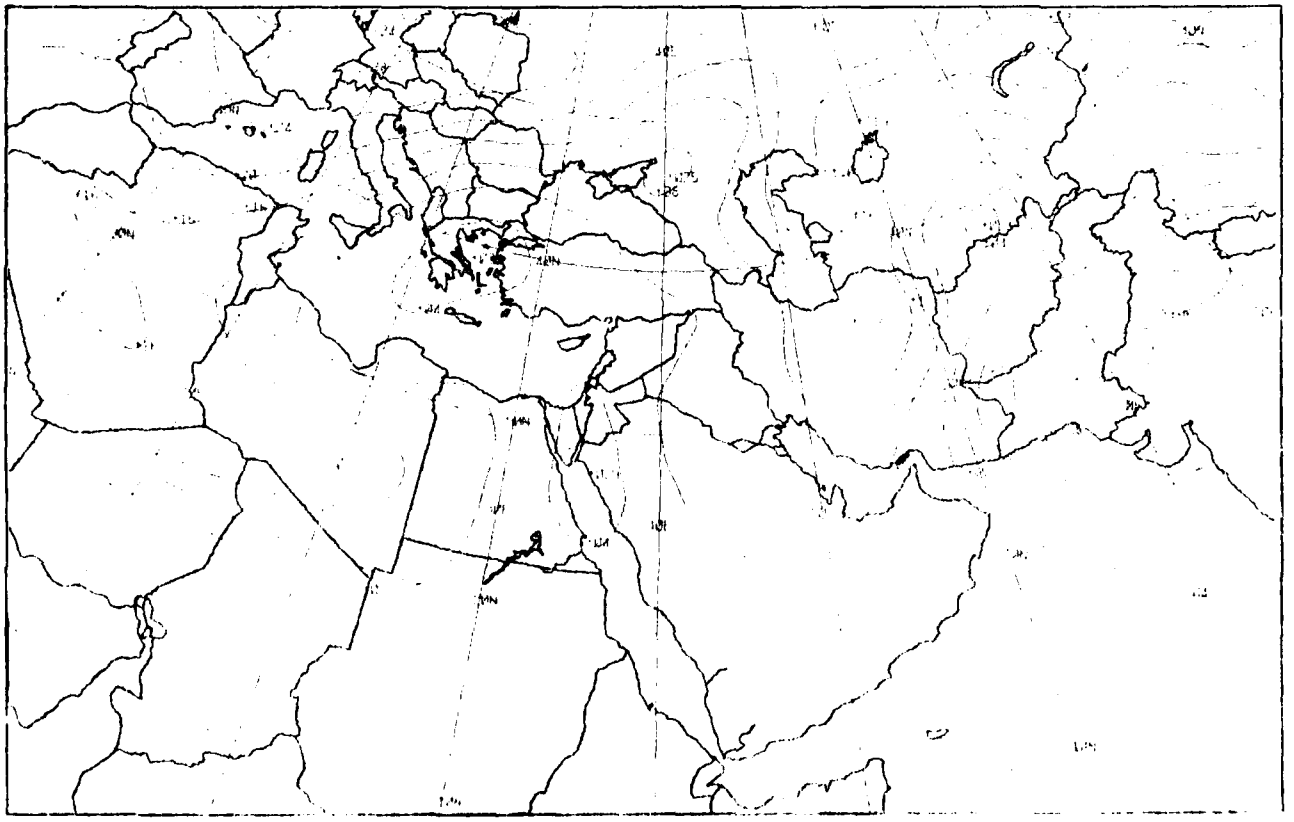

1D-8b. ENOC PE 36hr Surface Prognosis. Valid 1200 GMT 14 May 1979.

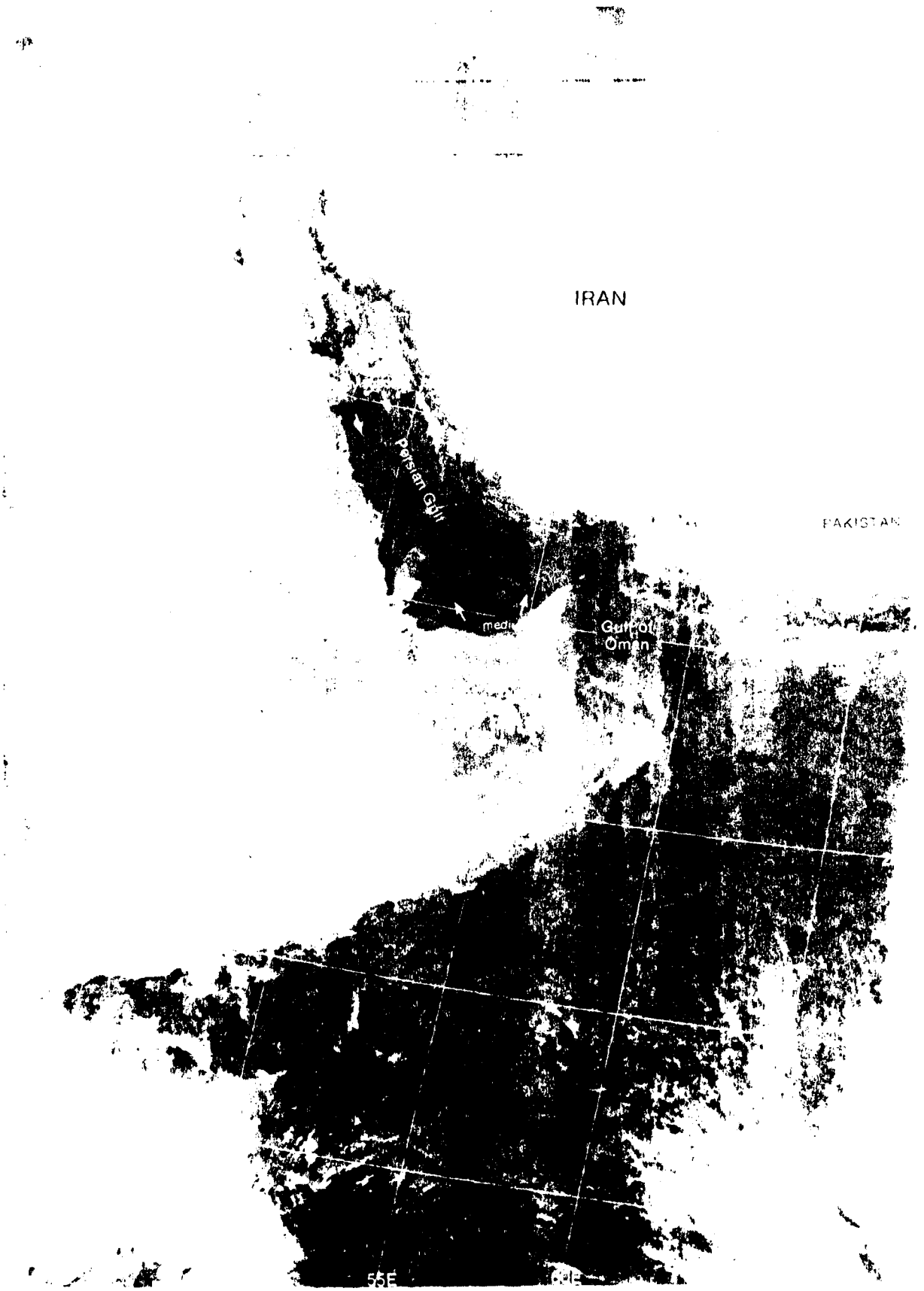

ID 2a. F-3 DMSP IR-1 Dust Enhancement 0243 GMT 11 May 1979

[illegible] DMSP [illegible] Data Collection [illegible] 0241 GMT [illegible] May 1979

Duststorms Generated by the Desert Front

ID 5a. GOES-Indian Ocean. Enlarged View. Visible Picture. 0730 GMT 13 May 1979

ID 5b. METEOSAT. Enlarged View. Water Vapor Picture. [illegible]

ED-4a METEOSAT Enlarged View, Visible Picture 1155 GMT 13 May 1979.

ED-4b METEOSAT Enlarged View, Infrared Picture 1155 GMT 13 May 1979.

850 mb

Duststorms Generated by the Desert Front

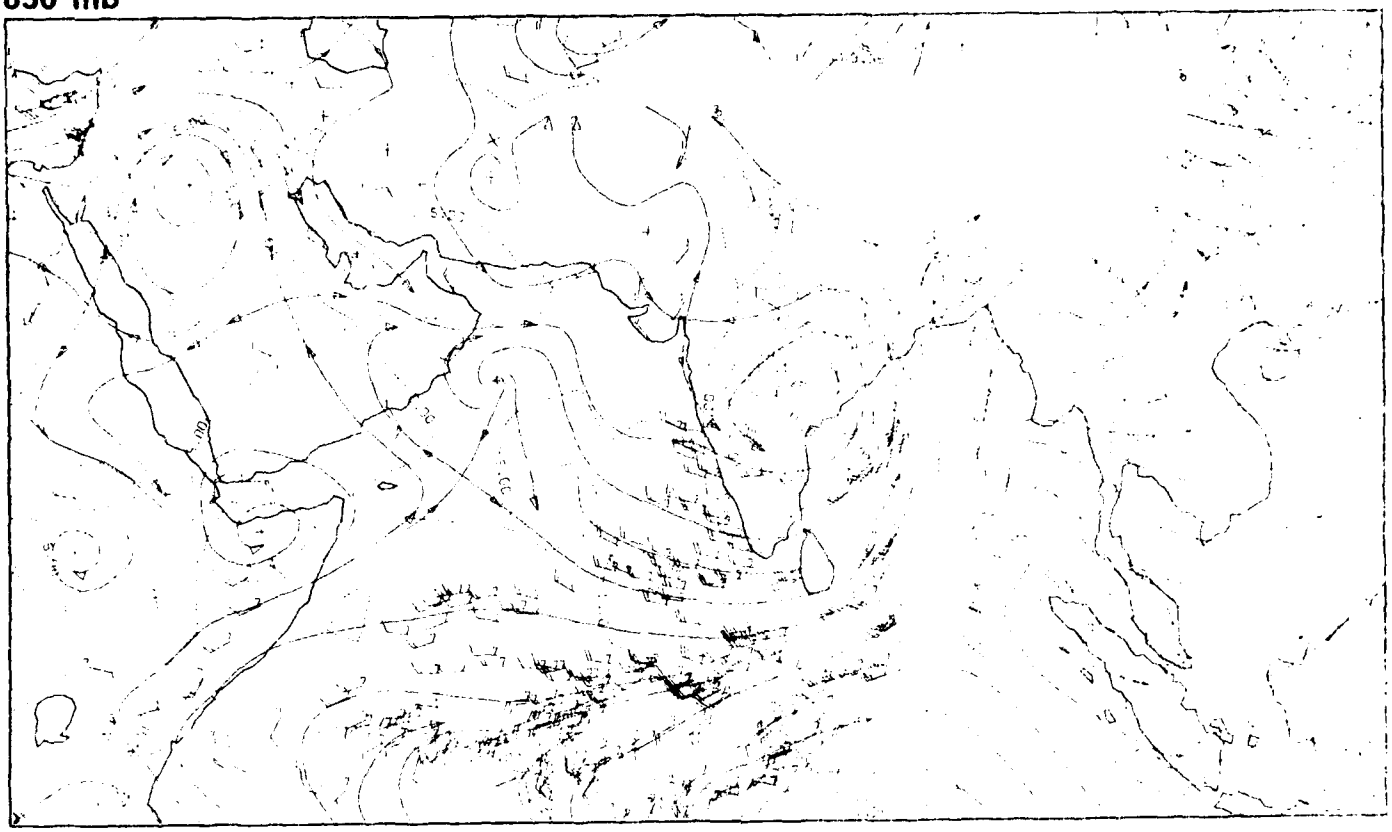

1D-3a. MONEX 850-mb Analysis, 1200 GMT 13 May 1979.

surface

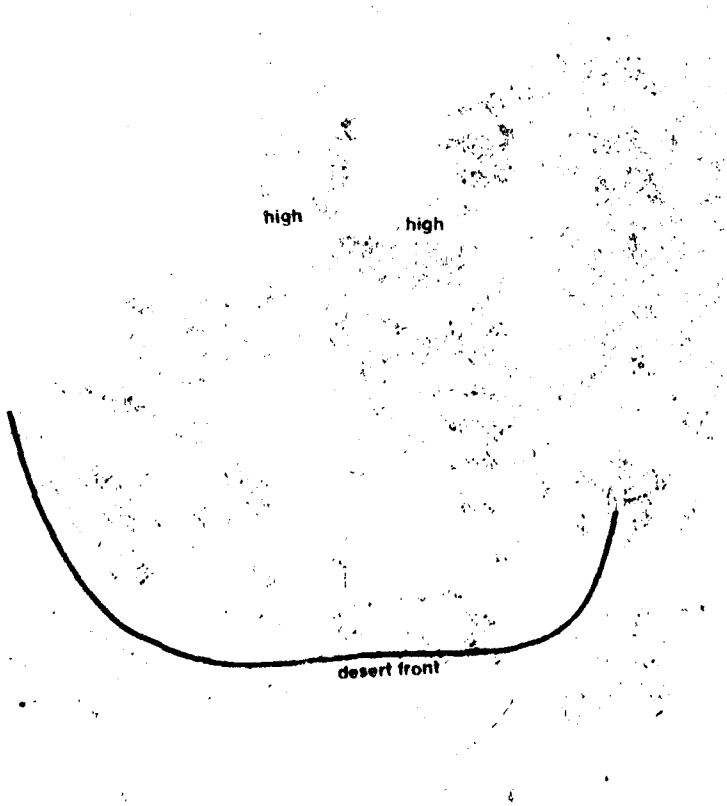

1D-3b. NMC Surface Analysis, 1200 GMT 13 May 1979.

Dust Storms Generated by the Desert Front
Arabian Peninsula
May 1979

13 May

The NMC surface analysis for 1200 GMT (1D-3b) shows a large high pressure cell over Western Europe, oriented from the northeast to the southwest. On the east side of the high, northerly winds flow southward across the Mediterranean into north Africa. Under this flow pattern, the desert front should be located between the northern near equatorial trough (NET) and the north African coastline.

The 850-mb analysis is useful in locating the position of the desert front, since the temperature contrast across the front is greater at levels above the surface. The NMC 850-mb analysis (1D-2b) shows a region of packed isotherms over the Sinai Peninsula, and to the northeast and southwest of the peninsula. The analysis also shows a closed low L over the Balkans, and a high pressure circulation over the Arabian Peninsula. The desert front lies between these two circulation features, in the region where the temperature gradient is the strongest. Note that winds of 40–60 kt are observed along the base of the Balkan low, indicating the potential for low-level turbulence and duststorm generation. The MONEX 850-mb flow field (1D-3a), shows in better detail the anticyclonic circulation over the northern Arabian Peninsula, with a flow of moderately strong northerly winds into the Persian Gulf.

On the NMC 300-mb analysis (1D-2a), a merger of the polar jet (**PJS**) and the subtropical jet (**STJ**) occurs near the Sinai Peninsula. The winds diverge downstream with one branch turning southward across the Persian Gulf and the other branch turning northward around the Balkan low. Such a strong wind configuration poses a strong potential for duststorm development over the Syrian desert, with advection of the dust southward over Iraq, Iran, and the Persian Gulf.

The METEOSAT visible picture at 1155 GMT (1D-4a) reveals cloud bands **A1–A1** which define the spiral vortex associated with the Balkan low and the active portion of the desert front over the Sinai Peninsula. Subtropical jet stream cirrus is observed [illegible] of the desert front over central Africa. This [illegible] is emphasized in the simultaneous METEOSAT infrared picture (1D-4b), which [illegible] cold cirrus temperatures and [illegible] features with excellent contrast against [illegible]

[illegible] METEOSAT water vapor picture (1D-5b) [illegible] circulation **A1–A1** [illegible] particular, the northern [illegible] cirrus and the desert [illegible] vapor to the north [illegible] defined by the dark [illegible] possible subsidence [illegible] shown on the 300-mb [illegible] area of convergence [illegible] PJS and the STJ. Such [illegible] vapor features [illegible] area of upper [illegible]

The GOES Indian Ocean visible picture for 0730 GMT (1D-5a) provides a view of the desert frontal cloud system. The picture confirms that there is no large-scale duststorm over the Red Sea or Persian Gulf. These pictures cannot be relied upon, however, to detect smaller scale dust advection because the resolution is inadequate to detect such small scale features.

The higher resolution DMSP visible picture at 0243 GMT (1D-6a), however, shows gray shades in the Persian Gulf which suggest dust in suspension. Note the clarity of the Zagros Mountains, as opposed to the surrounding regions. The clarity results from the fact that most of the higher elevations of the mountains are well above the dust and aerosol debris. The DMSP infrared picture (1D-7a) shows cool areas (medium gray shades) over the Persian Gulf, some of which may be attributable to long wave radiation from dust in the atmosphere. However, the fact that the Persian Gulf land boundaries are not obscured by this effect indicates that the dust at this time is not heavy or intense in character. Some sea surface temperature effects appear to be revealed in this picture; in particular, an apparent upwelling of cold water along the southern coast of Iran and Pakistan, extending eastward from the Gulf of Oman.

The FNOC 36-hr surface prognosis (1D-8b), based on the initial surface analysis (1D-8a), indicates that the low pressure is retained over the Balkan region, and that pressure will fall over the Sinai Peninsula and the northern Red Sea. A wedge of high pressure is shown building over the Persian Gulf region. The FNOC 36-hr 500-mb prognosis (1D-9b), based on the initial analysis (1D-9a), similarly, retains an almost stationary and slightly deeper low over the Balkans, with somewhat lower height contours extending over Saudi Arabia. A ridge extends northward from Iraq to the northern Caspian Sea. The flow pattern is such that any dust raised over the Syrian desert reaching this upper-level flow would be advected southeastward toward the Persian Gulf. The prognosis charts suggest some slight southward movement of the desert front into Syria, where duststorm conditions could be anticipated. A vigorous movement of the front into Saudi Arabia, however, appears unlikely.

continued on page 1D-1o

300 mb

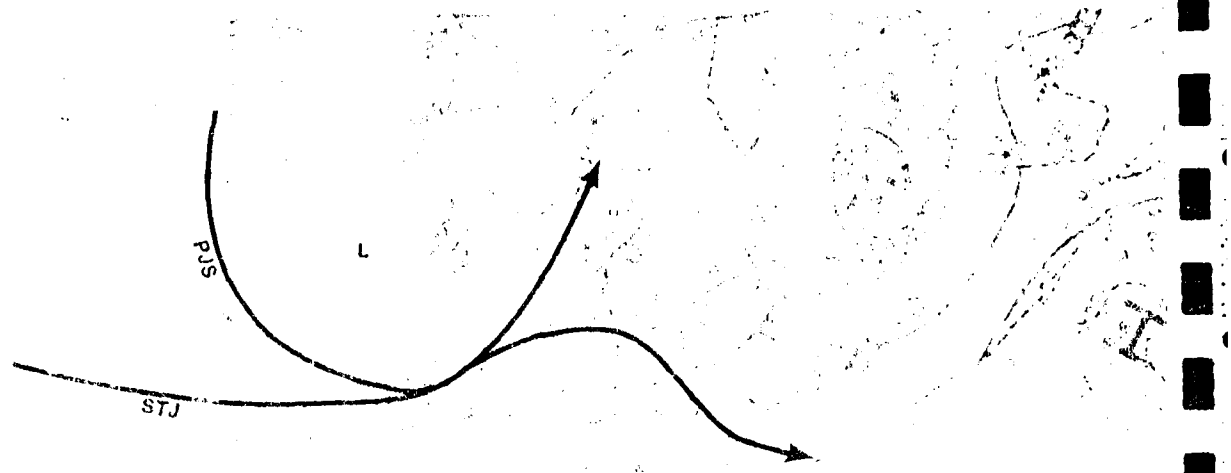

[illegible] NMC 300-mb Analysis 1200 GMT 13 May 1979

850 mb

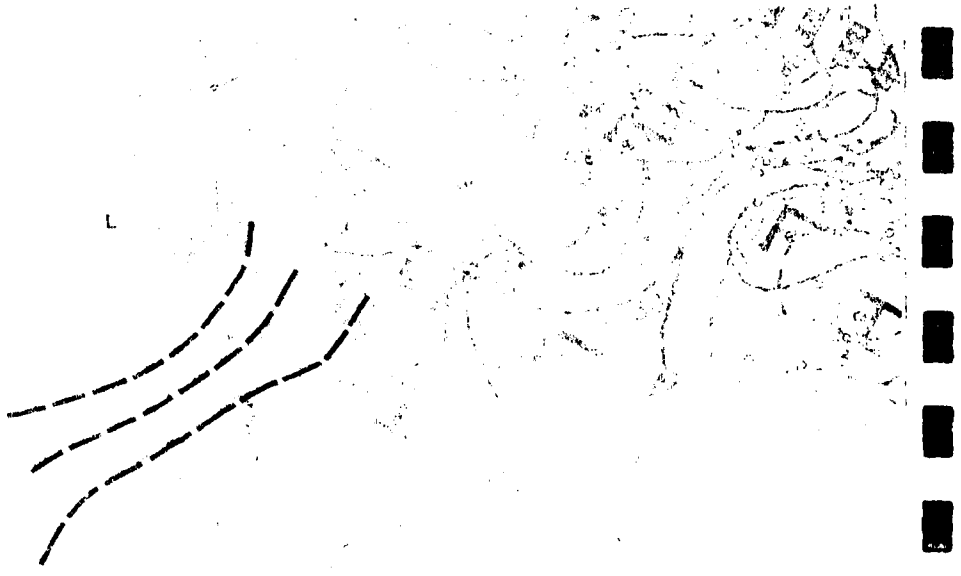

[illegible] NMC 850-mb Analysis 1200 GMT 13 May 1979

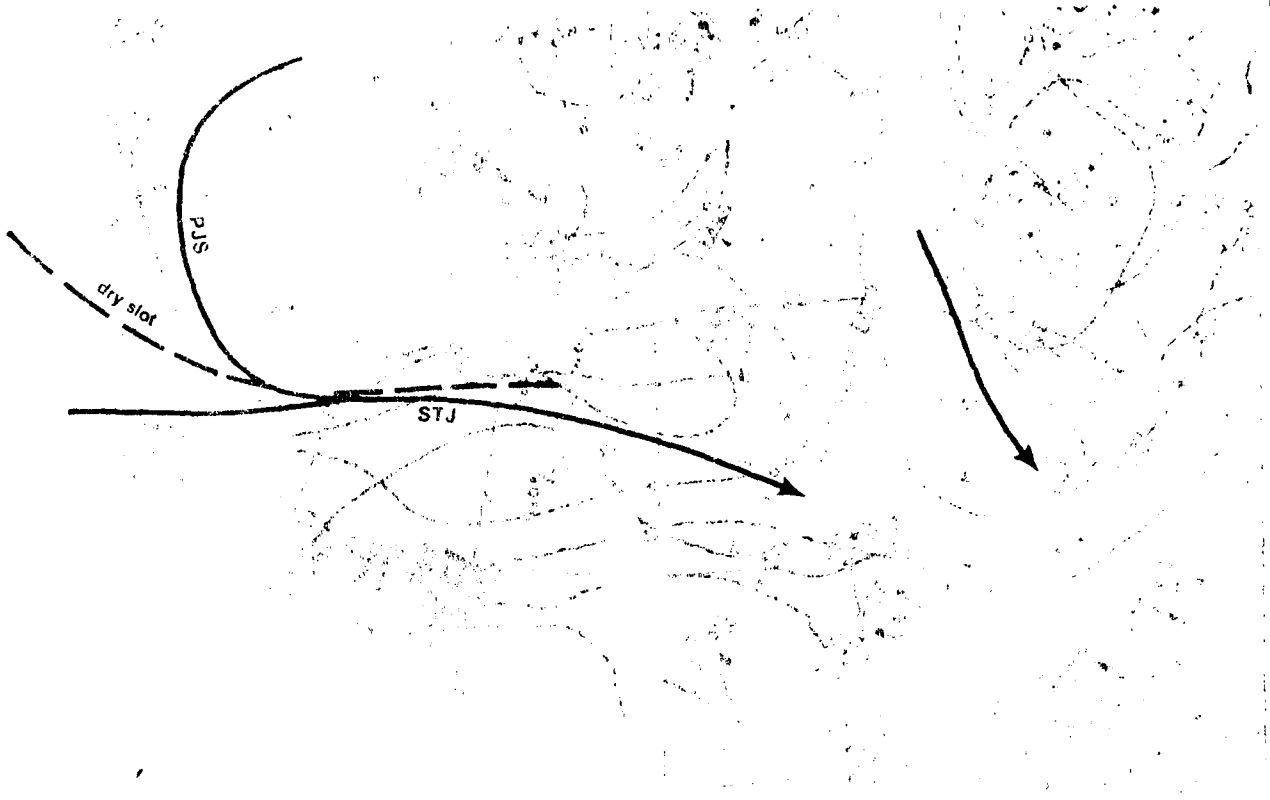

NMC [illegible] Valid [illegible] 1200 GMT 14 May 1979

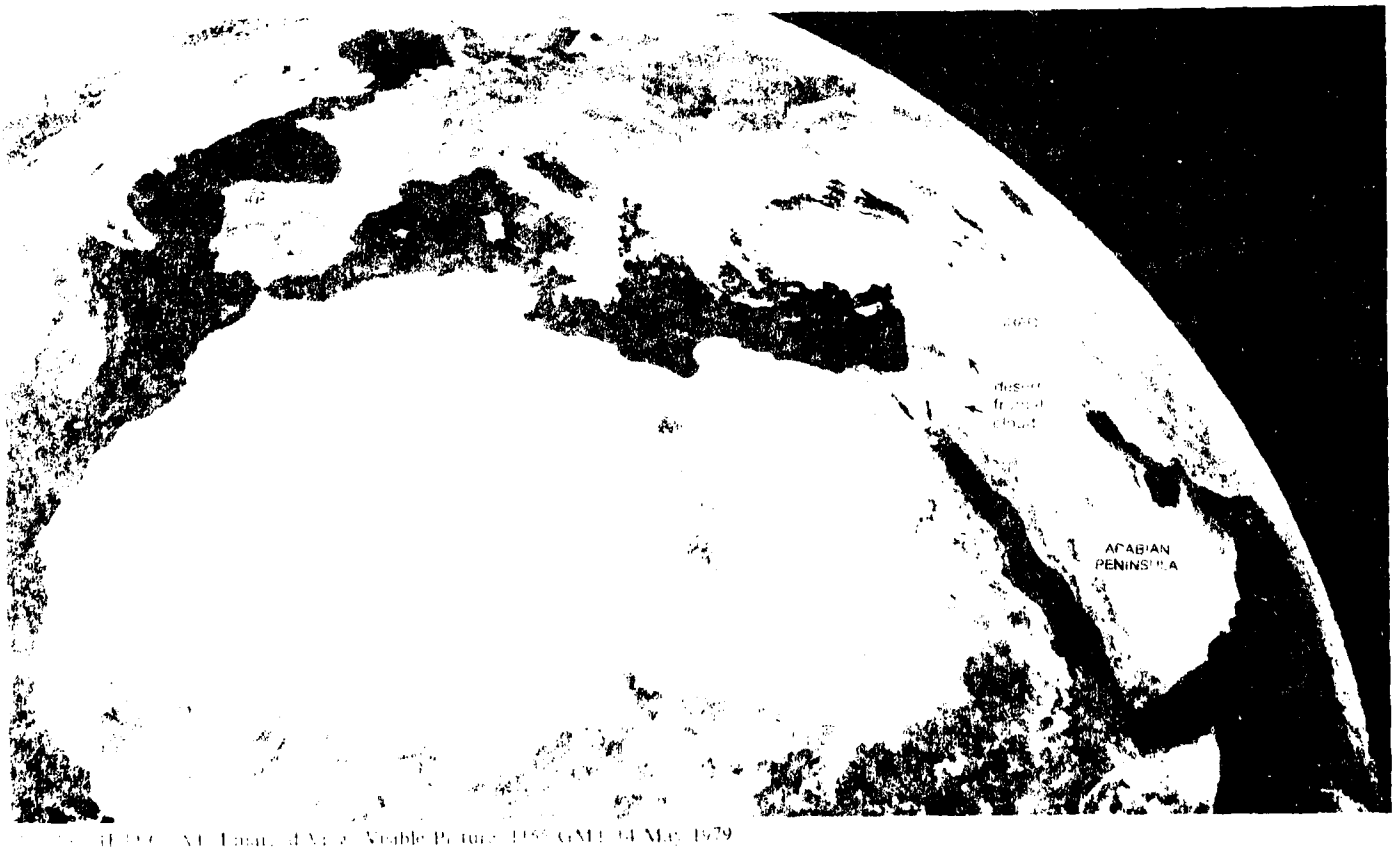

GOES-[illegible] Visible Picture 1145 GMT 14 May 1979

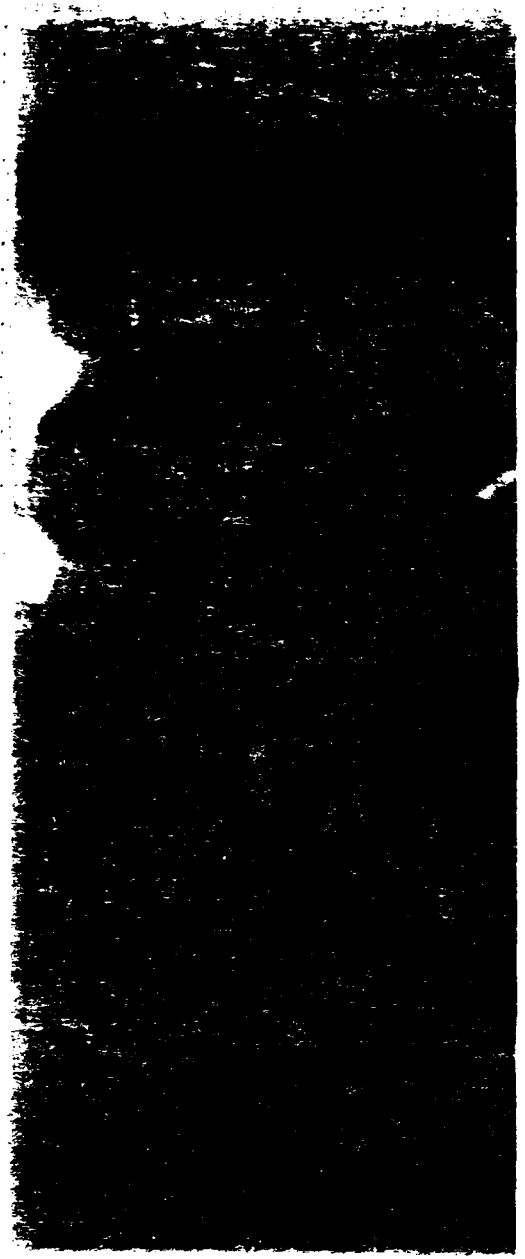

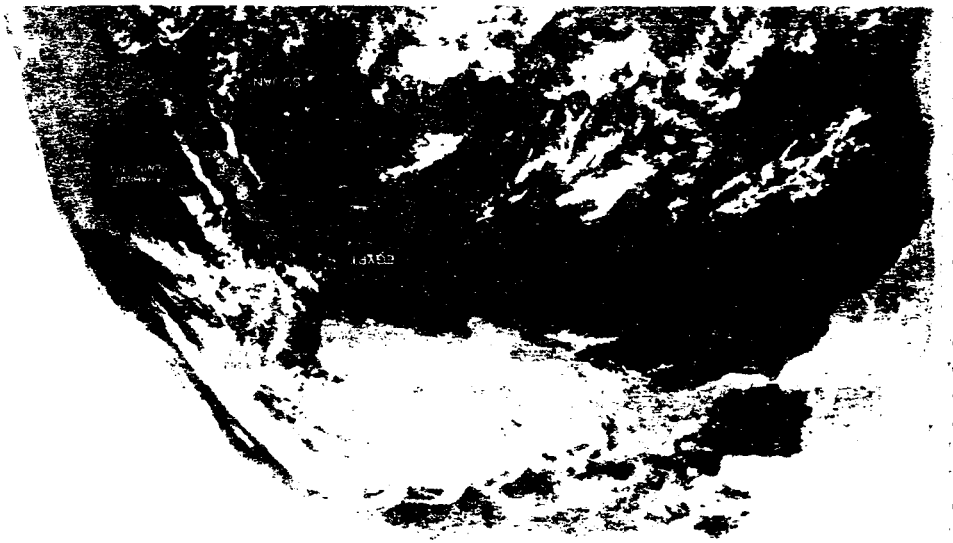

parent low to the north, which exhibits multiple centers and dense cloudiness covering a major portion of the Caspian Sea. Supercimposed surface observations reveal visibilities as low as 0.1 statute mile in obscured conditions, with a duststorm in progress in advance of the frontal band, just north of the Persian Gulf. A comparison of this image with that 24 hours earlier (1D-6a) reveals that many of the land, river, and lake features north of the Persian Gulf, which were clearly visible, have become obscured in the later pass. One useful but important change is the deteriorated contrast of the Zagros Mountain area in comparison to the previous view (1D-6a). This indicates that dust has been raised to and advected over the highest peaks in this region, reaching altitudes above 4,500 feet. The flow patterns at 850 mb and above (1D-11a, 11b, and 12a) favor such advection.

The DMSP infrared picture for 0223 GMT (1D-15a), however, indicates no pronounced obscurement of the Persian Gulf region, suggesting that most of this area is still free of extreme duststorm conditions.

It will be noted that the infrared pattern over the Persian Gulf varies from the previous view (1D-7a) in a non-uniform manner, indicating a difference in obscuring effects due to changed atmospheric conditions. A plume of dust water in the northern Persian Gulf and upwelling [illegible] the coast of Iran and Pakistan are common to both images, differentiating these oceanographic effects from those atmospherically-induced.

A comparison of the FNOC surface analysis at 1200 GMT (1D-16a), with the 36-hr prognosis valid at 1200 GMT (1D-16b), reveals that the movement of the desert front in its connection to the Balkan low was not well forecast. Whereas the analysis shows a trough along 40° E, the prognosis holds the trough back in the region from S[illegible] to the Caspian Depression. About 30° further [illegible] the prognosis [illegible]

[illegible]

A similar comparison of the FNOC surface analysis at 1200 GMT (1D-17a), with the 36-hr prognosis valid at 1200 GMT (1D-17b), also shows that the low was forecast to remain further west of its actual position by about 10° of longitude. The overall pattern, however, was forecast quite well, showing a ridge between low centers at [illegible] between 30° N and 40° N. It is apparent that [illegible] were associated with [illegible] and the area of duststorm generation over this date. Neither the 36-hr prognoses, nor the actual [illegible]

1D-11a, 12a. DMSP [illegible]

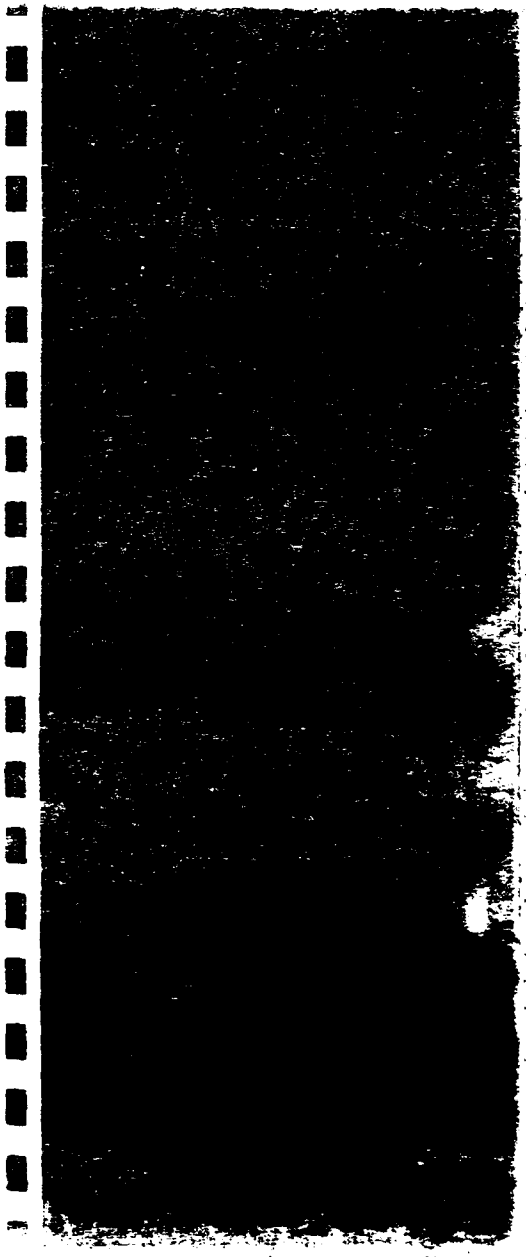

Duststorms Generated by the Desert Front

ID-15. U.S. DMSP IR Exploitation Enhancement 0223 GMT 14 May 1979.

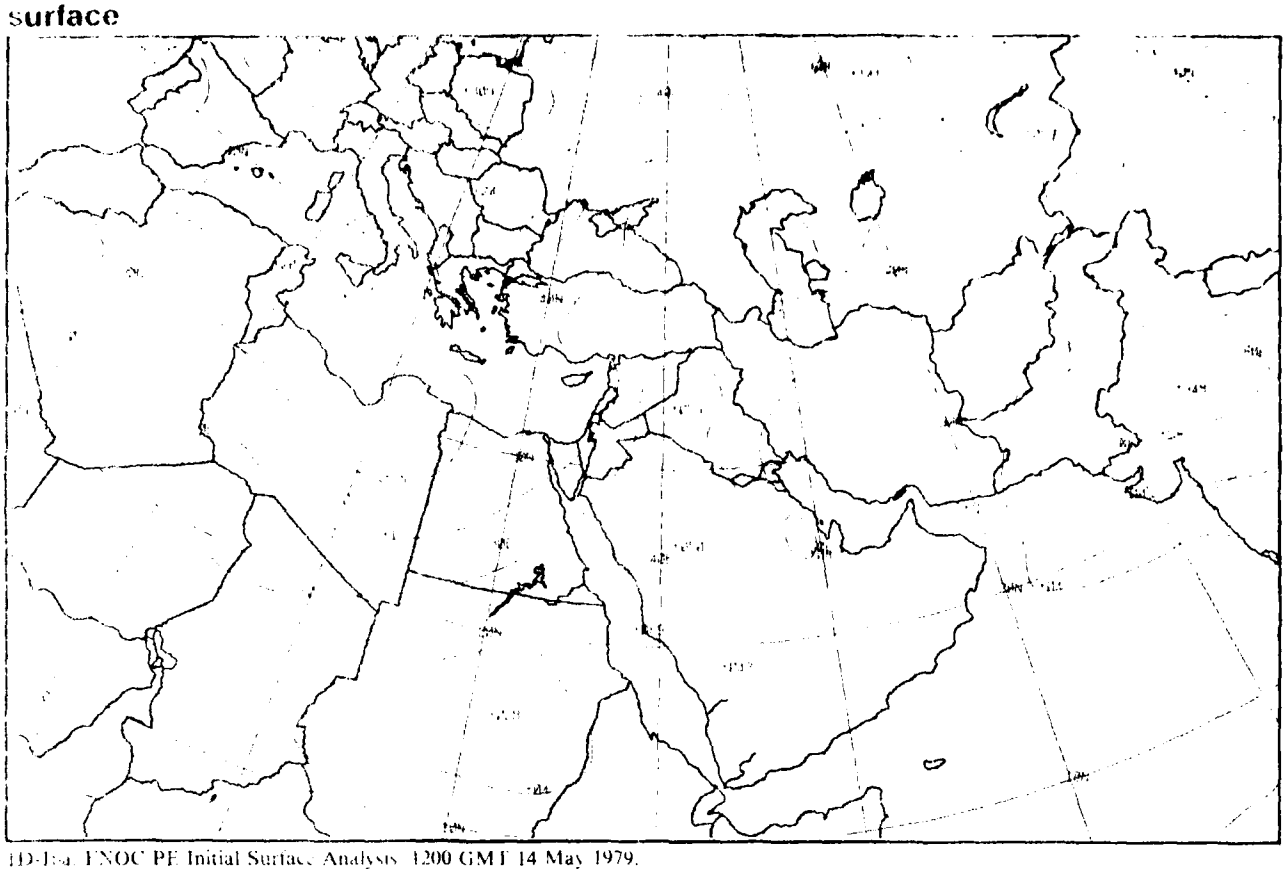

1D-15a. FNOC PE Initial Surface Analysis 1200 GMT 14 May 1979.

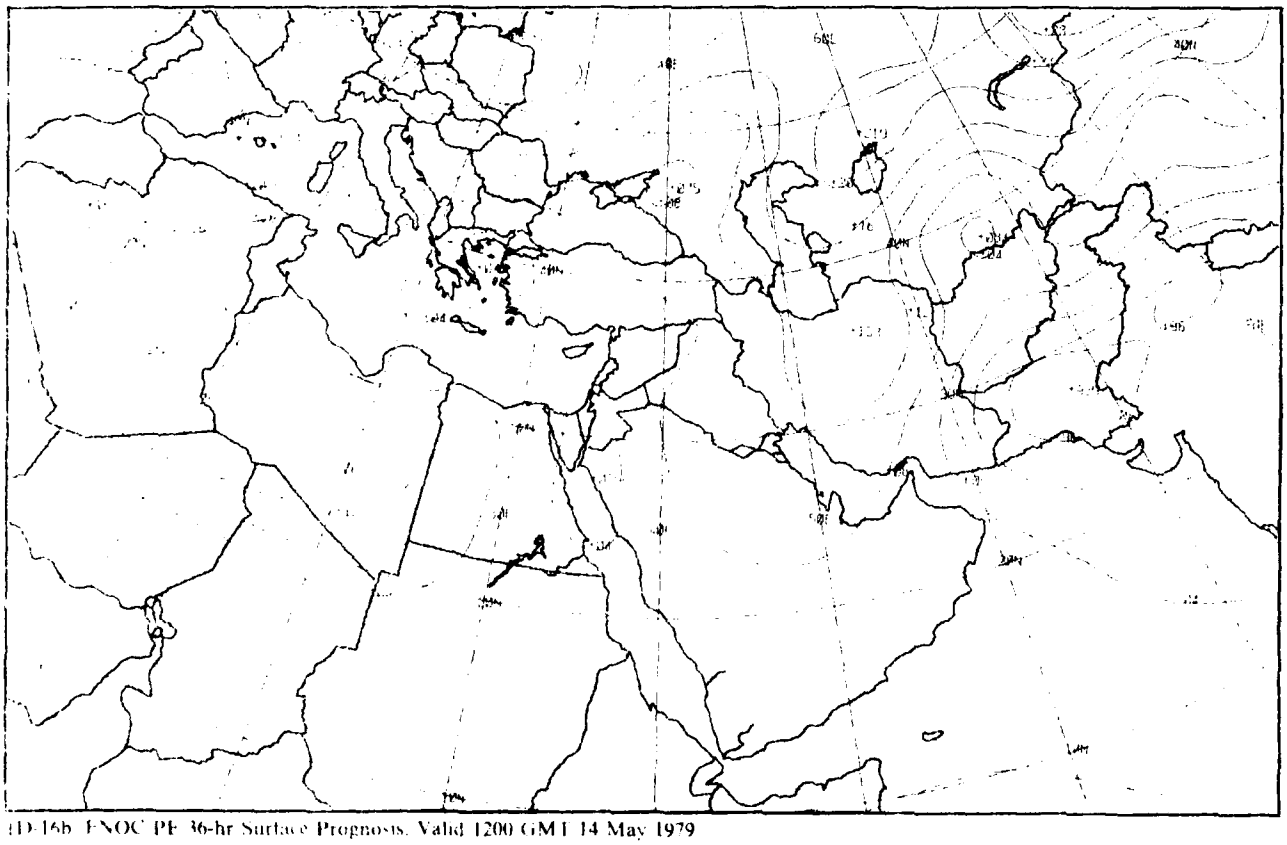

1D-16b. FNOC PE 36-hr Surface Prognosis. Valid 1200 GMT 14 May 1979

surface

1D-18a. NMC Surface Analysis. 1200 GMT 15 May 1979.

surface

1D-18b. NMC Tropical Surface Streamline Analysis. 1200 GMT 15 May 1979.

Duststorms Generated by the Desert Front

500 mb

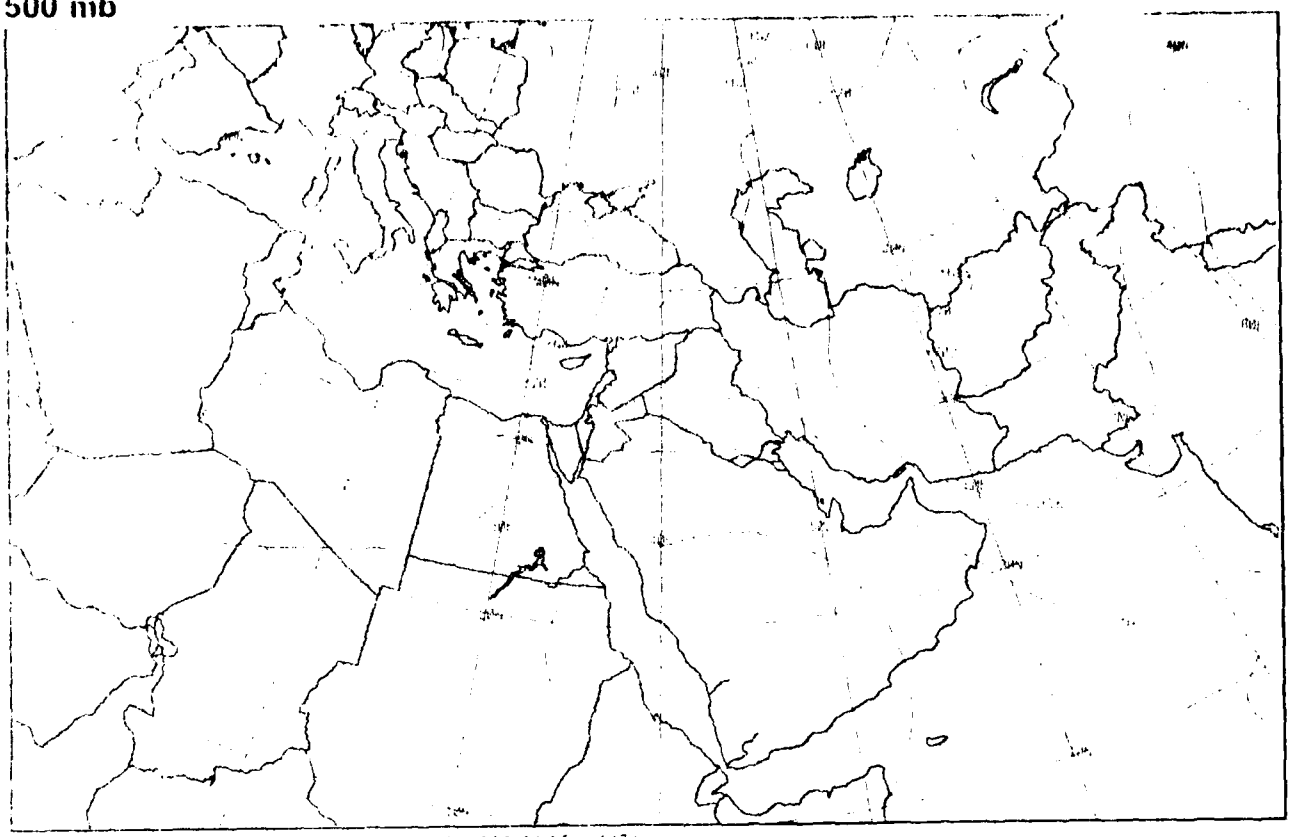

ID-17a ENOC PE Initial 500-mb Analysis, 1200 GMT 14 May 1979

500 mb

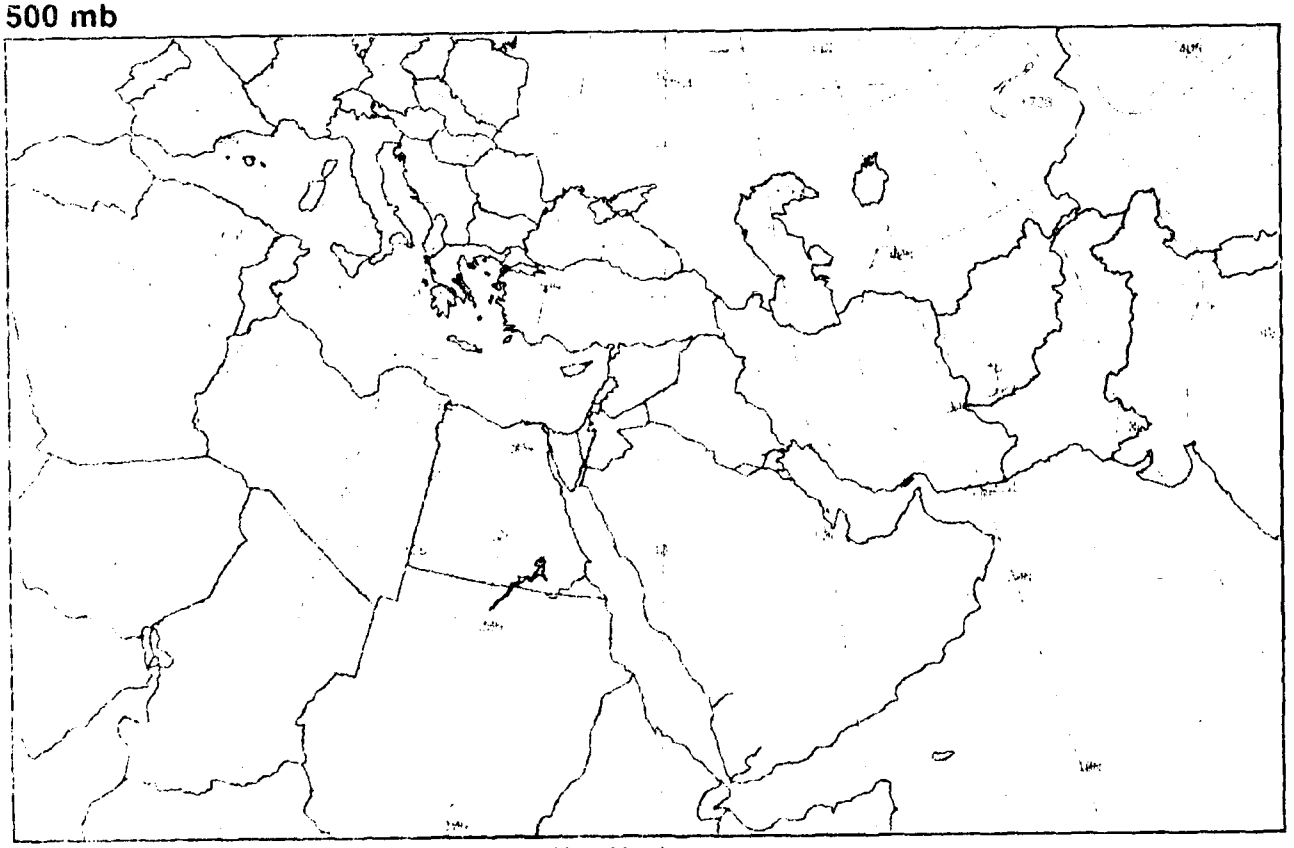

ID-17b ENOC PE 36-hr 500-mb Prognosis Valid 1200 GMT 14 May 1979

15 May

The NMC surface analysis at 1200 GMT (1D-18a) indicates that the low pressure center **L1** has moved eastward to the eastern portion of the Caspian Sea. Northerly polar flow continues to be directed southward around this center and in the region between this center and the high pressure cells to the west. The NMC surface streamline analysis (1D-18b) shows a cyclonic center **L1** north of the Persian Gulf over southern Iraq with abundant reports of dust in that region. Northerly winds are seen to extend to the southern Red Sea region and then turn cyclonically around a trough which crosses Saudi Arabia from the southwest to the northeast.

At 850 mb (1D-19a), a packing of isotherms continues to be shown in the northern Red Sea region. A trough **T1** extends from a low west of the Caspian Sea to the central portion of the Red Sea. The MONEX 850-mb flow field (1D-19b), shows the extension of westerly mid-latitude flow into central Saudi Arabia, as compared to 1D-3a when the desert front was still well to the north.

The 300-mb analysis (1D-20a) continues to show strong jet-force westerly winds crossing north of the Sinai Peninsula and turning anticyclonically into the Persian Gulf.

The METEOSAT visible picture at 1155 GMT (1D-20b), reveals a hazy streak (dust) extending across Saudi Arabia into southern Iraq, a few degrees south of the cloud band position shown in the visible picture on the previous day (1D-12b). The METEOSAT infrared picture (1D-21a), shows cooler temperatures over the region from the eastern Mediterranean into northern Saudi Arabia, and particularly over the region of southern Iraq. Cirrus plumes associated with the **STJ** are seen turning anticyclonically over north Africa.

These plumes and associated mid-tropospheric water vapor are shown in the METEOSAT water vapor picture (1D-21b). Again the area of the merger of the **PJS** and **STJ** is shown by the dry (dark) slot on the north side of the **STJ** cirrus. The darkest region in the western portion of the image coincides with the region where confluence of the respective jet streams is most pronounced, as shown in the 300-mb analysis (1D-20a).

The DMSP visible picture (1D-22a), approximately four hours prior to the METEOSAT imagery, also reveals the dust plume extending across Saudi Arabia into southern Iraq. The surface reports and streamlines superimposed on the DMSP image (1D-23a) clearly reveal the low over southern Iraq, where the Euphrates River and nearby lakes are seen to be obscured by the dust plume. The trough associated with the southward movement of the desert front is also clearly defined extending from southern Iraq into the Tokar Gap region of Sudan. Note the typically strong northerly winds in the northern Red Sea following the desert front, giving rise to localized dust production in adjacent areas.

The corresponding DMSP infrared picture (1D-23b) demonstrates the important capability of detecting the denser portion of the dust plume over southern Iraq which could seriously affect land and air operations in that area. Confirmation of strong winds in this region are shown by wave clouds in and near the dust plume.

Important Conclusions

1. Satellite data correlated with conventional surface and upper-air observations are required to detect the movement of the desert front and the region and extent of duststorm production. Numerical prognoses and conventional analyses in themselves do not provide the required accuracy or information content necessary to resolve and predict such occurrences.

2. Water vapor imagery provides useful information on jet stream location. Confluence of the **PJS** with the **STJ** can be detected as a dry (dark tone) slot in water vapor imagery.

3. GOFS imagery and imagery from other geostationary satellite systems of similar resolution are inadequate in terms of resolving light suspended dust in the atmosphere, readily detected by higher resolution systems such as DMSP.

4. Heavy or intense dust in the atmosphere is detectable as a cool or cold area in DMSP infrared data which will result in the obscurement of land-sea boundaries. Light dust in suspension is detectable but does not obscure land-sea boundaries.

5. Time sections for Beirut, Lebanon, and Damascus, Syria, based on RAOB data, are useful to maintain for detection of movement of the desert front past those locations and for evidence of strong winds at low elevations that could create severe duststorm conditions capable of affecting operations in the region over and surrounding the Persian Gulf.

6. Dust in the atmosphere over mountain ranges results in subdued contrast in satellite visible imagery thereby providing a means to detect such an effect when compared to earlier-obtained clear sky views.

7. Strong northerly winds should be anticipated in the Red Sea and Persian Gulf following a southward movement of the desert front through that region.

300 mb

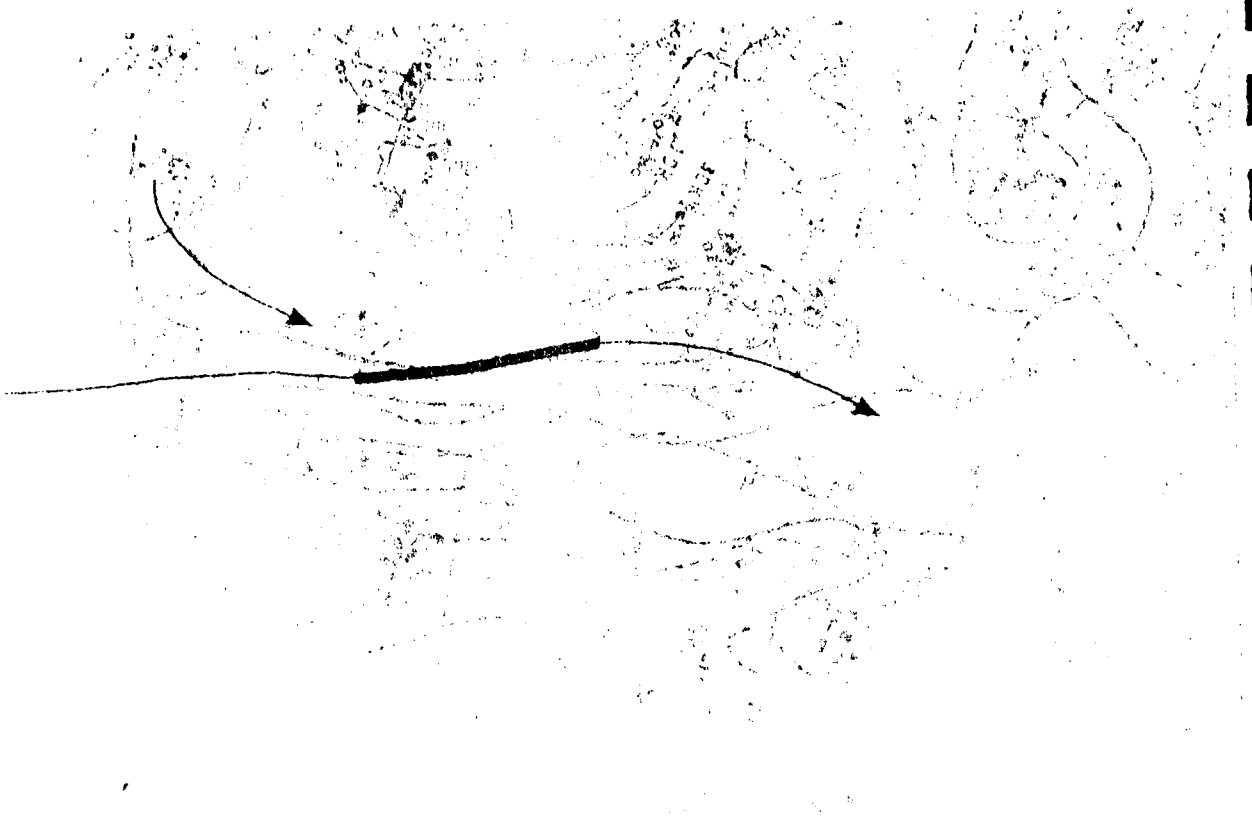

[illegible] SMS Second Anniversary Picture GMT 15 May 1979

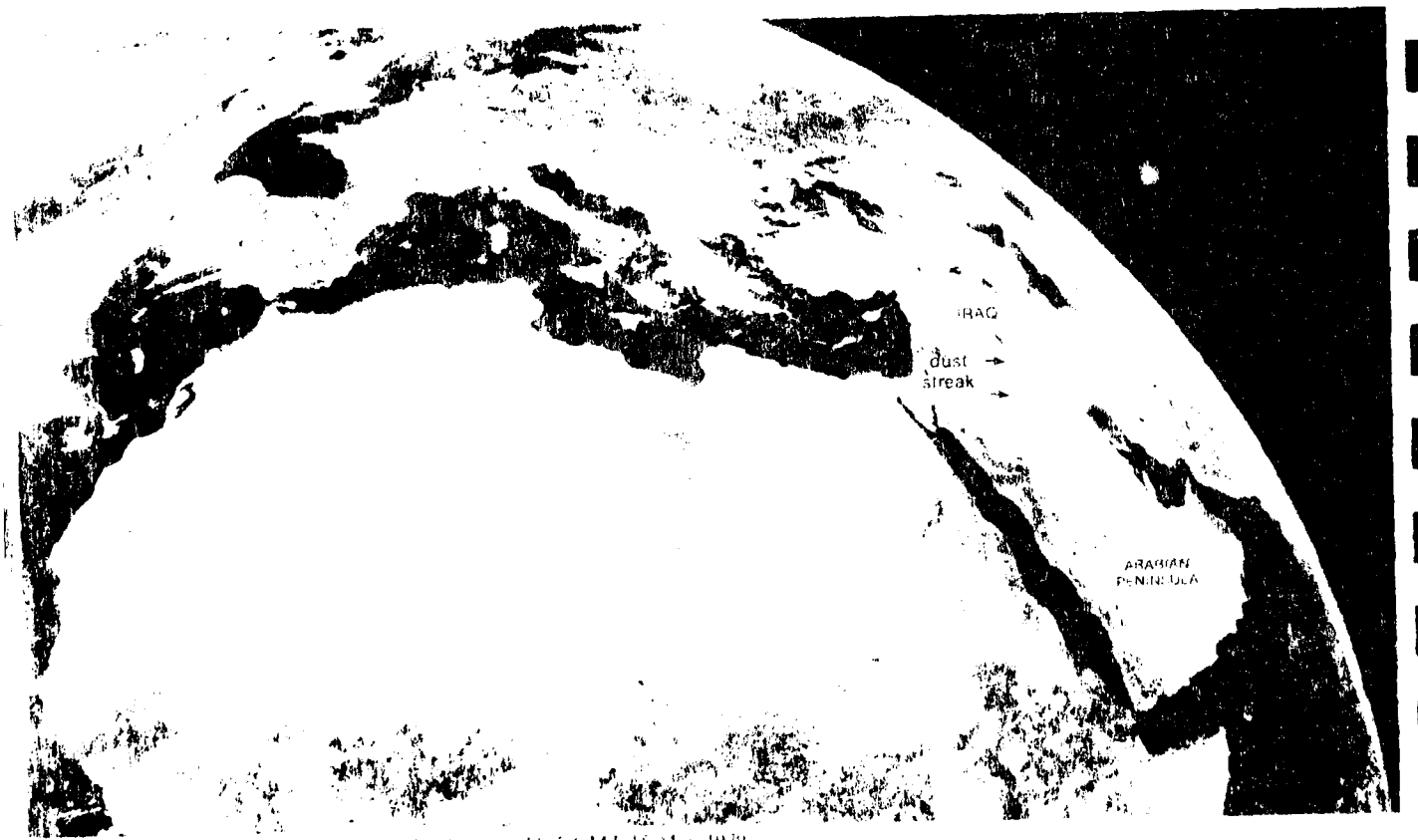

[illegible] METEOSAT Enlarged View Visible Picture GMT 15 May 1979

850 mb

ID-3a. NMC 850-mb Analysis, 1200 GMT 15 May 1979.

850 mb

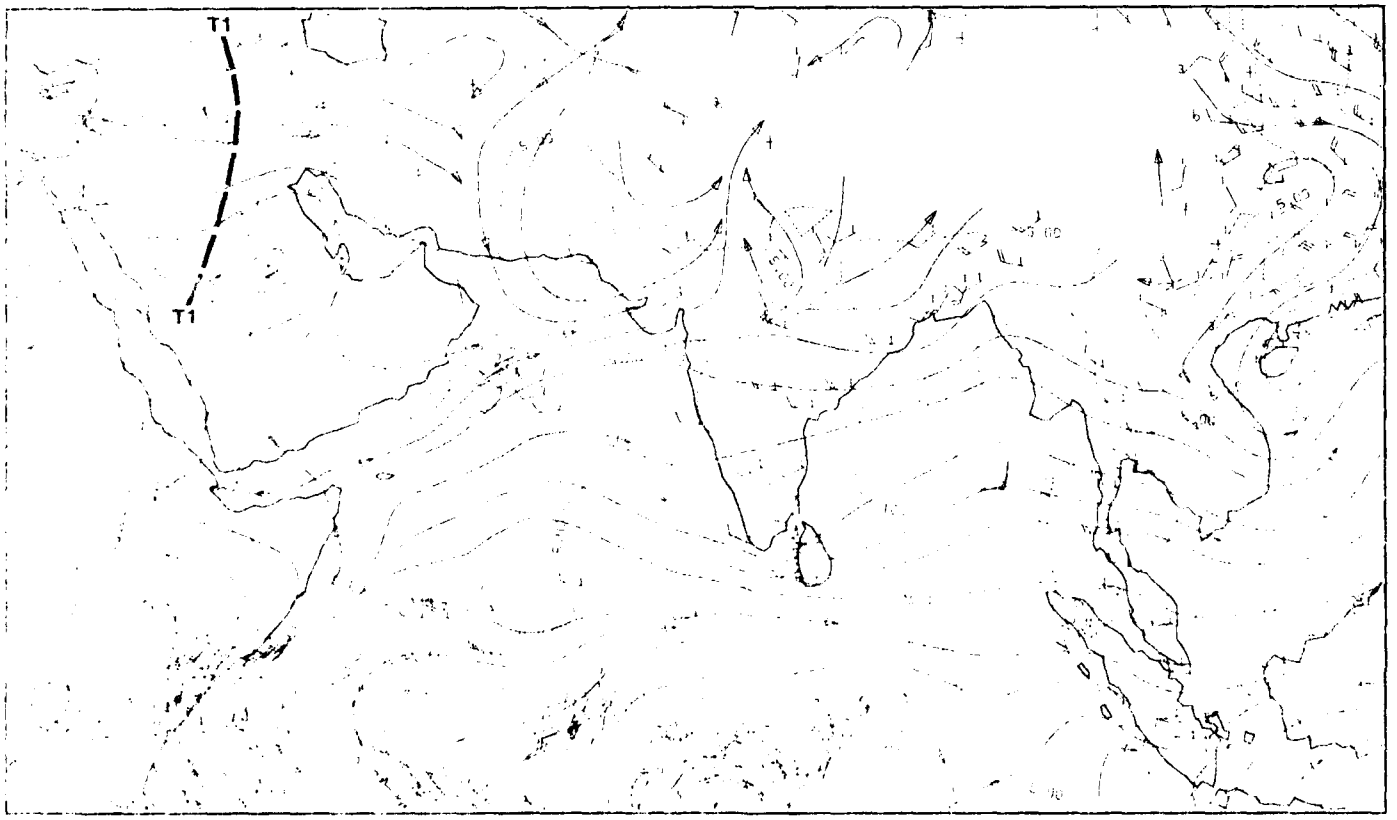

ID-3b. MONEX 850-mb Analysis, 1200 GMT 15 May 1979.

Duststorms Generated by the Desert Front

[illegible] ... EOSAT Enhanced View Infrared Picture 1155 GMT 15 May 1979.

[illegible] METEOSAT Enhanced View Water Vapor Picture 1155 GMT 15 May 1979.

FIG. 2(a). [illegible] DMSP [illegible] Low Enhancement [illegible] Note the [illegible] HD [illegible] Surface Wind Report [illegible] Arabian Sea [illegible]


IRAQ
dust
plume
30E
40E
45E
50E

AD-A154 718 NAVY TACTICAL APPLICATIONS GUIDE VOLUME 5 PART 1 INDIAN OCEAN (RED SEA/PE..(U) BOHAN (WALTER A) CO PARK RIDGE IL R W FETT ET AL. FEB 85 NEPRF-TR-83-03-REV 2/2

UNCLASSIFIED N00228-82-C-6222 F/G 4/2 NL

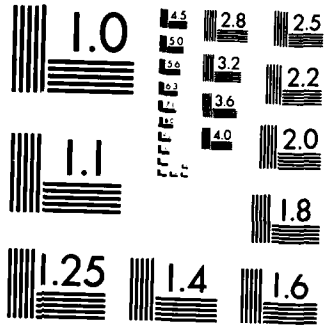

Case 2 Red Sea/Persian Gulf— Spring Transition

Detection of the Descending Offshore Branch in a Sea Breeze Circulation

The sea breeze circulation has a descending offshore branch which can be quite strong at low latitudes, where pressure gradients are generally weak and solar insolation very high. As an example, it has been noted in the Netherlands East Indies that pilot balloons blown out to sea in the upper return current of the sea breeze circulation have been observed returning to the coast at sea level in the low-level onshore flow (Kimble and Collaborators, 1946). The implication is that subsidence offshore was sufficient to overcome the free lift of the balloons.

The effect of the subsidence is to warm the air and stabilize the lapse rate in the descending branch of the sea breeze circulation. Moist haze droplets are evaporated or reduced in size by the warming of the air. At the same time, the stable lapse rate impedes the downward transfer of wind momentum to the sea surface so that a profound calming influence is maintained in the subsidence region.

The effects of the subsidence are often detected in satellite visible imagery in one of three distinct patterns: (1) An offshore cloud line may appear where the subsiding branch of the sea breeze circulation converges with the prevailing onshore flow; (2) When a uniform anomalous gray shade area is observed offshore, a clear channel may be produced along the coast under the subsiding branch of the sea breeze circulation where moist haze droplets composing the gray shade have been evaporated; and (3) Sunglint effects may be observed adjacent to the coastline. When the coastline is near the primary specular point, brilliant sunglint will be observed, and sometimes a black strip will also be observed as part of the sunglint pattern. Both of these occurrences — the brilliant sunglint and the black strips — indicate a calm sea state (NTAG Vol. 1, Sec 2A).

Reference
Kimble, G. H. T. and Collaborators, 1946: Tropical land and sea breezes. *Bull. AMS*, 27: 99–113.

700 mb

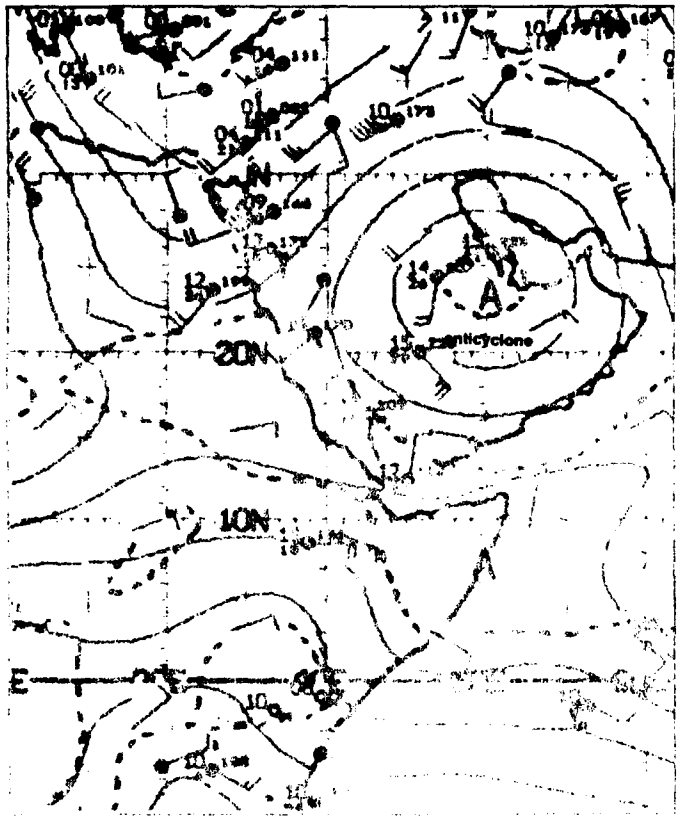

1D-26a. NMC Tropical 700-mb Streamline Analysis. 1200 GMT 21 May 1979.

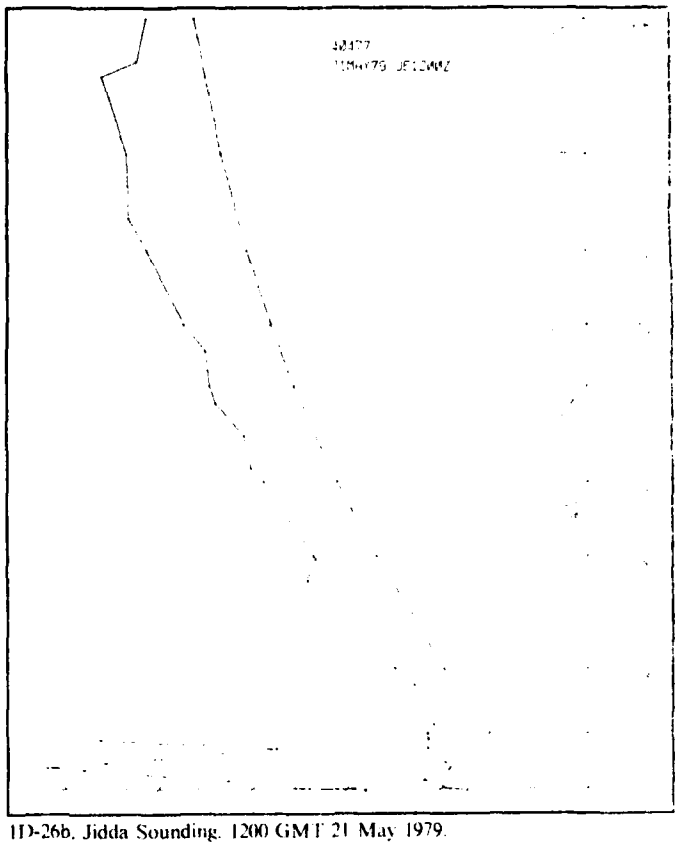

1D-26b. Jidda Sounding. 1200 GMT 21 May 1979.

surface

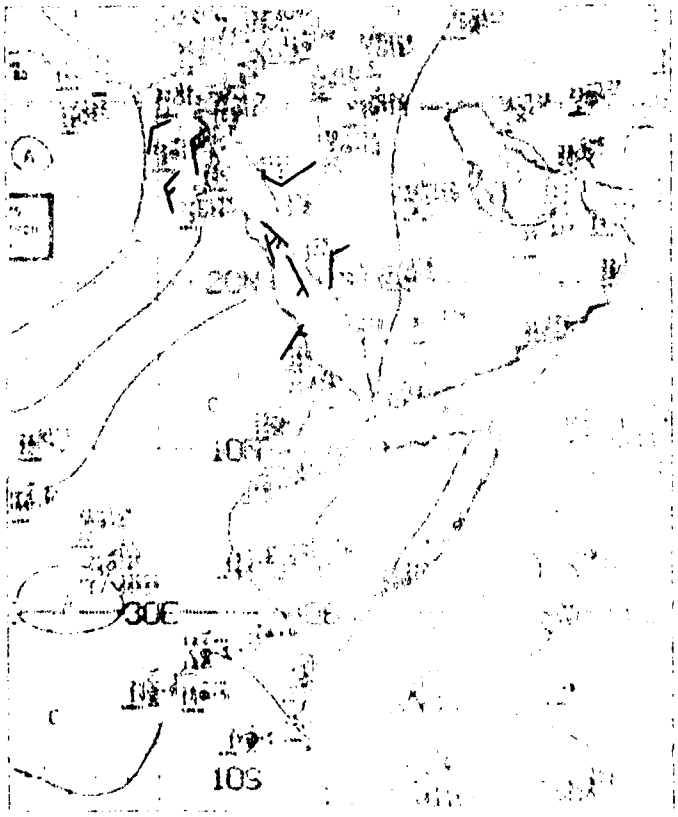

1D-26c. NMC Tropical Surface Streamline Analysis. 0000 GMT 21 May 1979.

surface

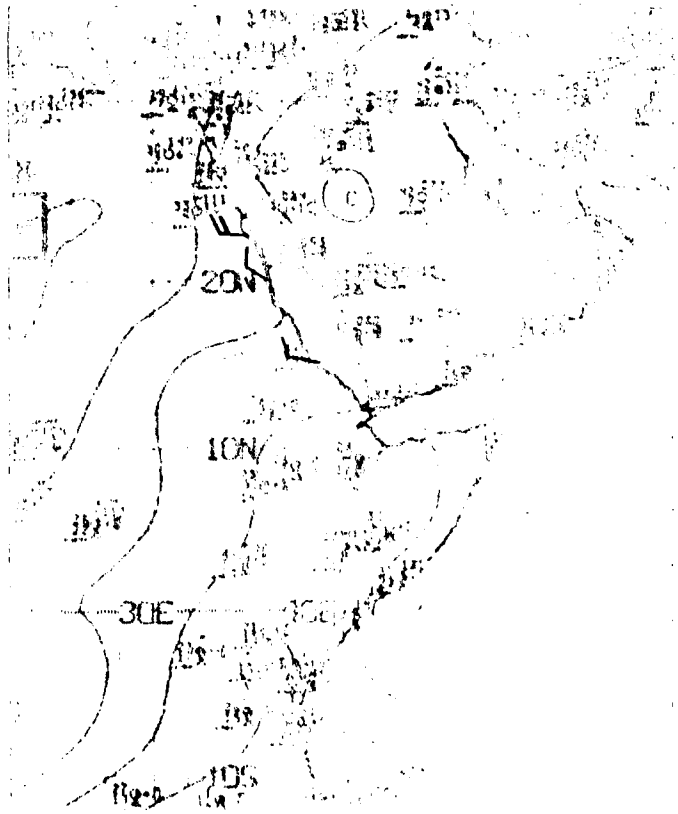

1D-26d. NMC Tropical Surface Streamline Analysis. 1200 GMT 21 May 1979.

The Use of Sunglint in Detecting Calm Sea Conditions in a Sea Breeze Circulation
Red Sea
May 19-9

21 May

The topography on the east coast of the Red Sea, facing the Al Hijaz mountain range, is ideal for the formation of strong land and sea breezes. The NMC surface streamline analysis for 0600 GMT (0900 LST, 1D-26c) reveals only light and variable winds over the central Red Sea region, but by 1200 GMT (1500 LST, 1D-26d) every wind report in the coastal Red Sea area indicates onshore flow, with speeds up to 20 kt, suggesting that a strong sea breeze has developed.

At 700 mb (1D-26a), southerly flow through the central Red Sea region curves anticyclonically around a high pressure (anticyclone) centered over southern Saudi Arabia. Near the surface, light northwest winds at Jidda (1D-26b) indicate the existence of the sea breeze within the overall southerly synoptic flow. A low-level inversion is also apparent based on this sounding.

The DMSP visible picture at 0816 GMT (1116 LST, 1D-27a) shows the central Red Sea to be cloud-free, as suggested by the low humidities in the Jidda sounding. There is, however, an elongated bright area along the Arabian coast. The question might be asked if this bright area could be due to a localized thunderstorm. This is precluded, however, because the DMSP infrared picture (1D-27b) shows no cold spot in the area of this unusually bright region. The effect is due to sunglint off the calm seas. Although winds are generally light and variable in the region, the added effect of the stabilizing influence exerted by the subsiding branch of the sea breeze circulation produces absolute calm and hence the brilliant sunglint pattern.

Important Conclusions

1. Regions of subsidence offshore associated with the subsiding branch of the sea breeze circulation produce a stable lapse rate at low levels which can result in calm seas and brilliant sunglint patterns offshore.

2. The tactical forecaster can use information of this type in several ways, including:
   a. The ability to locate regions in his area subject to strong land and sea breeze influence.
   b. Account for variations in localized coastal sea state conditions.
   c. Infer low-level wind direction in the absence of synoptic reports.

DMSP F-11 OLS Low Light Enhancement data (GMT 21 May 92 0)

Figure 3-1. DMSP Low Enhancement 0516 GMT 21 May 1979

Case 3 Red Sea/Persian Gulf— Spring Transition

Land Breeze Detection in Infrared Imagery

The land breeze forms during evening hours as a result of differential cooling between the land and the sea. The temperature of the land drops very rapidly after sunset, whereas the sea surface temperature drops very slowly. As an example, under ideal radiation conditions with a clear sky in a relatively dry atmosphere, land surfaces may cool as much as 20° - 30° F during the night, whereas the sea surface temperature during the same period rarely drops more than 0.5° - 1° F. The density difference between the air over the land and that over the sea results in a pressure gradient force directing the movement of the air to the sea, creating the land breeze. The strength of the land breeze is normally not as intense as that of the sea breeze. However, in coastal mountainous areas, cold air draining down the mountain side acquires a fall velocity which can reinforce the land breeze, creating strong, gusty conditions. The land breeze advance over the sea requires compensating subsidence onshore and rising motion over the sea at the seaward edge of the land breeze, which forms a closed cellular-type circulation similar to that of the sea breeze circulation, but reversed in direction.

Satellite evidence of land breeze effects, as described in the literature, has been chiefly concerned with a discussion of the offshore cloud line observed in visible and infrared imagery, parallelling the coastline. This cloud line results from speed convergence and upward vertical motion at the seaward limit of the land breeze, under favorable circumstances. However, due to DMSP infrared sensor water vapor absorption characteristics, these data can provide details which can be used to identify the presence of a land breeze circulation.


ARABIAN
PENINSULA
45E
50E

Land Breeze
Red Sea
May 1979

21 May

The DMSP visible picture at 0325 GMT (1D-30a) was acquired approximately one hour after sunrise. Sunglint is observed extending along the eastern portion of the image – the normal location of sunglint in an early morning DMSP pass. The Red Sea, therefore, is well removed from the sunglint area. The satellite picture shows the ridge line of the Al Hijaz Mountains along the eastern shore of the Red Sea, between 15° N and 20° N, in the region where the terrain rises very steeply from sea level. Some of the mountains in this range have peaks close to 10,000 ft; the average elevation of the prominent ridge paralleling the coastline is about 5,000 ft (1D-31d).

The satellite picture also shows subtropical jet stream cirrus over the northern Red Sea. With this cloud pattern it is common to have a cell of high pressure to the south over southern Saudi Arabia. The NMC 300-mb analysis for 0000 GMT (1D-31b) shows the subtropical jet stream over the northern Red Sea, and a high pressure cell over the southern Arabian Peninsula. The corresponding NMC surface streamline analysis (1D-31c) shows very light winds and clear sky conditions over the southern Arabian Peninsula, in agreement with the satellite evidence.

The nearest radiosonde station on the eastern Red Sea shore is Jidda, near 21° N, 39° E. The sounding at this station for 0000 GMT (1D-31e) reveals calm surface winds and a surface-based inversion, as the arid land was cooled through ideal radiation conditions during the nighttime hours. One might anticipate that under such circumstances a strong land breeze should develop, particularly along the shore facing the Al Hijaz Mountains. Yet little evidence of such an affect can be obtained from the DMSP visible picture, or the weather analyses.

The DMSP infrared picture for 0325 GMT (1D-31a), however, which is especially enhanced to provide information on variations in temperature at the warm end of the enhancement scale, gives strong evidence that a land breeze circulation has been established along the east coast of the Red Sea between latitudes 16° N and 20° N. In this region a warm (black-toned) area extending from roughly 40 to 70 n mi offshore is clearly evident. Over most of the Red Sea cooler temperatures with a slightly mottled appearance are observed. Water vapor absorption had a strong effect on the infrared signal for DMSP spacecraft, particularly for those of the Block 5-D series (F-1, F-2, and F-3), which had spectral bandwidths extending from 8 to 13 micrometers (see NIAG Vol. 2, Sec 3.V, Case 6).

In moist tropical or semi-tropical air masses, the problem was so severe that ocean thermal features could rarely be seen. In this F-3 example, such features appear to be completely blocked, and the variations of detail over the open ocean can be attributed to changes in the concentration and temperature of the water vapor in the atmosphere rather than sea surface temperature changes.

Why, then, should a land breeze, where cooler air is blowing from the land to the sea, produce a warm temperature reading? The answer to this question appears to be that the land breeze air is not only cooler than the air over the Red Sea but also much drier. Dry air from aloft, which has rolled down from the mountain side has been introduced into the boundary layer thereby reducing the total water vapor content per unit volume. With less water vapor in the land breeze region, atmospheric absorptive effects are reduced and the infrared sensor records faithfully the warmer temperatures of the actual sea surface. Conversely, in the surrounding region sea surface temperatures are masked by the over-lying water vapor which radiates at a much cooler temperature, characteristic of the low and mid-troposphere.

Apparently the Al Hijaz mountain region is strongly favored for the development of land breezes. An almost identical example is observed on 6 June 1979, in the DMSP (F-3) infrared picture at 0308 GMT (0608 LST, 1D-33a). Not only does the drying effect of the land breeze appear south of Jidda but also in a small region south of the Sinai Peninsula. The effect in that region is due to cold dry air drainage from a coastal mountain basin just south of the Sinai Peninsula (1D-31d). The converging effect of air draining down from such a basin would favor especially strong land breeze conditions. The corresponding DMSP visible picture (1D-32a) does not provide any evidence of a land breeze circulation south of the Sinai Peninsula or in the southern portion of the Red Sea due to suspended dust and haze at lower levels over the region.

Important Conclusions

1. Enhanced infrared data acquired during early morning hours over moist tropical regions are useful in determining areas exhibiting pronounced land breeze effects.

2. Such regions, because of reduced humidity, should be anticipated to be regions of increased low-level visibility, and will appear as a warm region in infrared imagery (even though reduced humidity is due to cold air drainage).

3. Concave coastal mountain basins or bay areas encircled by mountains should have especially pronounced land breeze effects.

ID Fig. F-3. DMSP 1S Low Enhancement, 0325 GMT 21 May 1979

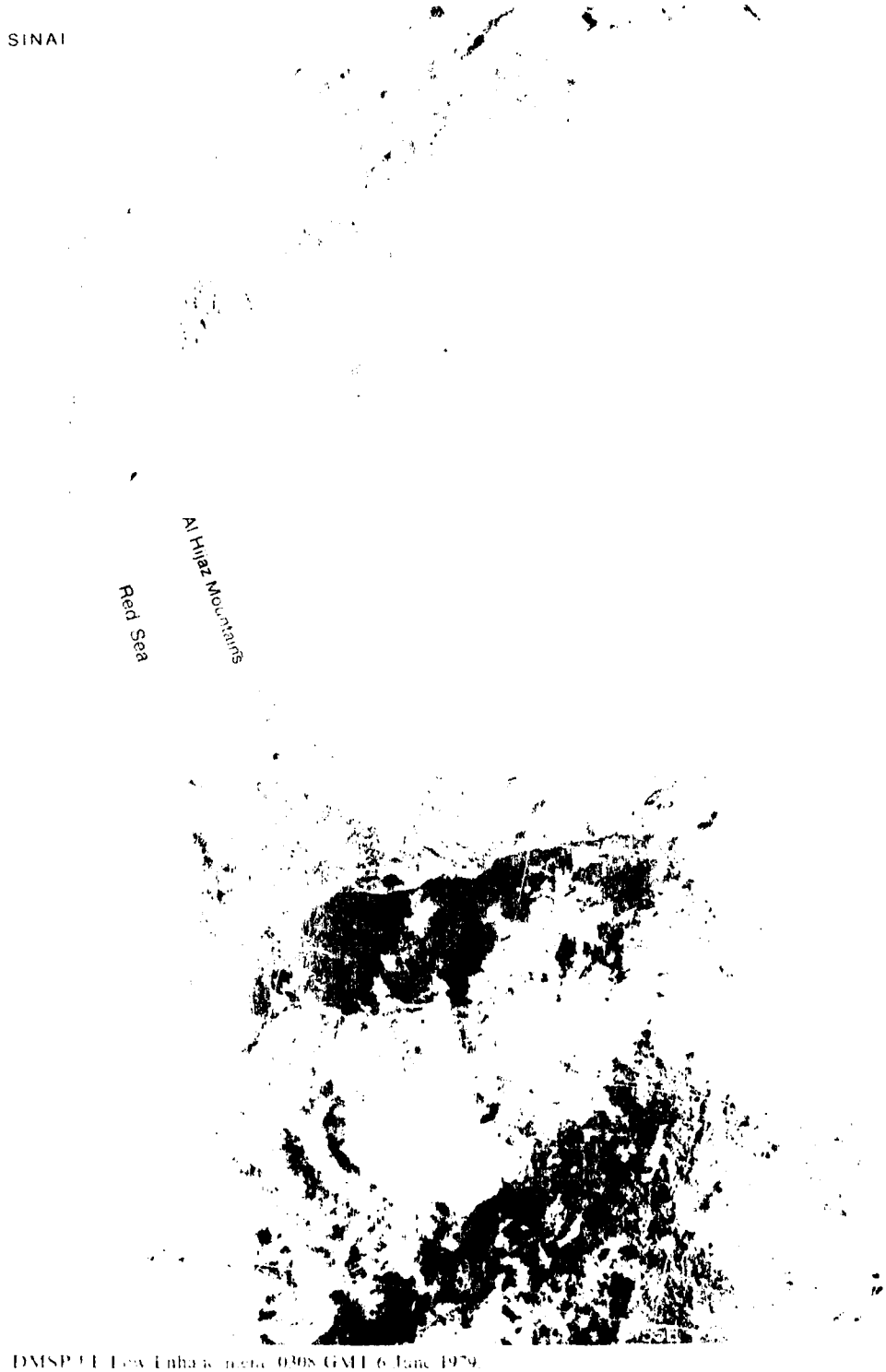

Fig. 2 U.S. DMSP Fine Enhanced 0308 GMT 6 June 1979

300 mb

surface

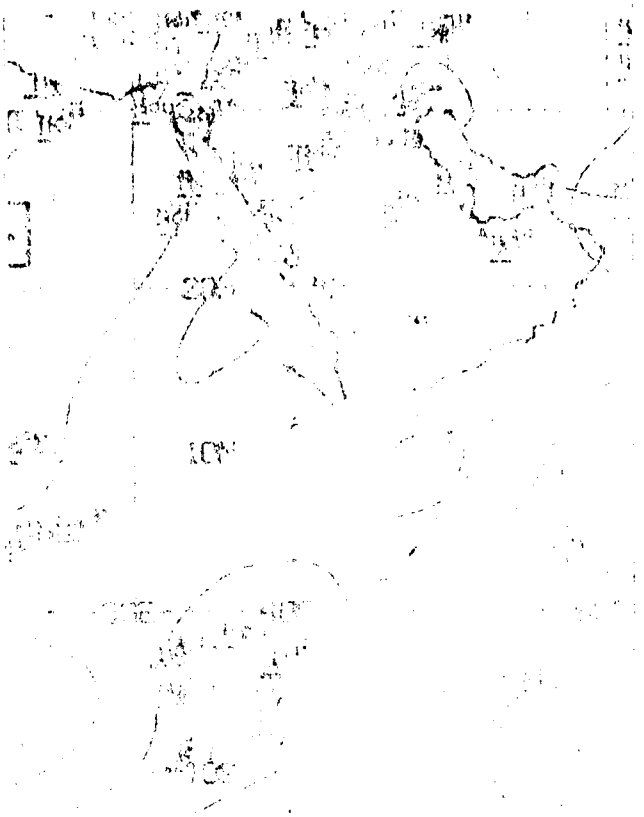

[illegible] NMC 300 mb Analysis 0000 GMT 21 May 1979.

ID-3b. NMC Tropical Surface Streamline Analysis 0000 GMT 21 May 1979.

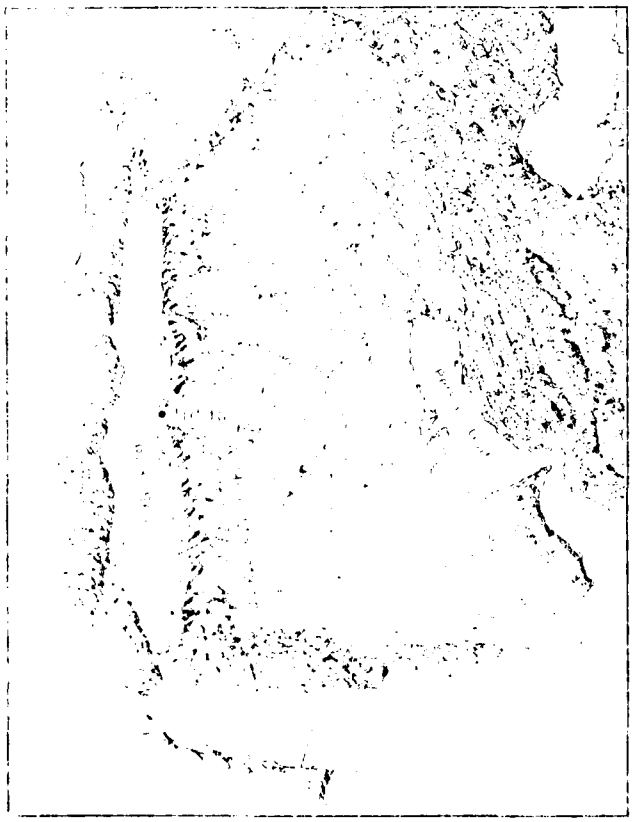

[illegible] Photographic Coverage of the Red Sea-Persian Gulf.

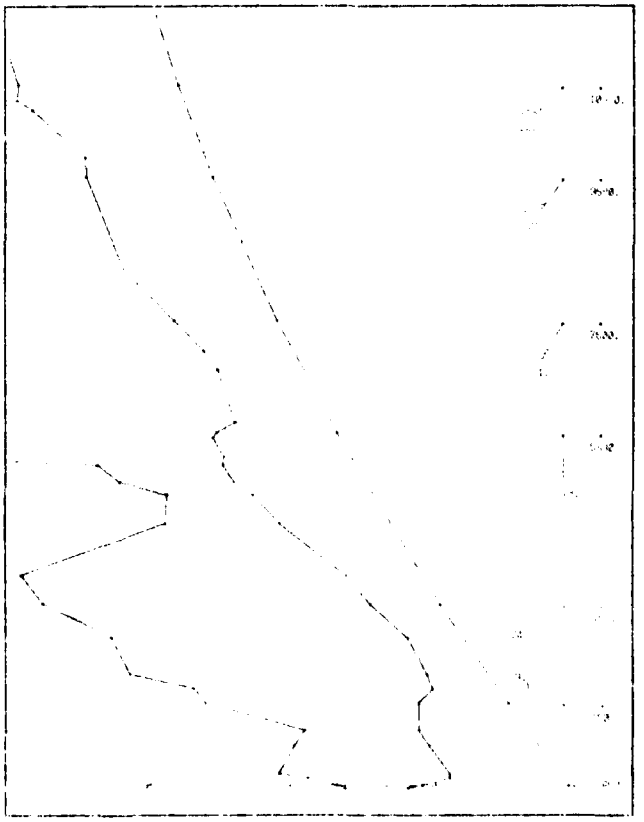

ID-3c. Tabla Streamline 0000 GMT 21 May 1979.

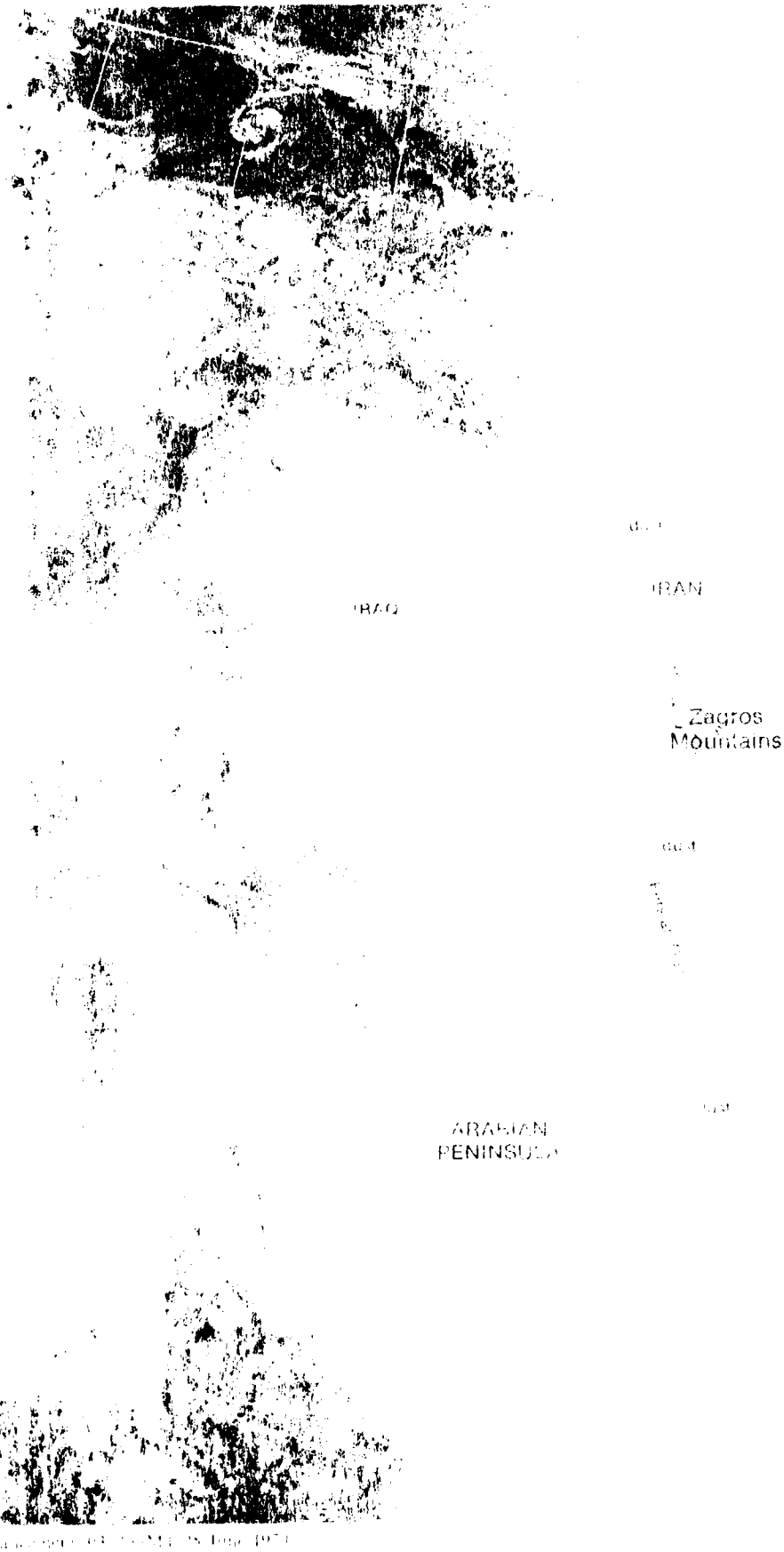
IRAN
IRAQ
Zagros
Mountains
ARABIAN
PENINSULA

Duststorms Generated by the Summer Shamal

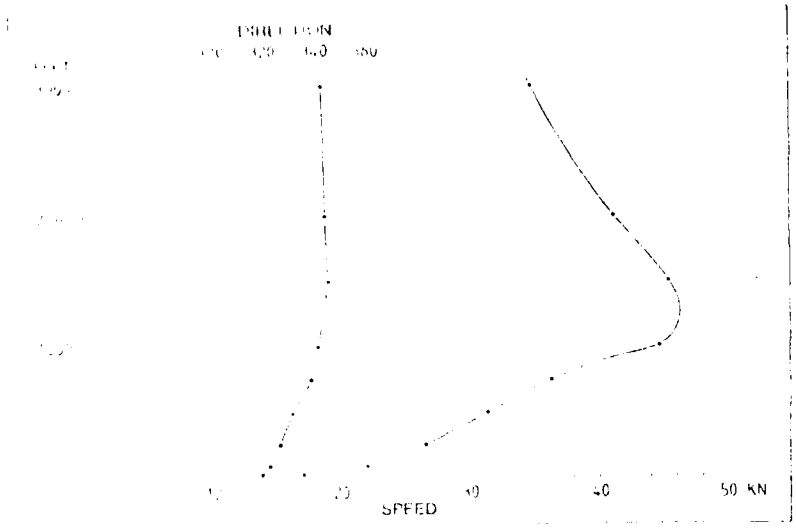

1E-51a. Average low-level wind profile for Bahrain.
After Membery, 1983.

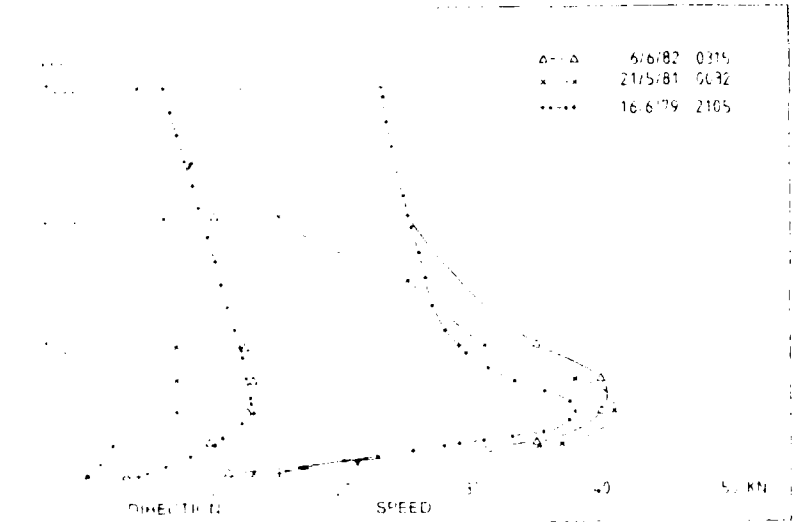

1E-51b. Example of low-level wind profile during shamal event.
After Membery, 1983.

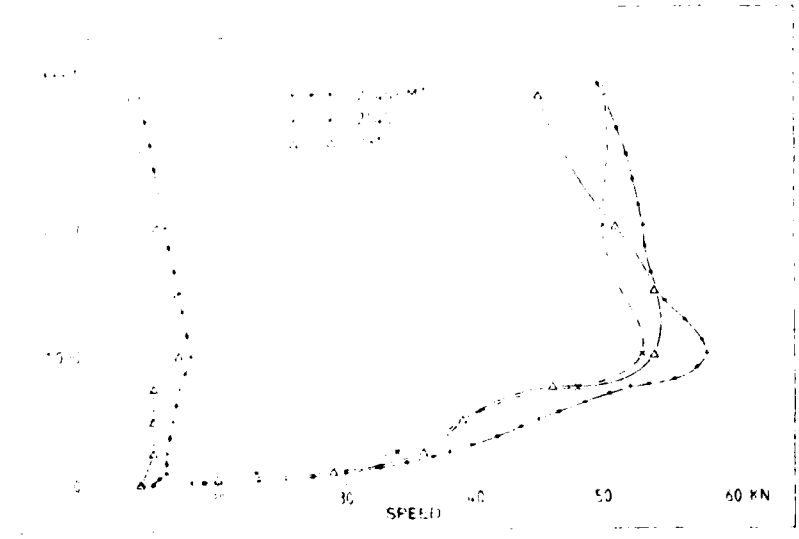

1E-51c. Low-level wind profile during strongest shamal on record.
After Membery, 1983.

The July mean monthly airflow at 850 mb (IE-50a) shows a speed maximum over the extreme northwestern Persian Gulf. Grant (1982) points out that the core of the northwesterly flow slopes westward with height and is still evident in the mid-troposphere near Riyadh, some 240 miles to the west of the Persian Gulf (IE-50b).

At night, very stable conditions develop and little mixing occurs over the Persian Gulf region. Maximum radiational cooling occurs over the desert under nighttime clear sky conditions. Inversions as strong as 9° C per 500 ft have been reported over Bahrain (Membery, 1983). These conditions during the summer shamal are occasionally related to the development of a nocturnal low-level jet that can cause extreme wind shear in the region from a few hundred feet down to the surface, as speeds

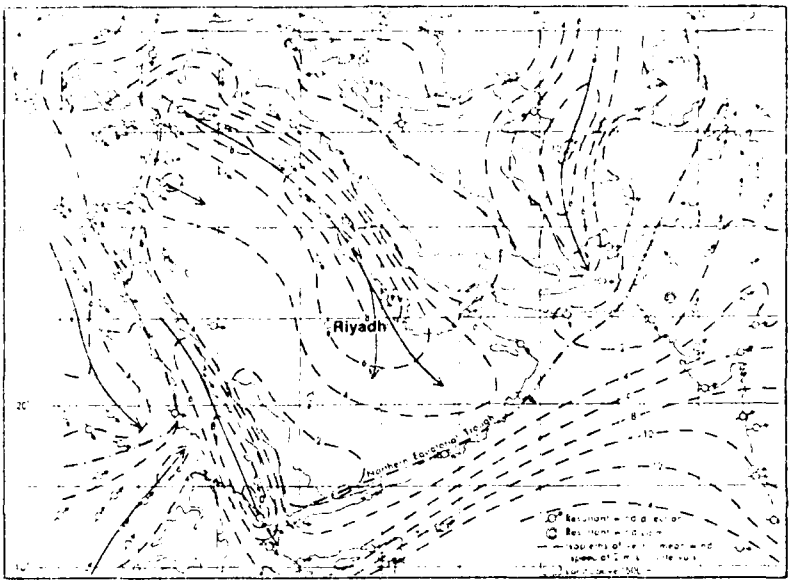

IE-50a. July mean monthly airflow at 850 mb.
After Grant, 1982.

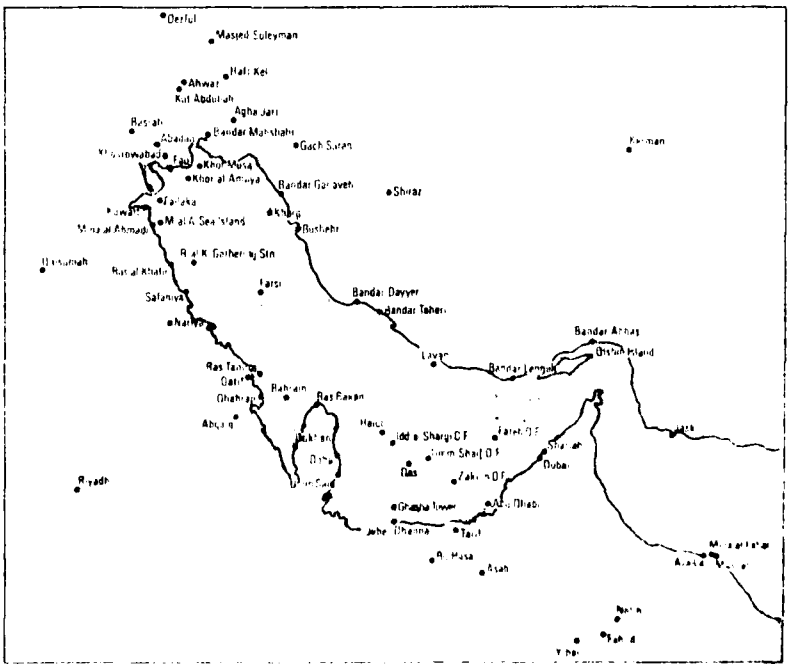

IE-50b. Map of the Persian Gulf region.

suddenly decrease very rapidly. The potential as an aircraft hazard during the landing process is great, and it could also pose a problem if an aircraft took off downwind and suddenly encountered a strong tailwind at low levels.

Development of the nocturnal jet appears to be maximized about 4½ hours after sunset at 26° N (Membery, 1983). This time period has been related to an inertial oscillation of the ageostrophic wind component of the total wind, with a period equal to the inverse of the coriolis parameter (which is latitude dependent).

What appears to happen is that during the daylight hours strong heating leads to turbulent mixing of the lower atmosphere. Sea breeze-induced wind flow at lower levels is mixed with winds at higher levels which are more geostrophic. This results initially in a resultant wind slower than would have occurred without mixing. At sunset, turbulence and mixing ceases. The sea breeze or ageostrophic component of the resultant wind begins to turn clockwise at upper levels in an inertial oscillation due to the coriolis force. About 4½ hours after sunset, at 26° N, the original upper-level wind and the ageostrophic component become aligned, and a rapid acceleration of the wind speed occurs, which produces the nocturnal jet. The mixing effect has been calculated to produce a wind as much as 80% stronger than otherwise would have occurred (Paegle and Rasch, 1973).

Membery (1983) shows an average low-level wind profile (1E-51a) for Bahrain determined from 12 reports from wide-bodied jets equipped with Inertial Navigation Systems (INS) during significant shamal outbreaks. Similar profiles (1E-51b) during shamal events when a marked low-level inversion existed (≥7° C between the surface and a level at or below 1,000 ft) show that a drop-off in speed both above and below the jet core is much more rapid in those instances when a marked temperature inversion is present. The height of the jet maximum also drops appreciably from over 1,000 ft under non-inversion dominated situations to as low as 600 or 700 ft, slightly above the top of the nocturnal inversion. The wind shear below the core is on the order of 6 kt per 100 ft, well above the 15 kt per 1,000 ft used in the classification of severe clear air turbulence by Navy forecasters (AG1 & C, 1974).

The development of the nighttime inversion is the key element in the formation of the nocturnal low-level jet. However, the temperature and wind profiles (1E-51c) for the strongest shamal case on record (11 June 1982) does not show a strong inversion. The wind profile in this case shows the low-level maximum near 1,000 ft, rather than near 600 ft as previously described (1E-51b), and a lack of strong shear above that level. The true nocturnal jet is not occurring in this case.

References

Grant, K., 1982: The July lower troposphere over the Middle East. *Met. Magazine*, **111**, 179–182.

Membery, D. A., 1983: Low level wind profiles during the Gulf shamal. *Weather*, **38**, 18–24.

Paegle, J. and G. E. Rasch, 1973: Three-dimensional characteristics of diurnally varying boundary-layer flows. *Mon. Wea. Rev.*, **101**, 746–756.

AG1 & C, 1974: Aerographer's Mate 1 & C. NAVEDTRA 10362-B. 659 pp.

Case 5 Red Sea/Persian Gulf—Summer

Summer Shamal over the Persian Gulf

From late May through mid-July persistent, moderately strong low-level northwesterly winds are observed over the northern and western Persian Gulf region. Locally this wind phenomenon is known as the 40-day shamal and is essentially a part of the southwest monsoon circulation. It results from the Persian Gulf region being under the influence of the thermal low that forms each spring over Pakistan and Afghanistan. The northerly flow over the western Persian Gulf is enhanced by a lee trough to the west of the Zagros Mountains, which border on the eastern Persian Gulf. The combination of a semi-permanent high pressure cell over northern Saudi Arabia, the thermal low, lee trough, and topographic features of the area tend to enhance the northerly flow below 5,000 ft.

The summer shamal is [illegible]n strong during the daytime, but typically decreases at night over land. [illegible]cal duststorms tend to develop daily over southern Iraq and Kuwait and diminish during the night. This is related to the typical unstable desert region conditions associated with the strong daytime heating which leads to a thoroughly mixed lower atmosphere. The summer shamal is basically a cloud-free feature. There is no flow of cold air over the Persian Gulf, as in the winter shamal; therefore no low-level clouds are likely to form. The existence of low-level dust plumes over southern Iraq and Kuwait, however, would be an indicator of an active summer shamal.

Red Sea/Persian Gulf
Summer Case 4

Tokar Gap Duststorms

II-47. DMSP F-5 Low Enhancement, 0731 GMT 20 June 1979

IE-46a. F-3 DMSP US Low Enhancement 0351 GMT 19 June 1979. (Note this picture is a repeat of IE-45a.) Surface Wind Reports and Streamline Analysis 0600 GMT 19 June 1979.

IF-45a. U.S. DMSP LS Low Enhancement 0351 GMT 19 June 1979

II-44c U.S. DMSP II Data Composite at 0330 GMT 15 June 1979. (Note this picture is a repeat of II-42a.) Surface Wind Reports and Streamline Analysis 0900 GMT 15 June 1979.

Lokar Cay Duststorms

Tokar Gap Duststorms
Southern Red Sea
June 1979

15 June

The DMSP visible picture at 0330 GMT (IE-42a) is an early morning pass (0030 LST) over the Red Sea region. Dense dust covers the southern half of the Red Sea. The Al Hijaz mountain range along the eastern coast rises steeply from the shoreline and in the higher elevations is an effective barrier to the advance of dust eastward over the Arabian Peninsula. The rugged western boundary of the higher elevations of the mountain range is barely discernible in the visible picture. However, in the DMSP infrared picture (IE-43a), the ridge line stands out as a cold, wavy northwest southeast-oriented line separating the warmer land along the coast from higher and colder land to the east. The dark tones over the southern Red Sea indicate that the dust is thinner over this area as compared to the light-toned area to the northwest. The cold area is an effect of long-wave radiation from dust carried to mid-tropospheric levels and debris from convective activity along the eastern shore. The convective activity is readily identified in the visible picture (IE-42a), and the dense dust band covers the Tokar Gap region. Note the numerous convective complexes that show shadows (dark areas) to the west, away from the sun in this early morning picture.

A streamline analysis based on the 0600 GMT surface observations is superimposed on the DMSP visible picture at 0330 GMT (IE-44a) to show the flow field over the southern half of the Red Sea. Note that northerly winds are located over the northern portion of the Red Sea, and that southerly flow through the Tokar Gap turns anticyclonically southward over the southern Red Sea. This flow pattern confines the dust to the southern Red Sea and shows that southerly winds are responsible for the dense dust band emerging from the Tokar Gap. Numerous stations report suspended dust or a duststorm in progress over the Sudan.

19 June

The DMSP visible picture at 0351 GMT (IE-45a) shows that dust in suspension covers the southern Red Sea to a much lesser degree on this day. The Tokar Gap is clearly discernible in this picture. Note how clearly the Al Hijaz mountain range appears along the eastern coastline of the northern half of the Red Sea. The streamline analysis superimposed on the DMSP visible picture at 0351 GMT (IE-46a) depicts wind flow patterns over the Sudan and the southern half of the Red Sea similar to that on the 15 June DMSP visible picture (IE-44a). On this day the main convective activity is well to the south, and surface observations show duststorms in progress with visibilities of less than ½ miles. Again the flow pattern confines the dust to the southern half of the Red Sea region.

20 June

The DMSP visible picture at 0731 GMT (IE-47a) shows a prominent dust plume emerging from the Tokar Gap and spreading out in an arch over the Red Sea. This is an outstanding example of a Tokar Gap duststorm produced by high winds. Winds tunneling through the valley under a strong low-level temperature inversion pick up speed due to the venturi effect, raising dust in the process which is advected out over the Red Sea. On this day, 60 kt southerly winds were observed near Tokar at the 850-mb level at 1200 GMT (MONEX winds, not shown, Krishnamurti, 1979).

Important Conclusions

1. The Tokar Gap is a preferred route for dust advection into the central and southern Red Sea.

2. Qualitative comparisons of satellite visible and infrared imagery are useful in determining relative severity of duststorm conditions.

3. Dust plumes emerging from the Tokar Gap may indicate strong southwesterly winds.

Reference

Krishnamurti, T. N., P. Ardanuy, Y. Ramanathan, and R. Pasch, 1979: Quick look summer MONEX atlas, part II, the onset phase. FSU report No. 79-5 Florida State University, Tallahassee, Florida. 205 pp

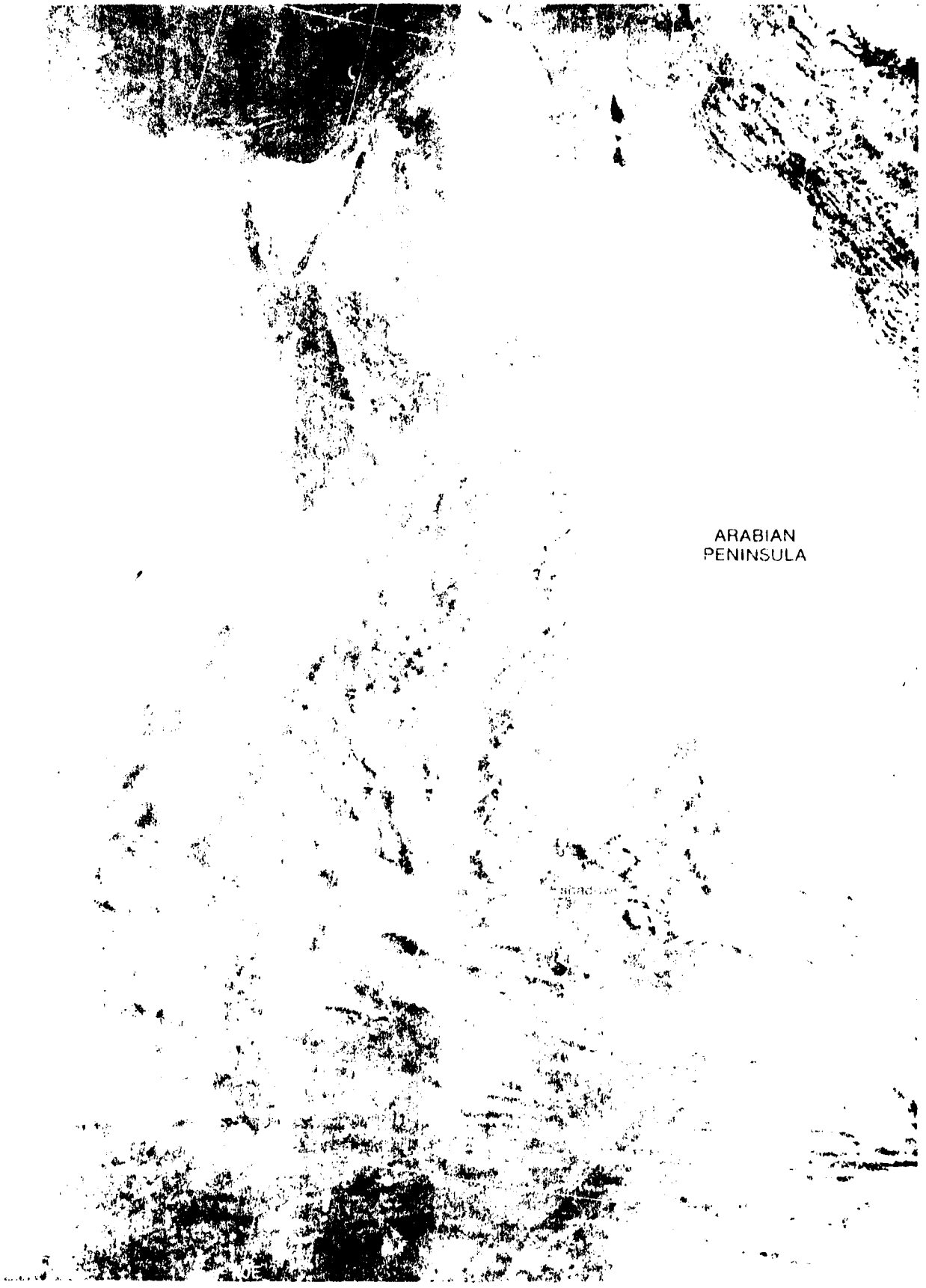

[illegible] COMPLETE Gas Fuel Inventory [illegible] GMT 15 June 1979

Case 4 Red Sea/Persian Gulf—Summer

Duststorms over the Southern Red Sea

An unstable atmosphere is necessary before duststorms can develop. Under such conditions, dust raised at the surface is lifted vertically to altitudes where stronger winds exist, permitting advection long distances downwind. In the southern half of the Red Sea, the maximum frequency of duststorms is during the summer months when convectively unstable air reaches the Red Sea region as part of the southwest monsoon flow from equatorial latitudes. The Tokar Gap is a southwest to northeast oriented valley that opens onto the western shore of the Red Sea (1E-41a). During the southwest monsoon, winds funneling through this valley pick up speed due to the venturi effect, and raise dust in the process which is advected out over the Red Sea. Dust may also be generated by local convective activity (haboobs) over the desert and be advected by the prevailing southwesterly winds through the Tokar Gap. Over the Red Sea, the flow tends to turn anticyclonically so that the entire southern portion of the Red Sea is affected by the dust. From an operational point of view, it is important to recognize that air to ground visibility in duststorms is generally a small fraction of the surface reported horizontal visibility, therefore it may not be possible to pick out an airfield from above, even when reported horizontal surface visibility is three miles or more.

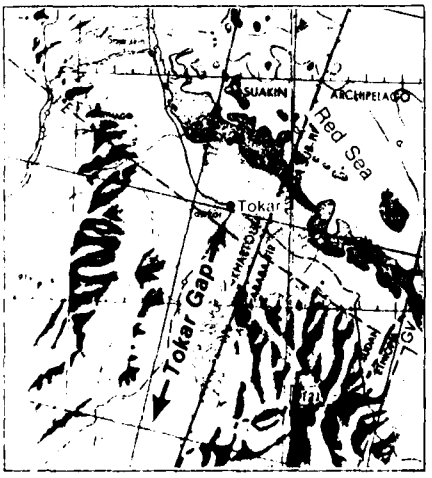

Inset: Tokar Gap, DOD Topographic Map

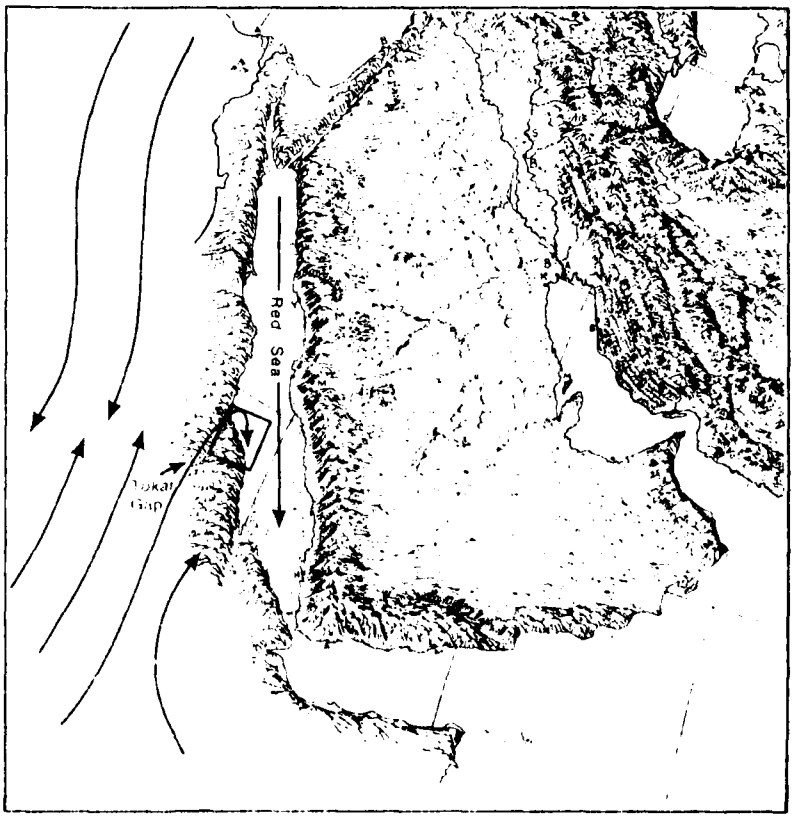

1E-41a Wind Flow during Southwest Monsoon Duststorms

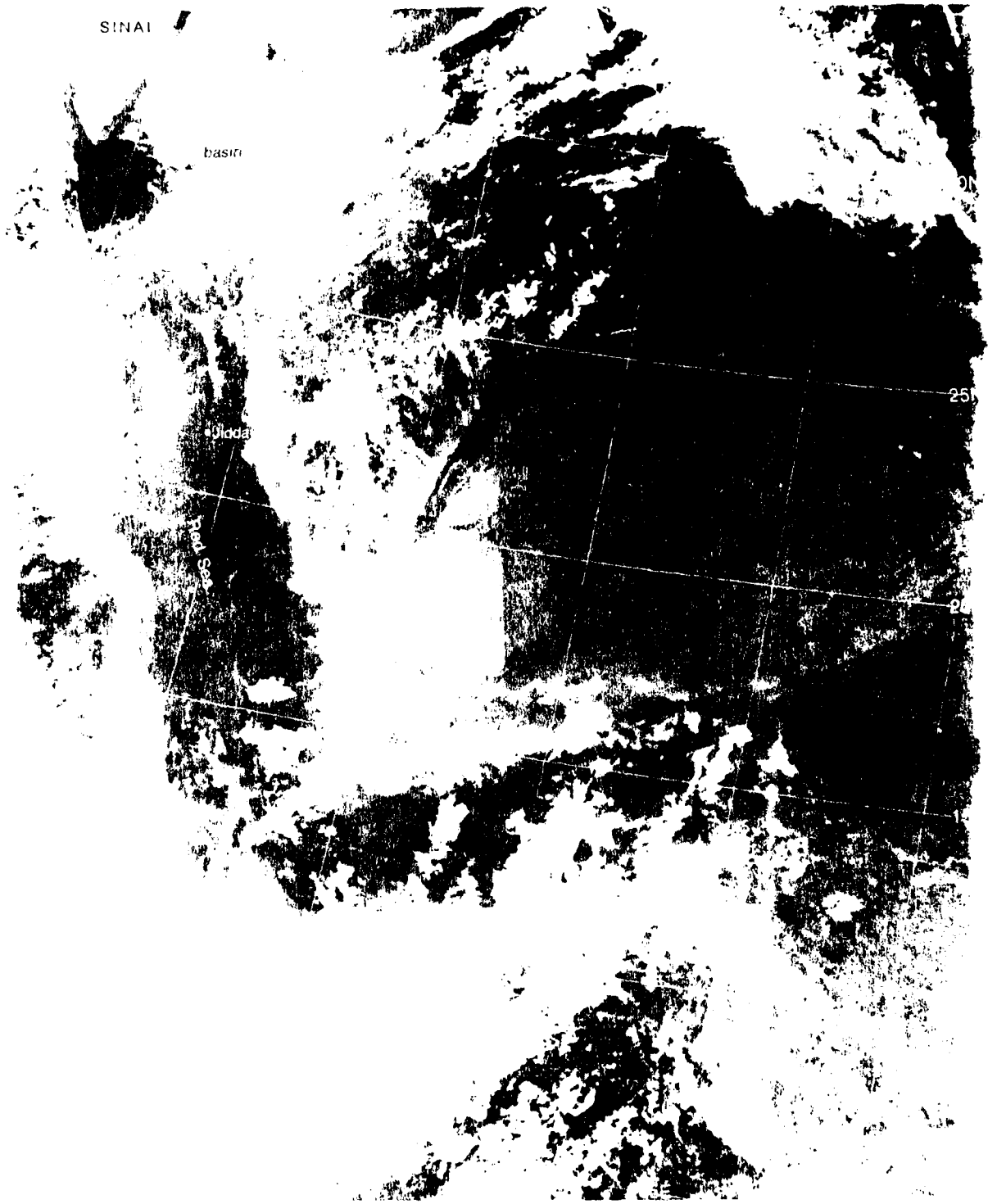

TD-33a. F-3 DMSP IR Low Enhancement 0308 GMT 6 June 1979.

Duststorms Generated by the Summer Shamal
Persian Gulf
June 1979

25 June

The DMSP visible picture at 0332 GMT (1E-52a) shows a large-scale duststorm generated by a summer shamal. At this time the primary dust source is over western Iran. Dust is also apparent in central Iraq where surface features, lakes, etc., are obscured; as well as over central Saudi Arabia; and over the central portion of the Red Sea. The Persian Gulf is totally obscured by dust. The NMC surface streamline analysis for 0600 GMT (not shown) reveals numerous reports of suspended dust north of the Persian Gulf, along coastal stations of the Persian Gulf, and westward to the Red Sea. The clockwise turning of the suspended dust is corroborated by the 850-mb wind pattern (not shown; see Krishnamurti, 1979) which shows an anticyclonic flow pattern over the region with 50-kt northerly winds at Kuwait. The surface to 850-mb wind conditions at Dhahran (1E-53a), for the period from 23/0000 GMT to 26/0000 GMT show that strong winds persisted throughout the period and that a nocturnal jet appears in evidence on the 0000 GMT (nighttime) data. This condition closely resembles the nocturnal jet profile (1E-53b) described by Meinbery (1983).

With the summer shamal being an extremely persistent feature, the forecasting of the development of the nocturnal low-level jet may be the most critical issue. One can be sure that it will not occur when nighttime surface winds are strong, implying the lack of a low-level inversion. Combining the use of satellite imagery to monitor the dust plume activity with conventional surface and upper-air observations will provide the information needed to forecast nocturnal jet events. By keeping a record of the surface temperatures as the night progresses and comparing these with an afternoon (1200 GMT) sounding, one can determine when a strong nocturnal surface inversion is developing and hence the likelihood of a jet formation aloft in the evening.

Important Conclusions

1. The summer shamal does not produce a cloud signature and therefore is not clearly indicated by cloud lines in satellite imagery.

2. Local as well as large-scale duststorms are daily events over the land areas north of the Persian Gulf, Iraq, and Kuwait during the summer shamal, and these events are evident in satellite imagery.

3. Nighttime strong low-level temperature inversions tend to form over the desert areas during the summer. A nocturnal low jet profile with the core near 600 to 700 ft develops under summer shamal conditions with strong surface inversions.

4. The nocturnal jet tends to develop under moderate summer shamal conditions, rather than under strong conditions where mechanical mixing tends to prevent the formation of a low-level inversion.

5. Forecasters should be alerted to the possibility of strong low-level wind shear, producing severe clear air turbulence at Persian Gulf locations during summer nighttime hours whenever a marked low-level inversion exists.

Reference

Krishnamurti, T. N., P. Ardanuy, Y. Ramanathan, and R. Pasch, 1979: Quick look summer MONEX atlas, part II, the onset phase. FSU report No. 79-5, Florida State University, Tallahassee, Florida. 205 pp.

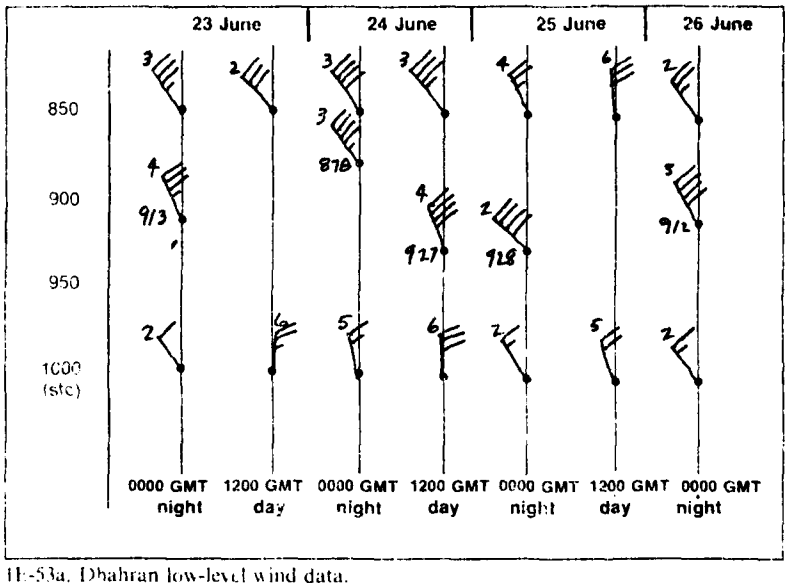

IE-53a. Dhahran low-level wind data.

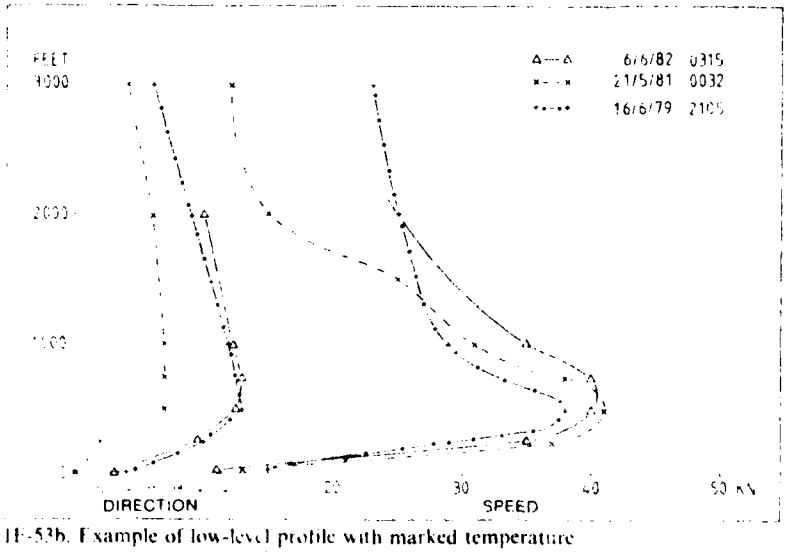

IE-53b. Example of low-level profile with marked temperature inversion present (nocturnal jet). After Membery, 1983.

END

FILMED

7-85

DTIC